AD-A047 953 STANFORD UNIV CALIF STANFORD ELECTRONICS LABS F/G 20/5
INTERACTION OF ELECTROMAGNETIC AND ACOUSTIC WAVES IN A STOCHAST--ETC(U)
JUL 77 N BHATNAGAR N00014-75-C-0601
UNCLASSIFIED SU-SEL-77-031 NL

1 OF 2
ADA047953

RADIOSCIENCE LABORATORY

STANFORD ELECTRONICS LABORATORIES
DEPARTMENT OF ELECTRICAL ENGINEERING
STANFORD UNIVERSITY · STANFORD, CA 94305

SEL-77-031

INTERACTION OF ELECTROMAGNETIC AND ACOUSTIC WAVES IN A STOCHASTIC ATMOSPHERE

by

NIRDOSH BHATNAGAR

July 1977

FINAL REPORT

Prepared under

Joint Services Electronics Program
Office of Naval Research
Contract N00014-75-C-0601
and
National Aeronautics and Space Administration
Grant NGL 05-020-014

(14) SU-SEL-77-031

(6) INTERACTION OF ELECTROMAGNETIC AND ACOUSTIC WAVES IN A STOCHASTIC ATMOSPHERE.

by

(10) NIRDOSH/BHATNAGAR

(12) 125p.

(11) July 1977

(9) FINAL REPORT.

Prepared under

Joint Services Electronics Program
(15) Office of Naval Research
~~Contract~~ N00014-75-C-0601
and
National Aeronautics and Space Administration
Grant NGL-05-020-014

Radioscience Laboratory
Stanford Electronics Laboratories
Stanford University Stanford, California

ABSTRACT

In the Stanford Radio Acoustic Sounding System (RASS), an electromagnetic signal is made to scatter from a moving acoustic pulse train. Under a Bragg-scatter condition, maximum electromagnetic scattering occurs. The scattered radio signal contains temperature and wind information as a function of the acoustic pulse position.

In the theoretical work on RASS to date, the effects of such atmospheric parameters as turbulence, humidity, mean temperature, and mean wind fields on the propagating acoustic pulse train have been ignored. By neglecting these parameters, the quantitative analyses have assumed that the acoustic wavefronts act as large perfect spherical reflectors. In this investigation, RASS performance is assessed in a real atmosphere where "coherency" of the acoustic pulse is degraded as it propagates vertically into the lower atmosphere. The only assumption made is that the electromagnetic wave is not affected by stochastic perturbations in the atmosphere.

Coherency of vertical acoustic-wave propagation is described through a perturbation-theoretic method and Feynman's diagrammatic technique. One of the most important attributes of this analysis is that it systematically and explicitly accounts for multiple scattering of acoustic waves in the presence of atmospheric fluctuations. The coherency results are then used to evaluate the strength of the scattered electromagnetic signal from the acoustic pulse train while taking into account the presence of turbulence, mean temperature gradients, and mean wind fields.

It is concluded that, for acoustic pulses with carrier frequencies below a few kilohertz propagating under typical atmospheric conditions,

turbulence has little effect on the strength of the received radio signal at heights up to a few kilometers. This result implies that focusing of RF energy by the acoustic wavefronts is primarily a function of sound intensity which decreases as x^{-2}, where x denotes altitude.

The effect of mean vertical wind and mean temperature on the strength of the received signal is also demonstrated to be insignificant. Mean horizontal winds, however, shift the focus of the reflected electromagnetic energy from its origin, resulting in a decrease in received signal level when a monostatic RF system is used. For a bistatic radar configuration with space-diversified receiving antennas, the shifting of the acoustic pulse makes possible the remote measurement of the horizontal wind component.

ACKNOWLEDGMENT

This research was supervised by Prof. Allen M. Peterson. His definitive work in remote sensing is the foundation upon which this research has been built. The author is deeply indebted to him for his continual guidance and encouragement throughout the course of this work.

Appreciation is also extended to Dr. M. S Frankel for his interest and numerous comments on the literary style of the manuscript. A special note of gratitude is in order to Prof. G. S. Kino for his comments and prompt attention. Mary Anne Larrimore typed the manuscript with obvious care and skill. The author would like to express his appreciation for her diligence, helpfulness, and patience. The literary eclecticism of Hortense Shirely has helped to improve the comprehensibility of this work.

This research was partially supported by Joint Services Electronics Program under contract N00014-75-C-0601 and by NASA grant NGL 05-020-014. This support is gratefully acknowledged.

CONTENTS

CONTENTS (Cont)

CONTENTS (Cont)

ILLUSTRATIONS

SYMBOLS

Symbols most often used in the text are defined below; others are defined as they occur.

a_g	temperature gradient in lower troposphere
A	proportionality constant measuring outer scale of turbulence
A_r	effective area of receiving antenna
B	proportionality constant measuring inner scale of turbulence
$B_p(\bar{r},\bar{r}')$	covariance of random field $p(\bar{r})$
$c(\bar{r})$	velocity of sound
c_o	reference velocity of sound
c_p	specific heat of air at constant pressure
c_v	specific heat of air at constant volume
C_f	Fresnel cosine integral
$C_p^2(x)$.	refractive-index structure parameter of random field $p(\bar{r})$ at altitude x
C_{no}^2	reference value of refractive-index structure parameter at altitude x_o
d	imaginary part of complex acoustic wave number h
d_{scv}	diameter of scattering volume for electromagnetic energy
d_t	total derivative with respect to time, d/dt
$d\alpha(x,\bar{\kappa}_\alpha)$	two-dimensional Fourier-Stieltjes measure of log-amplitude of a scattered sound wave
$d\nu(x,\bar{\kappa}_\alpha)$	two-dimensional Fourier-Stieltjes measure of acoustic refractive index

$d\rho(x,\bar{\kappa}_\alpha)$ . . . . . two-dimensional Fourier-Stieltjes measure of acoustic pressure

$d\sigma(x,\bar{\kappa}_\alpha)$ . . . . . two-dimensional Fourier-Stieltjes measure of phase of scattered sound wave

$d\phi(x,\bar{\kappa}_\alpha)$ . . . . . two-dimensional Fourier-Stieltjes measure of log-amplitude and phase of scattered sound wave

$D_p(\bar{r},\bar{r}')$ . . . . . structure function of random field $p(\bar{r})$

$\mathfrak{D}$ . . . . . Dyson's operator

e_{ij} . . . . . shear strain tensor

$E(\bar{r})$ . . . . . electric field component

$E_o(\bar{r})$ . . . . . electric field in free space

$E_1(0), E_1$ . . . . . scattered electromagnetic signal, collected at receiver

f_a . . . . . acoustic frequency

f_e . . . . . electromagnetic frequency

F^* . . . . . complex conjugate of F

$|F|$ . . . . . magnitude of complex number F

$F_p\left(\frac{\bar{r}+\bar{r}'}{2}, x-x', \bar{\kappa}_\alpha\right)$ . . two-dimensional spectral density of random field $p(\bar{r})$ in a medium with smoothly varying mean characteristics

$F_p(x,\bar{\kappa}_\alpha)$ . . . . . two-dimensional spectral density of random field $p(\bar{r})$ in the plane x = constant

$F_{\chi s}(x,\bar{\kappa}_\alpha)$ . . . . . two-dimensional log-amplitude phase spectra of scattered acoustic wave

G_{as} . . . . . maximum gain of acoustic source

$G_a(\bar{r},0)$ . . . . . Green's function for acoustic-wave propagation in the presence of turbulence

$G_a'(\bar{r},0)$ . . . . . varying part of $G_a(\bar{r},0)$

$G_{ao}(\bar{r},\bar{r}')$ . . . . . free-space Green's function for acoustic-wave propagation

G_r . . . . . maximum gain of electromagnetic receiver antenna

G_t . . . . . maximum gain of electromagnetic transmitter antenna

h . . . . . complex acoustic wave number

$H(\bar{r})$ . . . . . magnetic field component

H_e . . . . . entropy of air

i . . . . . $\sqrt{-1}$

$Im(F)$ . . . . . imaginary part of complex number F

I_i . . . . . identity operator

$\mathcal{I}$ . . . . . intensity operator

$J_o(x)$ . . . . . Bessel function of first kind and zeroth order

k_a . . . . . real part of complex acoustic wave number h

k_e . . . . . electromagnetic wave number

K_d . . . . . a constant indicating a measure of sound velocity

K_{re} . . . . . a constant indicating a measure of the varying part of electromagnetic refractive index

$\ell_o(x)$ . . . . . inner scale of turbulence at height x

$\mathscr{k}_o(x)$ . . . . . $\ell_o(x)/(2\pi)$

$\ln(x)$ . . . . . natural logarithm

$L_o(x)$ . . . . . outer scale of turbulence at height x

$\mathscr{L}_o(x)$ . . . . . $L_o(x)/(2\pi)$

$\mathcal{L}$ . . . . . linear stochastic differential operator

$\mathcal{L}'$ . . . . . varying part of linear stochastic differential operator

m_a . . . . . factor determining the refractive-index structure parameter in the presence of inhomogeneous turbulence

$M(\bar{r}',\bar{r}'')$ . . . . . coherence function for two points $\bar{r}'$ and $\bar{r}''$

$\mathfrak{M}$ . . . . . mass operator

$n(\bar{r})$ . . . . . acoustic refractive index

$n_1(\bar{r})$ . . . . . fluctuating component of acoustic refractive index

$n_e(\bar{r})$ . . . . . electromagnetic refractive index

$n_{e1}(\bar{r})$ . . . . . varying part of electromagnetic refractive index

n_{ac} . . . . . number of cycles in acoustic pulse

$p_a(\bar{r})$ . . . . . external acoustic pressure

p_o . . . . . reference pressure

P . . . . . total pressure in the fluid

P_a . . . . . acoustic radiated power

P_{av} . . . . . ensemble average operator ($P_{av} = \langle \cdot \rangle$)

P_{ij} . . . . . fluid stress sensor

P_r . . . . . power collected by electromagnetic receiver

P_{rw} . . . . . asymptotic value of power collected by electromagnetic receiver in presence of constant horizontal winds

P_t . . . . . power radiated by electromagnetic transmitter

r . . . . . magnitude of vector $\bar{r}$; $|\bar{r}|$

$\bar{r}$ . . . . . $(x,y,z) = (x,\bar{y}_\alpha)$ where $\bar{y}_\alpha = (y,z)$

R_1 . . . . . upper edge of acoustic pulse

R_2 . . . . . lower edge of acoustic pulse

$Re(F)$	real part of complex number F
R_{gc}	gas constant
$S(\bar{r})$	perturbed phase of acoustic wave
$S_o(\bar{r})$	unperturbed phase of acoustic wave
$S_1(\bar{r})$	perturbation in phase of acoustic wave $S_1(\bar{r}) \equiv (S(\bar{r}) - S_o(\bar{r}))$
$S_f(x)$	Fresnel sine integral
t	time variable
t_{ij}	total momentum flux tensor
$T(\bar{r})$	temperature of atmosphere
T_o	reference temperature of the medium
u_i	fluid-velocity caused by sound waves
$u_a(\bar{r})$	spatial variation of external acoustic pressure $p_a(\bar{r})$
$u_{ao}(\bar{r})$	$u_a(\bar{r})$ in absence of turbulence
V_{as}	scattering volume for electromagnetic wave
V_d	volume density of air
V_i	total fluid-velocity component
V_s	upper-half infinite space
w_h	magnitude of horizontal wind velocity
w_i	atmospheric fluid velocity in absence of sound
x	altitude
x_c	coherence length of acoustic-wave propagation
x_i	incoherence length of acoustic-wave propagation

$\bar{y}_\alpha$ . . . . . (y,z)

$Y(x)$ . . . . . Heaviside step function

γ . . . . . ratio of specific heats for air

$\Gamma(x)$ . . . . . gamma function

δ . . . . . dimensionless parameter

δ_e . . . . . dimensionless dummy parameter

δ_{ij} . . . . . Kronecker delta

$\delta(x)$ . . . . . Dirac delta measure

$\Delta f(x)$ . . . . . doppler shift in received electromagnetic signal scattered from traveling acoustic pulse at altitude x

$\Delta f_{av}(x)$ . . . . . averaged doppler shift

$\Delta T(x)$ . . . . . error in temperature measured at altitude x

$\Delta\varepsilon(\bar{r})$ . . . . . deviation of permittivity of the medium from its free-space value

$\varepsilon(\bar{r})$ . . . . . permittivity of the medium

ε_o . . . . . free-space permittivity

η_o . . . . . intrinsic impedance of free space

$\hat{\theta}$ . . . . . smaller of acoustic or radar beamwidths

$\hat{\theta}_a$ . . . . . half-power beamwidth of acoustic source

$\hat{\theta}_e$ . . . . . half-power beamwidth of electromagnetic transmitter and receiver

$\bar{\kappa}$ . . . . . spatial-frequency vector $(\kappa_x, \kappa_y, \kappa_z)$

$\bar{\kappa}_\alpha$ . . . . . (κ_y, κ_z)

λ_a . . . . . acoustic wavelength

λ_e . . . . . electromagnetic wavelength

λ_v . . . . . volume viscosity

μ_o . . . . . free-space permeability

μ_v . . . . . shear viscosity

$\rho(\bar{r})$ . . . . . density of air

ρ_o . . . . . static density of air

$\tau(\bar{r})$ . . . . . fractional variation of temperature from its reference

$\Phi_p(\bar{\kappa})$ . . . . . three-dimensional spectral expansion of random field $p(\bar{r})$

χ . . . . . perturbation in log amplitude of scattered sound wave

$\psi(\bar{r})$ . . . . . complex phase in the Rytov transformation

$\psi_o(\bar{r})$ . . . . . unperturbed value of complex phase of the acoustic wave

$\psi_1(r)$ . . . . . first-order perturbation of complex phase of the acoustic wave

ω_a . . . . . angular frequency of acoustic wave $(\omega_a = 2\pi f_a)$

ω_e . . . . . angular frequency of electromagnetic wave $(\omega_e = 2\pi f_e)$

∂_i	partial derivative with respect to space variable x_i $(\partial_i = \partial/\partial x_i)$
∂_t	partial derivative with respect to time $(\partial_t = \partial/\partial t)$
∇	gradient operator
$\nabla\cdot$	divergent operator
$\nabla\times$	curl operator
∇^2	Laplacian operator
$\langle\cdot\rangle$	ensemble average operator $(\langle\cdot\rangle = P_{av})$

Chapter I

INTRODUCTION

During the past few years, a Radio-Acoustic-Sounding-System (RASS) has been developed for real-time temperature profiling the first few kilometers of the lower troposphere [Marshall, 1972]. The basic physics of the RASS is as follows.

The electromagnetic refractive index of air (above 30 MHz) in the lower troposphere is not exactly unity but is a function of pressure, temperature, and humidity [Bean and Dutton, 1968]. Because of its pressure dependence, this refractive index can be altered by a short pulse of sound from an acoustic source. An electromagnetic RF signal generated by a radar passes through the sound pulse and is scattered as a result of the induced refractive-index variations. The scattered RF signal is collected by a receiver and is processed to determine atmospheric temperature as a function of the acoustic-pulse position (range). In a static atmosphere, the received signal is maximized when a Bragg condition is established between the acoustic and electromagnetic signals. This occurs if the electromagnetic wavelength is twice the acoustic wavelength and results in an in-phase addition at the receiver of the electromagnetic signal scattered from successive acoustic wavefronts in the pulse.

A doppler radar measures the speed of the sound pulse. Because the speed of sound in air depends on its temperature, the temperature profile of the lower atmosphere can be obtained with the RASS [Frankel and Peterson, 1976]. Fig. 1 illustrates the geometry of a bistatic RASS wherein the acoustic source is located between separated RF transmit and

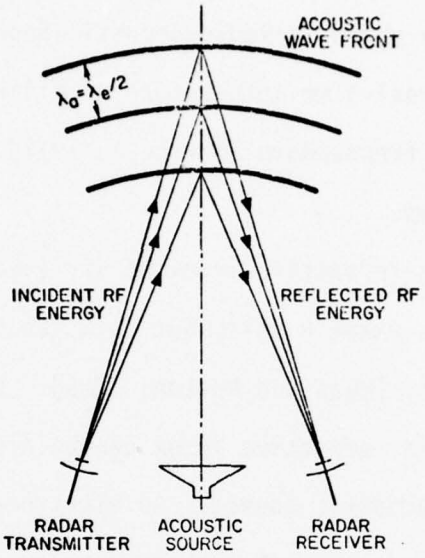

Fig. 1. REFLECTION OF ELECTROMAGNETIC ENERGY FROM AN ACOUSTIC PULSE FOR A RASS BISTATIC GEOMETRY.

receive antennas. In a monostatic RASS, the antennas and acoustic source are located at the same point.

In an early study at Stanford University , the reflection of electromagnetic energy from an acoustic pulse propagating vertically into the lower atmosphere was analyzed at a carrier frequency of 85 Hz [Marshall, 1972]. In that study Marshall assumed a static atmosphere (no turbulence and winds), and he made no attempt to determine the feasibility of operating the RASS at acoustic frequencies higher than 85 Hz which offers the advantage of a smaller system and an increase in the resolution of the measured atmospheric parameters.

In contrast to Marshall's analysis, this investigation considers the interaction of electromagnetic and acoustic waves when the RASS

is operated in a stochastic environment characterized by turbulence, winds, and mean-temperature gradients. These atmospheric parameters are important when evaluating RASS performance because they could affect the spatial coherency in and between the acoustic wavefronts of the transmitted acoustic pulse. This decrease in coherency would reduce the received signal levels.

An analysis of the effects of turbulence on the coherency of the acoustic wave shows that the acoustic wave amplitude at an altitude x is damped by a factor $\exp[-\langle|\psi_1(x,\bar{y}_\alpha)|^2\rangle/2]$ because of complex-phase intereference. In this damping factor, $\Psi_1(x,\bar{y}_\alpha)$ is the first-order perturbation in the complex phase of the acoustic wave due to turbulence. As shown herein , these complex-phase perturbations of the acoustic wave are small in the lower troposphere; consequently , for acoustic pulses with carrier frequencies below a few kilohertz propagating (under typical atmospheric conditions) to altitudes of a few kilometers, turbulence has little effect on the strength of the received radio signal. More particularly, it is shown in Chapter IV, that for an altitude x of the acoustic pulse much less than the coherence length of propagation x_c, the effect of turbulence on RASS performance is insignificant. This coherence length of propagation derived in this investigation is given by

$$x_c = \left[\frac{54.8\ (1.833 - m_a)}{C_{no}^2\ k_a^2\ A^{5/3}\ x_o^{m_a}}\right]^{6/(11-6\ m_a)} \tag{1.1}$$

In the above equation m_a is a factor determining the acoustic refractive-index structure parameter in the presence of inhomogeneous turbulence, C_{no}^2 is the refractive-index structure parameter at altitude x_o, k_a is the acoustic wave number, and A is a proportionality constant

measuring the outer scale of turbulence. It is observed that the coherence length varies inversely with frequency and the strength of the turbulence. As an example of the application of Eq. (1.1), consider a RASS operating at an acoustic frequency of f_a = 2 kHz and assuming the following typical values for the parameters in the equation ; $C_{no}^2 = 10^{-6}\ m^{-2/3}$, x_o = 1 m, A = 2 , m_a = 1.33, and the velocity of sound c_o = 340 m/sec, the coherence length is found to be $x_c = 4 \times 10^7$ m. This value of coherence length implies that the coherency of an acoustic wave is not affected by turbulence when f_a = 2 kHz and $x << 4 \times 10^7$ m.

Quiescent atmospheric conditions such as temperature gradients cause the dispersion of acoustic wavetrain. Under these circumstances, a match between electromagnetic and acoustic waves can be obtained by the use of a modified Bragg-scatter condition. This match depends on the temperature difference over the length of the acoustic wavetrain. This study shows, however, that typical temperature gradients in the lower atmosphere, which are on the order of - 6.5°K/km , have a negligible effect on the received power of a RASS. The effect of vertical winds on the strength of the received radio signal can be overcome similarly.

This investigation also shows that mean horizontal winds shift the focus of reflected electromagnetic energy from its origin, resulting in a decrease in received signal level when a monostatic RF system is used. Because the acoustic wavefronts act as large spherical reflectors, the principle of specular reflection , however, can be utilized in a bistatic radar geometry to remotely measure this wind component (in addition to atmospheric temperature profiles). In this RASS configuration, the radar antennas and acoustic sources are aligned in the wind direction -- the

transmit antenna upwind from the acoustic source and the receive antenna downwind. This technique offers the promise and potential of measuring horizontal wind velocities of magnitude up to a few tens of meters in the lower troposphere. Consistent with these theoretical predictions Frankel et al.,[1977] have utilized this principle of specular reflection to measure horizontal winds in the lower troposphere.

The analysis in this study was restricted to the lower troposphere ; however, it can be modified to study this diffraction phenomenon in any media. The mathematical and physical representations of the acoustic refractive-index field and atmospheric turbulence, following Tatarskii [1961, 1971] and Yaglom [1962], are presented in Chapter II. Acoustic-wave propagation in a turbulent medium is discussed in Chapter III, and Feynman's diagrammatic approach is used in Chapter IV to derive measures for the coherency of a vertically propagating acoustic wave. Results obtained in Chapter IV are applied in Chapter V to develop asymptotic expressions for the electromagnetic energy scattered from an acoustic wavetrain perturbed by atmospheric turbulence, mean temperature, and mean wind-fields. Chapter VI discusses the effect of the mean wind field on received doppler frequency. Chapter VII summarizes the conclusions of this research.

Chapter II

ACOUSTIC REFRACTIVE-INDEX FIELD

Acoustic and electromagnetic waves propagate in a stochastic medium; however, the naturally induced fluctuations in the acoustic refractive index are approximately one thousand times greater than those in the electromagnetic index [Little, 1969]. For this reason, natural fluctuations in the electromagnetic refractive index are ignored in this study.

The acoustic refractive index depends on wind, temperature, and humidity, and the stochastic variations in these parameters constitute the phenomenon known as "atmospheric turbulence." In this chapter, random fields are described; the mathematical analysis follows Tatarskii [1961, 1971] and Yaglom [1962]. This analysis is then extended to describe atmospheric turbulence and its effect on acoustic refractive-index fields in the lower troposphere.

A. Random Fields

Physical quantities such as atmospheric temperature, wind, density, and pressure are continuously distributed in space and time and, consequently, defy deterministic description. These can be described, however, in terms of random fields which are random space-time functions. In this section, random-field theory is described, with emphasis on meteorological applications.

1. Statistical Representation of Homogeneous Random Fields

Let $p(\bar{r})$ be a random field, where $\bar{r}$ is the space coordinate and let $\langle \cdot \rangle$ denote the mathematical expectation of a random function. The mean of the random field is $\langle p(\bar{r}) \rangle$, and its covariance is defined as

$$B_p(\bar{r},\bar{r}') = \left\langle \left[p(\bar{r}) - \left\langle p(\bar{r}) \right\rangle \right] \left[p^*(\bar{r}') - \left\langle p^*(\bar{r}') \right\rangle \right] \right\rangle \qquad (2.1)$$

(asterisks denote complex conjugates). A random field is "homogeneous" if its probability distribution function is invariant under a space translation; it is "homogeneous in the wide sense" if

$$\left\langle p(\bar{r}) \right\rangle = \text{constant} \qquad (2.2a)$$

and

$$B_p(\bar{r},\bar{r}') = B_p(\bar{r}-\bar{r}',0) \equiv B_p(\bar{r}-\bar{r}') \qquad (2.2b)$$

Henceforth, such fields will be referred to as "homogeneous random fields."

For an isotropic homogeneous random field, $B_p(\bar{r}) = B_p(r)$ where $|\bar{r}| \equiv r$ is the magnitude of the vector $\bar{r}$. When $\left\langle p(\bar{r}) \right\rangle = 0$, $p(\bar{r})$ has a Fourier-Stieltjes expansion,

$$p(\bar{r}) = \iiint_{-\infty}^{\infty} e^{i\bar{\kappa}\cdot\bar{r}} \, dW(\bar{\kappa}) \qquad (2.3a)$$

such that

$$\begin{aligned} \left\langle dW(\bar{\kappa}) \right\rangle &= 0 \\ \left\langle dW(\bar{\kappa}) dW^*(\bar{\kappa}') \right\rangle &= \delta(\bar{\kappa}-\bar{\kappa}') \Phi_p(\bar{\kappa}) d^3\bar{\kappa} \, d^3\bar{\kappa}' \end{aligned} \qquad (2.3b)$$

and $\Phi_p(\bar{\kappa}) \geq 0$ is the spectral density of the field where

$$B_p(\bar{r}) = \iiint_{-\infty}^{\infty} e^{i\bar{\kappa}\cdot\bar{r}} \, \Phi_p(\bar{\kappa}) d^3\bar{\kappa} \qquad (2.4)$$

When the medium is isotropic, $\Phi_p(\bar{\kappa}) = \Phi_p(\kappa)$.

The above equation describes globally homogeneous random fields; however, in the lower troposphere, meteorological variables are not statistically homogeneous. Homogeneity is violated by large-scale events and, therefore, it is necessary to consider locally homogeneous random fields.

2. Locally Homogeneous Random Fields and Structure Function

A random field is locally homogeneous if the probability distribution of $[p(\bar{r}) - p(\bar{r}')]$ is invariant under a joint space translation of the points $\bar{r}$ and $\bar{r}'$. Such fields are described by "structure functions" first introduced by Kolmogorov [1941]. This function, for a real-valued random field, is defined as

$$D_p(\bar{r},\bar{r}') = \left\langle \left| \left[p(\bar{r}) - \langle p(\bar{r}) \rangle \right] - \left[p(\bar{r}') - \langle p(\bar{r}') \rangle \right] \right|^2 \right\rangle \qquad (2.5a)$$

Physically, $D_p(\bar{r},\bar{r}')$ depends on the scale sizes of the inhomogeneities in the atmosphere, which are less than $|\bar{r} - \bar{r}'|$.

For a locally homogeneous random field,

$$D_p(\bar{r},\bar{r}') = D_p(\bar{r}-\bar{r}',0) \equiv D_p(\bar{r}-\bar{r}') \qquad (2.5b)$$

If the field is also locally isotropic, then $D_p(\bar{r}) = D_p(r)$.

The Fourier-Stieltjes expansion of a locally homogeneous random field is

$$p(\bar{r}) = p(0) + \bar{a}_p \cdot \bar{r} + \iiint_{-\infty}^{\infty} [e^{i\bar{\kappa}\cdot\bar{r}} - 1] \, dW(\bar{\kappa}) \qquad (2.6)$$

where $p(0)$ is a random variable and $\bar{a}_p$ is a random vector. If $\langle \bar{a}_p \rangle = 0$ and

$$p(\bar{r}) = p(0) + \iiint_{-\infty}^{\infty} [e^{i\bar{\kappa}\cdot\bar{r}} - 1]\, dW(\bar{\kappa}) \tag{2.7a}$$

such that

$$\langle dW(\bar{\kappa}) \rangle = 0 \tag{2.7b}$$

$$\langle dW(\bar{\kappa}) dW^{*}(\bar{\kappa}') \rangle = \delta(\bar{\kappa}-\bar{\kappa}')\Phi_p(\bar{\kappa})\, d^3\bar{\kappa}\, d^3\bar{\kappa}' \tag{2.7c}$$

$$\Phi_p(\bar{\kappa}) \geq 0 \tag{2.7d}$$

then

$$D_p(\bar{r}) = 2\iiint_{-\infty}^{\infty} [1 - \cos(\bar{\kappa}\cdot\bar{r})]\Phi_p(\bar{\kappa})\, d^3\bar{\kappa} \tag{2.8}$$

If this field is also isotropic, then $\Phi_p(\bar{\kappa}) = \Phi_p(\kappa)$. The covariance and structure function of a homogeneous and isotropic random field are related by

$$D_p(r) = 2[B_p(0) - B_p(r)] \tag{2.9a}$$

Because $B_p(\infty) = 0$ for a physical random field, $D_p(\infty) = 2B_p(0)$ and

$$B_p(r) = \frac{1}{2}[D_p(\infty) - D_p(r)] \tag{2.9b}$$

In this subsection, a three-dimensional spectral expansion of a locally homogeneous random field was made, and a two-dimensional spectral expansion is described below.

3. Two-Dimensional Fourier-Stieltjes Representation of Locally Homogeneous Random Fields

The two-dimensional Fourier-Stieltjes expansion of a random field $p(\bar{r})$ in the plane x = constant is

$$p(\bar{r}) = p(x,0,0) + \iint_{-\infty}^{\infty} \left[e^{i\bar{\kappa}_\alpha \cdot \bar{y}_\alpha} - 1 \right] ds_p(x,\bar{\kappa}_\alpha) \tag{2.10a}$$

where

$$\bar{\kappa}_\alpha = (\kappa_2,\kappa_3) \tag{2.10b}$$

$$\bar{y}_\alpha = (y,z) \tag{2.10c}$$

$p(x,0,0)$ is a random function and

$$\left\langle ds_p(x,\bar{\kappa}_\alpha) ds_p^*(x',\bar{\kappa}'_\alpha) \right\rangle = \delta(\bar{\kappa}_\alpha - \bar{\kappa}'_\alpha) F_p(x-x',\bar{\kappa}_\alpha)\, d^2\bar{\kappa}_\alpha\, d^2\bar{\kappa}'_\alpha \tag{2.10d}$$

$$F_p(x,\bar{\kappa}_\alpha) = F_p(-x,\bar{\kappa}_\alpha) \tag{2.10e}$$

As shown by Tatarskii [1971], the two-dimensional spectrum $F_p(x,\bar{\kappa}_\alpha)$ and the structure function are related by

$$D_p(\bar{r}-\bar{r}') - D_p(x-x',0,0) = 2\iint_{-\infty}^{\infty} [1 - \cos \bar{\kappa}_\alpha \cdot (\bar{y}_\alpha - \bar{y}'_\alpha)]\, F_p(x-x',\bar{\kappa}_\alpha) d^2\bar{\kappa}_\alpha \tag{2.10f}$$

When $\xi = x-x' = 0$, $y-y' = \eta$, and $z-z' = \zeta$, the above equation becomes

$$D_p(0,\eta,\zeta) = 2\iint_{-\infty}^{\infty} [1 - \cos(\kappa_2\eta + \kappa_3\zeta)]\, F_p(0,\kappa_2,\kappa_3)\, d\kappa_2\, d\kappa_3 \tag{2.10g}$$

The two- and three-dimensional spectral densities, defined in Eqs. (2.10a), (2.10d), (2.10e), and (2.4), respectively, are related by

$$F_p(\xi,\bar{\kappa}_\alpha) = \int_{-\infty}^{\infty} \Phi_p(\bar{\kappa})\cos(\kappa_1\ \xi)d\kappa_1 \qquad (2.11a)$$

and

$$\Phi_p(\bar{\kappa}) = \frac{1}{2\pi}\int_{-\infty}^{\infty} F_p(\xi,\bar{\kappa}_\alpha)\cos(\kappa_1\ \xi)d\xi \qquad (2.11b)$$

In addition,

$$D_p(\bar{r}) = 2\iint_{-\infty}^{\infty}[F_p(0,\bar{\kappa}_\alpha) - F_p(x,\bar{\kappa}_\alpha)\cos(\bar{\kappa}_\alpha\cdot\bar{y}_\alpha)]\ d^2\ \bar{\kappa}_\alpha \qquad (2.12)$$

and

$$B_p(\bar{r}) = \iint_{-\infty}^{\infty} F_p(x,\bar{\kappa}_\alpha)\cos(\bar{\kappa}_\alpha\cdot\bar{y}_\alpha)d^2\ \bar{\kappa}_\alpha \qquad (2.13)$$

The two-dimensional Fourier-Stieltjes representation of locally homogeneous random fields will be used in Chapters III and IV to describe the coherency of a propagating acoustic wave.

In the spectral expansion of random fields, it has been assumed that the medium has constant mean characteristics. In the lower troposphere, however, the intensity of fluctuations is smoothly varying, and the above descriptions of random fields must be modified.

4. Medium with Smoothly Varying Mean Characteristics

Following Tatarskii [1971], if the random field $p(\bar{r})$ is smoothly varying, then

$$D_p(\bar{r},\bar{r}') = C_p^2\left(\frac{\bar{r}+\bar{r}'}{2}\right) D_p^{(o)}(\bar{r}-\bar{r}') \qquad (2.14)$$

The function $D_p^{(o)}(\bar{r}-\bar{r}')$ represents the local variation of fluctuation intensity and is defined for arguments with magnitudes much smaller than the largest scale size events. The function $C_p^2((\bar{r}+\bar{r}')/2)$ represents the smooth variations and is approximately constant when $|\bar{r}-\bar{r}'|$ is much smaller than the largest scale size event. Tatarskii demonstrated that

$$C_p^2\left(\frac{\bar{r}+\bar{r}'}{2}\right)\Phi_p^{(o)}(\bar{\kappa}) = \Phi_p\left(\frac{\bar{r}+\bar{r}'}{2},\bar{\kappa}\right) \tag{2.15}$$

and that

$$C_p^2\left(\frac{\bar{r}+\bar{r}'}{2}\right)F_p^{(o)}(x-x',\bar{\kappa}_\alpha) = F_p\left(\frac{\bar{r}+\bar{r}'}{2},x-x',\bar{\kappa}_\alpha\right) \tag{2.16}$$

These equations will be used to describe a spherical wave traveling vertically into the lower atmosphere which is locally homogeneous and has smoothly varying mean characteristics.

B. Atmospheric Turbulence

The physical phenomenon associated with the deviations of energy transportation processes in the atmosphere from its deterministic description is called "atmospheric turbulence." The medium-describing variables are random functions of four coordinates, space and time. In this section, the effects of turbulence on the acoustic refractive index are considered. Let the acoustic refractive-index $n(\bar{r})$ be defined as

$$n(\bar{r}) = \langle n(\bar{r})\rangle + n_1(\bar{r}) \tag{2.17}$$

where $\langle n(\bar{r})\rangle \simeq 1$ and $\langle n_1(\bar{r})\rangle = 0$. In addition, $n_1(\bar{r})$ is the fluctuating component of $n(\bar{r})$ and is usually much smaller than unity.

The random medium, the lower part of the troposphere, generally is not statistically homogeneous; however, the fluctuating acoustic refractive-index field is locally homogeneous. As discussed in subsection A.2, such fields can be described in terms of the structure function of $n(\bar{r})$, defined as

$$D_n(\bar{r},\bar{r}') = \left\langle \{n_1(\bar{r}) - n_1(\bar{r}')\}^2 \right\rangle \qquad |\bar{r}-\bar{r}'| \lesssim L_o \tag{2.18}$$

In this equation, $\langle n(\bar{r}) \rangle$ is approximately constant for $|\bar{r}-\bar{r}'| \lesssim L_o$, where L_o is called the "outer scale of turbulence" and is the least distance between coordinates $\bar{r}$ and $\bar{r}'$ for which $B_n(\bar{r},\bar{r}') \approx 0$. For points separated spatially by distances greater than L_o, the covariance function is zero.

The structure function for locally homogeneous isotropic turbulence was first obtained by Kolmogorov [1941]; according to his theory,

$$D_n(r) = \begin{cases} C_n^2 \, \ell_o^{2/3} \left(\dfrac{r}{\ell_o}\right)^2 & r \ll \ell_o \\ \\ C_n^2 \, r^{2/3} & \ell_o \ll r \ll L_o \end{cases} \tag{2.19}$$

where C_n^2 is the "structure parameter" and is a measure of the intensity of fluctuations. The quantity ℓ_o is called the "inner-scale of turbulence," and the interval between ℓ_o and L_o is the inertial subrange. Energy is injected through some outside mechanism into L_o. According to Kolmogorov's cascade theory of turbulence, this energy is then successively transferred to smaller scales of turbulence until it reaches the size of ℓ_o where the viscous forces dominate and energy

is converted into heat. The scales of turbulence between ℓ_o and L_o are also often referred to as "eddies" [Tatarskii, 1971]. Generally, ℓ_o and L_o are functions of the vertical distance x above the ground. According to Lawrence and Strohbehn [1970], L_o is on the order of one to hundreds of meters, depending on the altitude; Gray and Waterman [1970] show ℓ_o to be on the order of a few millimeters. A model for the outer scale of turbulence as a function of altitude x is

$$L_o(x) = Ax^{1/2} \tag{2.20a}$$

where A varies from 1 to 10, with a typical value of 2 [Taylor, 1968]. Because only limited measurements exist for the inner scale of turbulence [Lawrence and Strohbehn, 1970] and for mathematical simplicity, the functional dependence of the inner scale as a function of altitude is modeled as the outer scale. Therefore,

$$\ell_o(x) = Bx^{1/2} \tag{2.20b}$$

where $A/B = 10^3$ to 10^5. For example, at $x = 1000$ m and $B = 10^{-4}$, the size of the inner scale of turbulence is $\ell_o \simeq 3$ mm.

In the lower troposphere, the refractive-index field is locally homogeneous and has smoothly varying mean characteristics in the vertical direction x [Brown and Keeler, 1975]. The refractive-index structure parameter C_n^2, as defined in Eq. (2.19), is a function of altitude x. Consequently,

$$C_n^2(x) = C_{no}^2\left(\frac{x}{x_o}\right)^{-m_a} \qquad 1.33 \geq m_a > 0 \tag{2.20c}$$

where $C_{no}^2 = C_n^2(x_o)$. As x increases, $C_n^2(x)$ decreases and has a maximum value near the ground. According to Brown and Keeler [1975], m_a is approximately equal to 1.33, and C_{no}^2 ranges from 10^{-6} to $10^{-8} m^{-2/3}$ at $x_o = 1m$.

C. Refractive-Index Spectrum in the Lower Troposphere

For isotropic homogeneous turbulence in the inertial subrange, Kolmogorov's two-third structure function law results in the spectrum,

$$\Phi_n(\kappa) = 0.033 C_n^2 \kappa^{-11/3} \qquad \frac{2\pi}{L_o} << \kappa << \frac{2\pi}{\ell_o} \tag{2.21a}$$

For wave numbers $\kappa >> 2\pi/\ell_o$, $\Phi_n(\kappa)$ is small and the corresponding range of the structure function given in Eq. (2.19) for $r << \ell_o$. Tatarskii [1971] used the following form for the spectrum.

$$\Phi_n(\kappa) = 0.033 C_n^2 \kappa^{-11/3} e^{-\kappa^2/\kappa_m^2} \qquad \frac{2\pi}{L_o} < \kappa \tag{2.21b}$$

where $\kappa_m = 5.92/\ell_o \simeq 2\pi/\ell_o$.

A disadvantage of the above representation for $\Phi_n(\kappa)$ is that it has a singularity at $\kappa = 0$. As a result Tatarskii's spectrum does not possess an autocovariance function. An alternative representation of the spectrum, as suggested by Strohbehn [1968] and Lutomirski and Yura [1971], is

$$\Phi_n(\kappa) = \frac{0.033 C_n^2 e^{-(\kappa \ell_o)^2}}{(\kappa^2 + L_o^{-2})^{11/6}} \tag{2.22}$$

where $\ell_o = 2\pi \ell_o$ and $L_o = 2\pi L_o$. This spectrum is flat for $\kappa \lesssim L_o^{-1}$.

In the lower troposphere, the turbulent medium generally has a smoothly varying mean characteristic; therefore, substituting Eqs. (2.20a), (2.20b) and (2.20c) into Eq. (2.22) yields

$$\Phi_n(x,\kappa) = \frac{0.033C_n^2(x)\, e^{-[\kappa \ell_o(x)]^2}}{[\kappa^2 + \ell_o^{-2}(x)]^{11/6}} \tag{2.23}$$

in the plane, x = constant. This spectral expansion of the acoustic refractive-index field will be used in subsequent chapters to describe acoustic-wave propagation in a turbulent atmosphere.

Chapter III

ACOUSTIC-WAVE PROPAGATION IN THE LOWER ATMOSPHERE

In this chapter, the basic equations for acoustic-wave propagation are derived. The theory developed by Tatarskii [1961, 1971] is valid for acoustic wavelengths λ_a much smaller than the inner scale of turbulence ℓ_o. By considering dissipation, however, log-amplitude, phase, and log-amplitude-phase spectra of the scattered acoustic wave can be obtained over the range of acoustic wavelengths pertinent to this study. It is shown that Tatarskii's results for optical propagation are good approximations for acoustic waves. These results are discussed in Section A.

The equations governing acoustic-wave propagation are determined in Section B. Assuming that variation of the acoustic refractive-index is much smaller than unity, which is justifiable under typical atmospheric conditions, the acoustic-wave equation and the Rytov technique developed in Section B are applied in Chapter IV to describe the coherency of a spherical acoustic wave propagating vertically into the lower atmosphere.

A. Sound Propagation in a Dissipative Atmosphere

A first-order perturbation solution of the pressure equation derived by Clifford and Brown [1970] forms the basis for computing the log-amplitude, phase, and log-amplitude phase spectra of the scattered acoustic wave. The atmosphere is considered to be dissipative, and tensor notation is used. The ground is the reference level for deviations in other physical parameters such as temperature. A static atmosphere is defined as one in which ground-level parameters exist throughout the atmosphere.

1. Fluid Dynamics

In the absence of sound, the atmospheric fluid velocity is $w_i = \langle w_i \rangle + w_i'$, $(i = 1, 2, 3)$ in the half space $x \geq 0$; the constant mean-wind velocity is $\langle w_i \rangle$ and w_i' is the fluctuating component having zero mean. The acoustic pulse is assumed to be beamed in the positive x-direction from the origin and, in its presence, fluid motion is $V_i = w_i + u_i$ where u_i is the velocity caused by sound waves. Mass flow is expressed by ρV_i, where ρ is the fluid density and ρ_o is the static fluid density. The following notation is used: $\partial_i = \partial/\partial x_i$, $\partial_t = \partial/\partial t$, and $d_t = d/dt$ where $d_t = \partial_t + V_i \partial_i$. The total pressure in the fluid is $P = p_o + p_a$; here p_o is the constant static pressure and p_a is the acoustic pressure. In practice $|p_a/p_o| << 1$ and $\rho = \rho_o(1 + \xi)$ where $|\xi| << 1$. The shear strain e_{ij}, fluid stress P_{ij}, and total momentum flux tensor t_{ij} are defined as

$$e_{ij} = \frac{1}{2} (\partial_i V_j + \partial_j V_i) \tag{3.1a}$$

$$P_{ij} = (P - \lambda_v \partial_k V_k)\delta_{ij} - 2\mu_v e_{ij} \tag{3.1b}$$

$$t_{ij} = P_{ij} + \rho V_i V_j \tag{3.1c}$$

In these equations, $\delta_{ij} = 1$ for $i = j$ and $\delta_{ij} = 0$ for $i \neq j$, and λ_v and μ_v are the volume and shear viscosities, respectively.

For an ideal gas H_e, the entropy, is

$$H_e = c_v \ln P - c_p \ln \rho \tag{3.1d}$$

The specific heats of air at constant volume and pressure are c_v and c_p

respectively, and the Laplace constant γ is equal to c_p/c_v. The magnitude of the fluid velocity c can be determined from $c^2 = \gamma^2 P/\rho = \gamma R_{gc} T$, where R_{gc} is the gas constant and T is temperature. If c_o and T_o are the reference fluid-velocity magnitude and temperature, respectively, then $c^2 = c_o^2(1+\tau)$; here τ is the fractional variation of temperature from the reference. In addition $\tau = \langle\tau\rangle + \tau'$, $\langle\tau'\rangle = 0$, and τ' contributes to the turbulence fluctuations. Assuming that the external source terms are zero, the basic equations of fluid motion, conservation of mass, momentum, and adiabatic propagation of sound are

$$\partial_t \rho + \partial_i(\rho V_i) = 0 \tag{3.2a}$$

$$\partial_t(\rho V_i) + \partial_j t_{ij} = 0 \tag{3.2b}$$

$$d_t H_e = 0 \tag{3.2c}$$

Defining $\nu_f = \mu_v/\rho_o$, $\eta_f = 2\nu_f + \lambda_v/\rho_o$ and $\pi_a = p_a/(\gamma p_o)$, then, for slowly varying turbulence, $\pi_a(x_i,t) = e^{-i\omega_a t}\Pi(x_i)$; here ω_a is the acoustic angular frequency. Combining the above equations and linearizing, results in the following equation for the acoustic pressure field

$$\nabla^2\Pi + h^2\Pi = -\frac{h^2}{k_a^2}\partial_i(\tau\partial_i\Pi) + \frac{2ih^2}{c_o k_a^3}\partial_i\partial_j(w_i\partial_j\Pi) \tag{3.3}$$

In this equation, $\nabla^2 = \partial_i^2$ is the Laplacian operator, $k_a = \omega_a/c_o$, $h = k_a + id$, and $d = k_a^2\,\eta_f/(2c_o)$.

2. First-Order Perturbation Solution of the Pressure Equation

Letting $\Pi = \Pi_o + \Pi_1$, then

$$\nabla^2\Pi_o + h^2\Pi_o = 0; \qquad \Pi_o = A_o e^{ihx} \tag{3.4a}$$

and

$$\nabla^2\Pi_1 + h^2\Pi_1 = 2i \frac{h^3}{k_a^2} \partial_x(n_1\Pi_o) \tag{3.4b}$$

where the fluctuation in the acoustic refractive index n_1 is

$$n_1 = -\left[\frac{\tau}{2} + \frac{w_x}{c_o}\right]; \qquad \langle n_1 \rangle = 0 \tag{3.4c}$$

Assuming this field to be locally homogeneous n_1 and Π_1 are expanded in their Fourier-Stieltjes measure as

$$\Pi_1(x,\bar{y}_\alpha) = \Pi_1(x,0,0) + \iint_{-\infty}^{\infty}\left[e^{i\bar{\kappa}_\alpha\cdot\bar{y}_\alpha} - 1\right] d\rho(x,\bar{\kappa}_\alpha) \tag{3.5a}$$

and

$$n_1(x,\bar{y}_\alpha) = n_1(x,0,0) + \iint_{-\infty}^{\infty}\left[e^{i\bar{\kappa}_\alpha\cdot\bar{y}_\alpha} - 1\right] d\nu(x,\bar{\kappa}_\alpha) \tag{3.5b}$$

where $n_1(x,\bar{y}_\alpha)$ real implies

$$d\nu(x,\bar{\kappa}_\alpha) = d\nu^*(x,-\bar{\kappa}_\alpha) \tag{3.5c}$$

$$d\nu(x,-\bar{\kappa}_\alpha) = d\nu^*(x,\bar{\kappa}_\alpha) \tag{3.5d}$$

Because $|\Pi_1| << |\Pi_0|$, $\ln(\Pi/\Pi_0) \simeq \Pi_1/\Pi_0$. If $\ln(\Pi/\Pi_0) = \chi + iS_1$, where χ and S_1 are the perturbations in the log-amplitude ratio and phase of the scattered wave, the Fourier Stieltjes measure $d\phi(x,\bar{\kappa}_\alpha)$ of the complex-phase $\chi + iS_1$ is related to that of $\Pi_1(x,\bar{y}_\alpha)$ by

$$d\phi(x,\bar{\kappa}_\alpha) = \frac{d\rho(x,\bar{\kappa}_\alpha)}{\Pi_0(x,\bar{y}_\alpha)} \tag{3.6}$$

Let $q = (h^2 - \kappa_\alpha^2)^{1/2}$, then

$$q = (a+ib)Y(k_a^2-\kappa_\alpha^2) + (b+ia)Y(\kappa_\alpha^2-k_a^2) \tag{3.7a}$$

where $Y(\cdot)$ is the Heaviside step function defined by

$$Y(x) = \begin{cases} 0 & x < 0 \\ 1/2 & x = 0 \\ 1 & x > 0 \end{cases} \tag{3.7b}$$

and

$$a(\kappa_\alpha) = \frac{1}{2}\left(|q|^2 + 2k_a d\right)^{1/2} + \frac{1}{2}\left(|q|^2 - 2k_a d\right)^{1/2} \tag{3.7c}$$

$$b(\kappa_\alpha) = \frac{1}{2}\left(|q|^2 + 2k_a d\right)^{1/2} - \frac{1}{2}\left(|q|^2 - 2k_a d\right)^{1/2} \tag{3.7d}$$

Writing

$$Y_+ = Y(\kappa_\alpha^2 - k_a^2) \tag{3.8a}$$

and

$$Y_- = Y(k_a^2 - \kappa_\alpha^2) \tag{3.8b}$$

yields

$$q = (a+ib)Y_- + (b+ia)Y_+ \tag{3.8c}$$

Using the forward-scatter approximation,

$$d\phi(x,\bar{\kappa}_\alpha) = ik_a \int_0^x d\nu(x',\bar{\kappa}_\alpha)\, e^{(ig_1+g_2)(x'-x)}\, dx' \qquad (3.9)$$

Here, $g_1 = (k_a - bY_+ - aY_-)$ and $g_2 = (-d + bY_- + aY_+)$. Note that a, b, g_1, and g_2 are functions of κ_α^2.

3. Log-Amplitude, Phase, and Log-Amplitude-Phase Spectra

Assuming that turbulence is homogeneous, the Fourier-Stieltjes measure of the log-amplitude ratio and phase of the scattered acoustic wave $d\alpha(x,\bar{\kappa}_\alpha)$ and $d\sigma(x,\bar{\kappa}_\alpha)$ are [Tatarskii, 1961]

$$d\phi(x,\bar{\kappa}_\alpha) = d\alpha(x,\bar{\kappa}_\alpha) + id\sigma(x,\bar{\kappa}_\alpha) \qquad (3.10a)$$

$$d\alpha(x,\bar{\kappa}_\alpha) = \frac{[d\phi(x,\bar{\kappa}_\alpha) + d\phi^*(x,-\bar{\kappa}_\alpha)]}{2} \qquad (3.10b)$$

$$d\sigma(x,\bar{\kappa}_\alpha) = \frac{[d\phi(x,\bar{\kappa}_\alpha) - d\phi^*(x,-\bar{\kappa}_\alpha)]}{2i} \qquad (3.10c)$$

The log-amplitude, phase, and log-amplitude-phase spectra of the acoustic wave can be obtained by computing certain auxiliary spectra. From Chapter II.A.3, the two-dimensional refractive-index spectrum $F_n(x'-x'',\bar{\kappa}_\alpha)$ is

$$\left\langle d\nu(x',\bar{\kappa}_\alpha) d\nu^*(x'',\bar{\kappa}'_\alpha) \right\rangle = \delta(\bar{\kappa}_\alpha - \bar{\kappa}'_\alpha) F_n(x'-x'',\bar{\kappa}_\alpha) d^2\bar{\kappa}_\alpha d^2\bar{\kappa}'_\alpha \qquad (3.11a)$$

and

$$\left\langle d\phi(x,\bar{\kappa}_\alpha) d\phi^*(x,\bar{\kappa}'_\alpha) \right\rangle = \delta(\bar{\kappa}_\alpha - \bar{\kappa}'_\alpha) F_1(x,0,\bar{\kappa}_\alpha) d^2\bar{\kappa}_\alpha d^2\bar{\kappa}'_\alpha \qquad (3.11b)$$

$$\left\langle d\phi(x,\bar{\kappa}_\alpha) d\phi(x,\bar{\kappa}'_\alpha) \right\rangle = \delta(\bar{\kappa}_\alpha + \bar{\kappa}'_\alpha) F_2(x,0,\bar{\kappa}_\alpha) d^2\bar{\kappa}_\alpha d^2\bar{\kappa}'_\alpha \qquad (3.11c)$$

where, from Eq. (3.9),

$$F_1(x,0,\bar{\kappa}_\alpha) = k_a^2 \int_0^x \int_0^x F_n(x'-x'',\bar{\kappa}_\alpha)\, e^{[ig_1(x'-x'') + g_2(x'+x''-2x)]}\, dx'dx'' \tag{3.12a}$$

$$F_2(x,0,\bar{\kappa}_\alpha) = -k_a^2 \int_0^x \int_0^x F_n(x'-x'',\bar{\kappa}_\alpha)\, e^{(ig_1+g_2)(x'+x''-2x)}\, dx'dx'' \tag{3.12b}$$

The above equations can be evaluated by noting that $F_n(\xi,\bar{\kappa}_\alpha)$ is even in ξ and, by using the substitution $x'-x'' = \xi$, $(x'+x'')/2 = \eta$,

$$F_1(x,0,\bar{\kappa}_\alpha) = \frac{k_a^2}{g_2} \int_0^x F_n(\xi,\bar{\kappa}_\alpha)\, e^{-g_2\xi} \cos(g_1\xi)\, d\xi$$

$$- \frac{k_a^2}{g_2} e^{-2g_2x} \int_0^x F_n(\xi,\bar{\kappa}_\alpha)\, e^{g_2\xi} \cos(g_1\xi)\, d\xi \tag{3.13a}$$

and

$$F_2(x,0,\bar{\kappa}_\alpha) = \frac{-k_a^2}{(ig_1+g_2)} \int_0^x F_n(\xi,\bar{\kappa}_\alpha)\, e^{-(ig_1+g_2)\xi}\, d\xi$$

$$+ \frac{k_a^2}{(ig_1+g_2)} e^{-2(ig_1+g_2)x} \int_0^x F_n(\xi,\bar{\kappa}_\alpha)\, e^{(ig_1+g_2)\xi}\, d\xi \tag{3.13b}$$

Because the major contribution in these expressions arise from $\xi \leq L_o$, the contribution of real terms in the exponent factor of the integrands is negligible, and

$$\int_0^x F_n(\xi,\bar{\kappa}_\alpha)e^{ig_1\xi}d\xi = \int_0^x F_n(\xi,\bar{\kappa}_\alpha)\cos(g_1\xi)d\xi \qquad (3.14a)$$

Furthermore, significant contribution to $F_1(x,0,\bar{\kappa}_\alpha)$ and $F_2(x,0,\bar{\kappa}_\alpha)$ results from $\xi \leq L_o << x$, hence the upper limits in the integrals in Eqs. (3.13a) and (3.13b) can be replaced by infinity. As shown in Chapter II.A.3, the three-dimensional refractive-index spectrum, $\Phi_n(\kappa)$, is

$$2\pi\Phi_n\left(\sqrt{\kappa_\alpha^2+\kappa_x^2}\right) = \int_{-\infty}^{\infty} F_n(\xi,\bar{\kappa}_\alpha)e^{i\kappa_x\xi}\,d\xi \qquad (3.14b)$$

therefore

$$F_1(x,0,\bar{\kappa}_\alpha) = \frac{\pi k_a^2}{g_2}\,\Phi_n\left(\sqrt{\kappa_\alpha^2+g_1^2}\right)\left[1 - e^{-2g_2x}\right] \qquad (3.15a)$$

$$F_2(x,0,\bar{\kappa}_\alpha) = \frac{\pi k_a^2}{(ig_1+g_2)}\,\Phi_n\left(\sqrt{\kappa_\alpha^2+g_1^2}\right)\left[-1 + e^{-2(ig_1+g_2)x}\right] \qquad (3.15b)$$

Because $F_1(x,0,\bar{\kappa}_\alpha)$ is real and a function of κ_α^2 and $F_2(x,0,\bar{\kappa}_\alpha)$ is complex and a function of κ_α^2,

$$\left\langle d\alpha(x,\bar{\kappa}_\alpha)d\alpha^*(x,\bar{\kappa}'_\alpha)\right\rangle = \delta(\bar{\kappa}_\alpha-\bar{\kappa}'_\alpha)F_\chi(x,0,\bar{\kappa}_\alpha)\,d^2\bar{\kappa}_\alpha\,d^2\bar{\kappa}'_\alpha \qquad (3.16a)$$

$$\left\langle d\sigma(x,\bar{\kappa}_\alpha)d\sigma^*(x,\bar{\kappa}'_\alpha)\right\rangle = \delta(\bar{\kappa}_\alpha-\bar{\kappa}'_\alpha)F_s(x,0,\bar{\kappa}_\alpha)\,d^2\bar{\kappa}_\alpha\,d^2\bar{\kappa}'_\alpha \qquad (3.16b)$$

$$\left\langle d\alpha(x,\bar{\kappa}_\alpha)\,d\sigma(x,\bar{\kappa}'_\alpha)\right\rangle = \delta(\bar{\kappa}_\alpha+\bar{\kappa}'_\alpha)F_{\chi s}(x,0,\bar{\kappa}_\alpha)\,d^2\bar{\kappa}_\alpha\,d^2\bar{\kappa}'_\alpha \qquad (3.16c)$$

where

$$F_\chi = \frac{[F_1 + \mathrm{Re}(F_2)]}{2} \qquad (3.17a)$$

$$F_s \simeq \frac{[F_1 - \mathrm{Re}(F_2)]}{2} \tag{3.17b}$$

$$F_{\chi s} = \frac{\mathrm{Im}(F_2)}{2} \tag{3.17c}$$

$\mathrm{Re}(F_2)$ and $\mathrm{Im}(F_2)$ denote the real and imaginary part of the complex number F_2. Here $F_\chi(x,0,\bar{\kappa}_\alpha)$, $F_s(x,0,\bar{\kappa}_\alpha)$, and $F_{\chi s}(x,0,\bar{\kappa}_\alpha)$ are the log-amplitude, phase, and log-amplitude phase spectra of the scattered acoustic wave, respectively, and F_χ, F_s, and $F_{\chi s}$ can be calculated from Eqs. (3.15) and (3.17). Limiting forms of F_χ, F_s and $F_{\chi s}$ are examined in the following cases.

Case 1: $\kappa_\alpha << k_a$.

In this case, $Y_+ = 0$, $Y_- = 1$, $h \simeq k_a$, $a = |q|$, $k_a - a \simeq \kappa_\alpha^2/(2k_a)$, $b \simeq d$, $g_1 = \kappa_\alpha^2/(2k_a)$, and $g_2 \simeq 0$. As a result,

$$F_1 = 2\pi k_a^2 x \Phi_n(\kappa_\alpha) \tag{3.18a}$$

$$F_2 = 2\pi k_a^2 \frac{\left[e^{-i\kappa_\alpha^2 x/k_a} - 1\right]}{(i\kappa_\alpha^2/k_a)} \Phi_n(\kappa_\alpha) \tag{3.18b}$$

and

$$F_\chi = \pi k_a^2 x \left[1 - \frac{\sin(\kappa_\alpha^2 x/k_a)}{(\kappa_\alpha^2 x/k_a)}\right] \Phi_n(\kappa_\alpha) \tag{3.19a}$$

$$F_s = \pi k_a^2 x \left[1 + \frac{\sin(\kappa_\alpha^2 x/k_a)}{(\kappa_\alpha^2 x/k_a)}\right] \Phi_n(\kappa_\alpha) \tag{3.19b}$$

$$F_{\chi s} = \pi k_a^2 x \left(\frac{k_a}{\kappa_\alpha^2 x}\right)\left[1 - \cos(\kappa_\alpha^2 x/k_a)\right] \Phi_n(\kappa_\alpha) \qquad (3.19c)$$

The above expressions are identical to those derived by Tatarskii [1971] but were obtained via a different approach.

Case 2: $\kappa_\alpha = k_a$.

In this case, $Y_+ + Y_- = 1$, $|q| = (2k_a d)^{1/2}$, $a = b = (k_a d)^{1/2}$, $g_1 \simeq k_a$, and $g_2 = (k_a d)^{1/2}$; therefore,

$$F_1 = 2\pi k_a^2 \, e^{-(k_a d)^{1/2} x} \left(\frac{\sinh[(k_a d)^{1/2} x]}{(k_a d)^{1/2}}\right) \Phi_n(\sqrt{2}\,\kappa_\alpha) \qquad (3.20a)$$

$$F_2 = (\pi k_a^2) \frac{\left[e^{-(ik_a + (k_a d)^{1/2})2x} - 1\right]}{ik_a} \Phi_n(\sqrt{2}\,\kappa_\alpha) \qquad (3.20b)$$

and

$$F_\chi = \pi k_a^2 \, e^{-(k_a d)^{1/2} x} \, \Phi_n(\sqrt{2}\,\kappa_\alpha) \left[\frac{\sinh((k_a d)^{1/2} x)}{(k_a d)^{1/2}} - e^{-(k_a d)^{1/2} x}\left(\frac{\sin(2k_a x)}{2k_a}\right)\right] \qquad (3.21a)$$

$$F_s = \pi k_a^2 \, e^{-(k_a d)^{1/2} x} \, \Phi_n(\sqrt{2}\,\kappa_\alpha) \left[\frac{\sinh((k_a d)^{1/2} x)}{(k_a d)^{1/2}} + e^{-(k_a d)^{1/2} x}\left(\frac{\sin(2k_a x)}{2k_a}\right)\right] \qquad (3.21b)$$

$$F_{\chi s} = \frac{\pi k_a}{2}\left[1 - e^{-(k_a d)^{1/2} 2x} \cos(k_a 2x)\right] \Phi_n(\sqrt{2}\,\kappa_\alpha) \qquad (3.21c)$$

Case 3: $\kappa_\alpha >> k_a$.

In this case $Y_+ = 1$, $Y_- = 0$, $h = k_a$, $a \simeq |q|$, $g_1 \simeq k_a$, and $g_2 \simeq a - d \simeq \kappa_\alpha$. Consequently,

$$F_1 = \frac{\pi k_a^2}{\kappa_\alpha} \Phi_n(\kappa_\alpha) \tag{3.22a}$$

$$F_2 = -\frac{\pi k_a^2}{\kappa_\alpha} \Phi_n(\kappa_\alpha) \tag{3.22b}$$

and

$$F_\chi = 0 \tag{3.23a}$$

$$F_s = \frac{\pi k_a^2}{\kappa_\alpha} \Phi_n(\kappa_\alpha) \tag{2.32b}$$

$$F_{\chi s} = 0 \tag{3.23c}$$

Normalized F_χ, F_s, and $F_{\chi s}$, that is, $f_\chi = F_\chi/(\pi k_a^2 x \Phi_n(\kappa_\alpha))$, $f_s = F_s/(\pi k_a^2 x \Phi_n(\kappa_\alpha))$, and $f_{\chi s} = F_{\chi s}/(\pi k_a^2 x \Phi_n(\kappa_\alpha))$ are plotted vs normalized wave number $\kappa_\alpha/(k_a/x)^{1/2}$ in Fig. 2, which shows the behavior of these normalized spectral functions. It can be observed that these functions are oscillatory at low wave numbers and that for large wave numbers, f_χ and f_s are equal but $f_{\chi s}$ decreases rapidly. The function $f_{\chi s}$ is negligibly affected by damping over the entire range of wave numbers; however, the shape of the f_χ and f_s spectra is altered slightly.

These log-amplitude, phase, and log-amplitude-phase spectra are largely dependent on wave numbers $\kappa_\alpha << k_a$ that correspond to

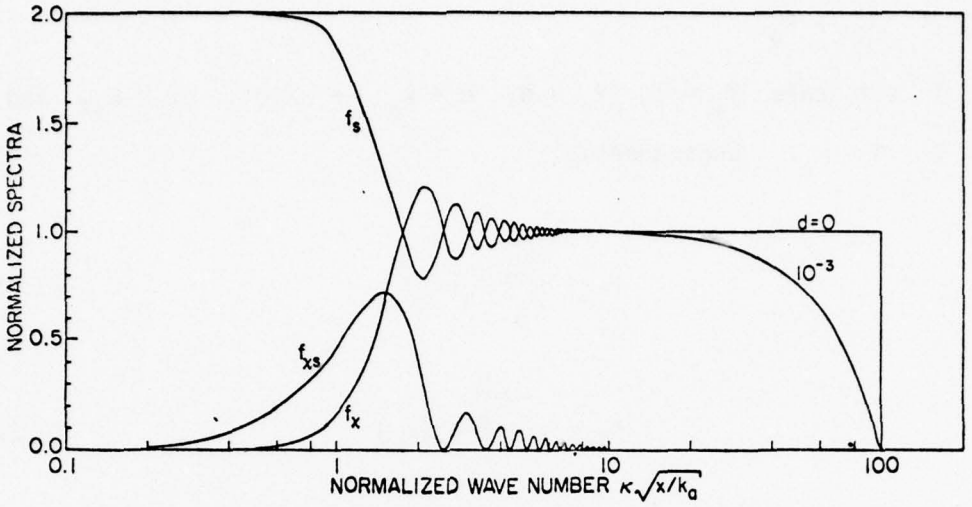

Fig. 2. NORMALIZED SPECTRAL FUNCTIONS VS NORMALIZED WAVE NUMBER. $k_a = 10\ m^{-1}$ and $x = 1000$ m.

turbulent eddies which determine the spectrum of the refractive-index fluctuations. Eddies with $\kappa_\alpha \geq k_a$ produce evanescent waves. It can be concluded that, because $\Phi_n(\kappa_\alpha) \propto \kappa_\alpha^{-11/3}$, these spectra are determined by refractive-index fluctuations rather than by absorption in the medium. As a result Tatarskii's results derived for $\lambda_a << \ell_o$ are good approximations for $L_o > \lambda_a > \ell_o$.

In this section plane-wave propagation was assumed; however, the conclusion that 'the formulas derived on the assumption that $\lambda_a << \ell_o$ are good approximations for $\lambda_a > \ell_o$' are unaffected, whether the type of propagation is plane, spherical, or beam.

B. Acoustic-Wave Propagation

In this section, the equations governing acoustic-wave propagation are developed.

1. Acoustic Time-Harmonic Wave Equation

Let the acoustic pressure impressed on the medium resulting from an external source be $p_a(\bar{r},t) = u_a(\bar{r})e^{-i\omega_a t}$. Because p_a is directly proportional to π_a which, in turn, is directly proportional to Π, an equation for $u_a(\bar{r})$ can be written similar to Eq. (3.3). In the lower atmosphere, $d \ll k_a$ and, as a result, the effect of dissipation is neglected in this analysis. In practice, $|\tau| \ll 1$ and $|\bar{w}|/c_o \ll 1$, where $|\bar{w}|$ is the magnitude of atmospheric fluid velocity. After preserving the terms linear in τ and w_i/c_o, it can be demonstrated that [Tatarskii, 1971]

$$\nabla^2 u_a(\bar{r}) + k_a^2 n^2(\bar{r}) u_a(\bar{r}) = 0 \qquad x > 0 \tag{3.24}$$

where

$$n^2(\bar{r}) = \left\langle n^2(\bar{r}) \right\rangle + 2n_1(\bar{r})\delta \tag{3.25a}$$

$$\left\langle n^2(\bar{r}) \right\rangle = 1 - \left\langle \tau \right\rangle - 2\frac{\left\langle w_i \ell_i \right\rangle}{c_o} \tag{3.25b}$$

$$n_1(\bar{r}) = -\frac{\tau'}{2} - \frac{1}{c_o}\left(w_i \ell_i - \left\langle w_i \ell_i \right\rangle \right) \tag{3.25c}$$

$$\left\langle n_1(\bar{r}) \right\rangle = 0 \tag{3.25d}$$

ℓ_i = unit vector tangent to the ray

The dummy parameter δ measures the smallness of $n_1(\bar{r})$, which is the variation of the acoustic refractive-index from its average value; generally, $\left\langle n(\bar{r}) \right\rangle$ is approximately unity and $|n_1(\bar{r})| \ll 1$. The above time-harmonic scalar wave equation describes the acoustic-

wave propagation in the half space $V_s = \{(x,\bar{y}_\alpha) : 0 < x < +\infty, 0 < |\bar{y}_\alpha| < +\infty\}$.

When $n(\bar{r}) = 1$, Eq. (3.24) reduces to the Helmholtz wave equation. Tatarskii [1971] demonstrated that the structure parameters for the acoustic refractive index, atmospheric wind, and atmospheric temperature (C_n^2, C_w^2, and C_T^2) are related as

$$C_n^2 = \frac{C_T^2}{4T_o^2} + \frac{C_w^2}{c_o^2} \tag{3.25e}$$

This equation also reveals the relationship between the structure parameters of the acoustic refractive index, temperature, and wind velocity. Eqs. (3.24) and (3.25) are applied in the next section and in Chapter IV to compute the first and second statistical moments of a spherical acoustic-wave propagating vertically into the atmosphere.

2. Rytov's Technique

Using Rytov's transformation, $u_a = \exp \psi$ [Barabanenkov et al, 1971]. The perturbation in complex phase-amplitude, ψ, is computed as

$$u_a(\bar{r}) = A_a(\bar{r}) \exp[iS(\bar{r})] \tag{3.26a}$$

$$\psi(\bar{r}) = \ln A_a(\bar{r}) + iS(\bar{r}) \tag{3.26b}$$

When this transformation is applied to the scalar-wave equation, the Ricatti equation in ψ

$$\nabla^2\psi + (\nabla\psi)^2 + k_a^2 n^2 = 0 \tag{3.27}$$

is obtained and $\psi(\bar{r})$ is then expanded in power series of a dimensionless parameter δ as

$$\psi(\bar{r}) = \sum_{j=0}^{\infty} \delta^j \psi_j(\bar{r}) \tag{3.28}$$

Using Eqs. (3.25a), (3.27) and (3.28) and equating to zero terms of like powers in δ result in

$$\nabla^2\psi_o + \nabla\psi_o \cdot \nabla\psi_o = - k_a^2 \langle n^2 \rangle \tag{3.29a}$$

$$\nabla^2\psi_1 + 2\nabla\psi_o \cdot \nabla\psi_1 = -2k_a^2 n_1 \tag{3.29b}$$

Note that solving Eq. (3.29a) is equivalent to solving

$$\nabla^2 u_{ao} + k_a^2 \langle n^2 \rangle u_{ao} = 0$$

which is Eq. (3.24) with $\delta = 0$, and $u_{ao} = \exp \psi_o$. Equation (3.29b) can be solved via the technique outlined in Schmeltzer [1967]. Assuming that $\langle n(\bar{r}) \rangle = 1$,

$$\psi_1(\bar{r}) = -2k_a^2 \int_{V_s} n_1(\bar{r}') \frac{u_{ao}(\bar{r}')}{u_{ao}(\bar{r})} G_{ao}(\bar{r},\bar{r}')\, d^3\bar{r}' \tag{3.30}$$

where

$$G_{ao}(\bar{r},\bar{r}') = - \frac{e^{ik_a|\bar{r}-\bar{r}'|}}{4\pi|\bar{r}-\bar{r}'|} \tag{3.31}$$

If $u_{ao}(\bar{r}) = A_{ao}(\bar{r}) \exp[iS_o(\bar{r})]$, $(\psi - \psi_o)$ measures the fluctuation in logarithmic-amplitude and phase of the scattered sound wave.

$$\psi - \psi_o = \ln \left| \frac{A_a}{A_{ao}} \right| + i(S - S_o) \equiv \chi + iS_1 \qquad (3.32)$$

where χ and S_1 are the perturbations in logarithmic amplitude and phase, respectively. Equations (3.30) and (3.31) will be used to determine the coherency of spherical acoustic-wave propagation in a turbulent medium.

Chapter IV

COHERENCY DESCRIPTION OF ACOUSTIC-WAVE PROPAGATION

The degree of interaction between electromagnetic and acoustic waves depends on the coherency of the latter. As a result, coherency of spherical acoustic-wave propagation in an inhomogeneous atmosphere is examined in this chapter via a perturbation theoretic approach.

A diagrammatic technique, introduced by Feynman [1948], serves as a basis for the analysis and is used to perform a selective summation of the perturbation series. Its basic philosophy is similar to that of the method of smoothing which, in turn, is related to the Bogoliubov-Krylov-Mitropolski method for solving nonlinear differential equations [Bogoliubov and Mitropolski, 1961]. These techniques are reviewed by Frisch [1968] and Nayfeh [1973].

The coherency of an acoustic pulse propagating in a turbulent medium is a measure of random fluctuations in and between successive wavefronts and is determined by atmospheric parameters. To simplify the analysis, it will be assumed that the mean of the acoustic refractive index $\langle n(\bar{r}) \rangle$ is unity and that the varying part of this refractive-index field $n_1(\bar{r})$ has a gaussian probability density function [Fante, 1975]. The acoustic source is modeled as a delta measure at the origin of the coordinate system. Source parameters are restricted to be deterministic.

A. First Moment of Acoustic-Wave Propagation

The first moment of a spherical acoustic wave propagating in a turbulent atmosphere is derived in this section and is then used to

estimate the coherence length of the wave. This length is defined as the altitude over which the mean acoustic field is attenuated by e^{-1} resulting from complex-phase interference. Given the notation $\bar{r} = (x,\bar{y}_\alpha)$, the coherence length x_c is

$$\left\langle G_a(x_c,\bar{y}_\alpha;0)\right\rangle = G_{ao}(x_c,\bar{y}_\alpha;0)e^{-1} \tag{4.1}$$

where $G_a(x,\bar{y}_\alpha;0)$ is Green's function for the spherical acoustic wave propagating in the turbulent medium. To derive $\left\langle G_a(x,\bar{y}_\alpha;0)\right\rangle$, Dyson's equation [Frisch, 1968] will be solved by means of Feynman's diagrammatic technique.

1. Dyson's Equation

Operator notation is used to simplify the following presentation. Equation (3.24) plus the source function determine the amplitude of the pressure wave as

$$\mathfrak{L}G_a = S_{ac} \tag{4.2}$$

Here, S_{ac} is assumed to be a delta measure at the origin of the coordinate system and $\mathfrak{L} \equiv (\nabla^2 + k_a^2 n^2)$ is the linear stochastic differential operator. In the above equation

$$\mathfrak{L} = \left\langle \mathfrak{L} \right\rangle + \mathfrak{L}' \qquad \left\langle \mathfrak{L}' \right\rangle = 0 \tag{4.3a}$$

$$G_a = \left\langle G_a \right\rangle + G_a' \qquad \left\langle G_a' \right\rangle = 0 \tag{4.3b}$$

where $\mathfrak{L}'$ and G_a' are the varying components of $\mathfrak{L}$ and G_a. Using Eqs. (3.24), (3.25a), (4.2), and (4.3),

$$\langle \mathfrak{L} \rangle = \nabla^2 + k_a^2 \langle n^2 \rangle \tag{4.4a}$$

$$\mathfrak{L}' = 2k_a^2 n_1 \tag{4.4b}$$

Therefore, from Eqs. (4.2) and (4.3a)

$$(\langle \mathfrak{L} \rangle + \mathfrak{L}')G_a = S_{ac} \tag{4.4c}$$

$$G_a = G'_{ao} S_{ac} - G'_{ao} \mathfrak{L}' G_a \tag{4.4d}$$

where G'_{ao} is the inverse operator of $\langle \mathfrak{L} \rangle$. It is nontrivial to solve the above equation for G_a; however, after formal iteration,

$$G_a = \sum_{j=0}^{\infty} \{-G'_{ao}\mathfrak{L}'\}^j G'_{ao} S_{ac} \tag{4.5}$$

This is called the Liouville-Neumann series and, because the random medium is semi-infinite, this series diverges with finite probability. Because $\langle G_a \rangle$ is to be computed, a relationship governing $\langle G_a \rangle$, called the Dyson equation, can be obtained by the method of smoothing; therefore, averaging Eq. (4.2) yields

$$\langle \mathfrak{L} \rangle \langle G_a \rangle + \langle \mathfrak{L}' G'_a \rangle = S_{ac} \tag{4.6}$$

Subtracting this result from Eq. (4.2) yields

$$\langle \mathfrak{L} \rangle G'_a + (I_i - P_{av}) \mathfrak{L}' G'_a = -\mathfrak{L}' \langle G_a \rangle \tag{4.7}$$

therefore,

$$G'_a = -G'_{ao}(I_i - P_{av})\mathfrak{L}' G'_a - G'_{ao}\mathfrak{L}' \langle G_a \rangle \tag{4.8}$$

where I_i is the identity operator and P_{av} denotes the operation of ensemble averaging. By iteration, G'_a can be determined as

$$G'_a = - \sum_{j=0}^{\infty} \left\{ -G'_{ao}(I_i - P_{av})\mathfrak{L}' \right\}^j G'_{ao}\, \mathfrak{L}' \langle G_a \rangle \tag{4.9}$$

Substituting for G'_a in Eq. (4.6) results in

$$\mathfrak{D} \langle G_a \rangle = S_{ac} \tag{4.10a}$$

where

$$\mathfrak{D} = \langle \mathfrak{L} \rangle - \mathfrak{M} \tag{4.10b}$$

and

$$\mathfrak{M} = \sum_{j=0}^{\infty} \left\langle \mathfrak{L}' \left\{ -G'_{ao}(I_i - P_{av})\mathfrak{L}' \right\}^j G'_{ao}\, \mathfrak{L}' \right\rangle \tag{4.10c}$$

Here $\mathfrak{M}$ is called the mass operator and $\mathfrak{D}$, the Dyson operator [Frisch, 1968]. Equations (4.10a) and (4.10b) yield

$$\langle G_a \rangle = G'_{ao} S_{ac} + G'_{ao} \mathfrak{M} \langle G_a \rangle \tag{4.11}$$

The success of Dyson's method depends on the fact that $\langle G_a \rangle$ is obtained by iterating from Eq. (4.11) after approximating $\mathfrak{M}$ instead of iterating G_a as in the Liouville-Neumann series and then averaging. Because the expression for $\mathfrak{M}$ is complicated, use of Feynman's diagrammatic technique in the following section is justified.

2. Series Solution of the Dyson Equation Using Feynman's Diagrams

Feynman's diagrammatic procedure is used to obtain a series solution of the Dyson equation. In this technique, the source S_{ac} is the Dirac-delta measure $\delta(\bar{r})$. Noting that $G'_{ao}\delta(\bar{r} - \bar{r}')$ is equal to $G_{ao}(\bar{r},\bar{r}')$, the integral representation of Eq. (4.2) then becomes

$$G_a(\bar{r},0) = G_{ao}(\bar{r},0) - 2k_a^2 \int G_{ao}(\bar{r},\bar{r}_1) n_1(\bar{r}_1) G_a(\bar{r}_1,0)\, d^3\bar{r}_1 \qquad (4.12)$$

Formal iteration of this equation results in the expansion of Eq. (4.5)

$$\begin{aligned} G_a(\bar{r},0) = {} & G_{ao}(\bar{r},0) - 2k_a^2 \int G_{ao}(\bar{r},\bar{r}_1) n_1(\bar{r}_1) G_{ao}(\bar{r}_1,0)\, d^3\bar{r}_1 \\ & + (-2k_a^2)^2 \iint G_{ao}(\bar{r},\bar{r}_2) n_1(\bar{r}_2) G_{ao}(\bar{r}_2,\bar{r}_1) \\ & \cdot n_1(\bar{r}_1) G_{ao}(\bar{r}_1,0)\, d^3\bar{r}_1\, d^3\bar{r}_2 \\ & + \cdots \end{aligned} \qquad (4.13)$$

The above series can be represented graphically with the following conventions:

C_1 -- $G_{ao}(\bar{r}_1,\bar{r}_2)$ is denoted by a short line whose end points are $\bar{r}_1$ and $\bar{r}_2$:

$G_{ao}(\bar{r}_1,\bar{r}_2) \sim$ —— ($\bar{r}_1$, $\bar{r}_2$)

C_2 -- The random operator $-\mathcal{L}' = -2k_a^2 n_1(\bar{r})$ is designated by a dot placed on the diagram at $\bar{r}$, sometimes called a vertex:

$-2k_a^2 n_1(\bar{r}) \sim \bullet_{\bar{r}}$

C_3 -- A dashed line joins the vertices for which $4k_a^4 \langle n_1(\bar{r}_2) n_1(\bar{r}_1) \rangle$ is evaluated:

$$4k_a^4 \langle n_1(\bar{r}_2) n_1(\bar{r}_1) \rangle \sim \bullet_{\bar{r}_2} \text{ - - - - } \bullet_{\bar{r}_1}$$

$$C_4 \text{ -- } \langle G_a \rangle \sim \text{————————}$$

For example,

$$\langle G'_{ao}(-\mathfrak{L}') G'_{ao}(-\mathfrak{L}') G'_{ao} \rangle \delta(\bar{r}-\bar{r}') =$$

$$(-2k_a^2)^2 \iint G_{ao}(\bar{r},\bar{r}_2) G_{ao}(\bar{r}_2,\bar{r}_1) G_{ao}(\bar{r}_1,\bar{r}')$$

$$\cdot \langle n_1(\bar{r}_2) n_1(\bar{r}_1) \rangle \, d^3\bar{r}_1 \, d^3\bar{r}_2$$

$$\sim \overset{\bar{r}}{\bullet}\!\!-\!\!-\!\!-\overset{\bar{r}_2}{\bullet}\!\!-\!\!-\!\!-\overset{\bar{r}_1}{\bullet}\!\!-\!\!-\!\!-\overset{\bar{r}'}{\bullet} \qquad (4.14)$$

The series in Eqs. (4.5) and (4.13) can be expanded diagrammatically as

$$G_a(\bar{r},0) \sim \overset{\bar{r}}{\bullet}\!\!-\!\!-\!\!-\!\!-\!\!-\!\!-\overset{0}{\bullet} + \overset{\bar{r}}{\bullet}\!\!-\!\!-\!\!-\overset{\bar{r}_1}{\bullet}\!\!-\!\!-\!\!-\!\!-\overset{0}{\bullet}$$

$$+ \overset{\bar{r}}{\bullet}\!\!-\!\!-\!\!-\overset{\bar{r}_2}{\bullet}\!\!-\!\!-\!\!-\overset{\bar{r}_1}{\bullet}\!\!-\!\!-\!\!-\!\!-\overset{0}{\bullet} + \ldots \qquad (4.15a)$$

One of the most significant attributes of this method is its systematic and explicit account of multiple scattering. For example, the third term represents a wave excited at the origin; it travels freely to and scatters at the vertex $\bar{r}_1$, travels freely to and scatters at the vertex $\bar{r}_2$, then travels freely to $\bar{r}$. Averaging Eq. (4.15a) and

because $n_1(\bar{r})$ is a centered gaussian random field, the following diagrammatic series is obtained [Tatarskii, 1971]:

$\langle G_a(\bar{r},0)\rangle \sim$ 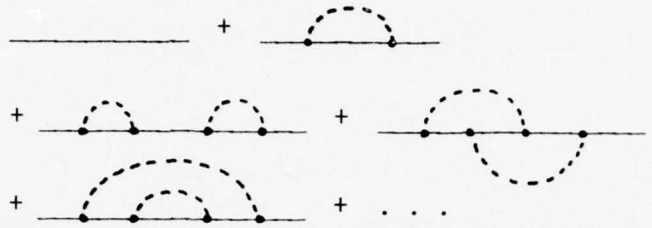

(4.15b)

This series is selectively summed by substituting the zeroth term in Eq. (4.10c) in Eq. (4.11), and (4.11) then simplifies to the following diagrammatic equation in $\langle G_a \rangle$:

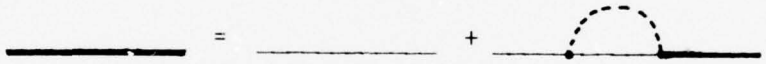

(4.16)

On iteration,

$\langle G_a(\bar{r},0)\rangle \sim$ 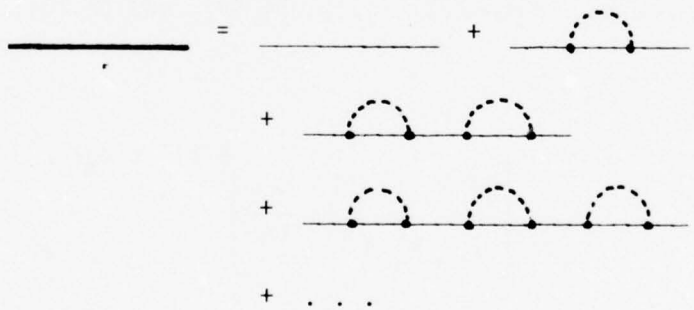

(4.17)

Using these equations, the coherence length of acoustic-wave propagation is computed in the next section, where the condition of forward scatter, $\lambda_a << L_o(x)$, exists (because the correlation length of the refractive-index fluctuations is on the order of $L_o(x)$).

3. Coherence Length of Propagation

An analytic representation of Eq. (4.16) is

$$\left\langle G_a(\bar{r},0)\right\rangle = G_{ao}(\bar{r},0) + (-2k_a^2)^2 \int_{V_s}\int_{V_s} G_{ao}(\bar{r},\bar{r}_2)G_{ao}(\bar{r}_2,\bar{r}_1)$$
$$\cdot \left\langle n_1(\bar{r}_1)n_1(\bar{r}_2)\right\rangle \left\langle G_a(\bar{r}_1,0)\right\rangle$$
$$\cdot\, d^3\bar{r}_1 d^3\bar{r}_2 \qquad (4.18)$$

Using the principle of stationary phase [Popoulis, 1968] and the mathematics in Appendix B, this equation can be solved for $\left\langle G_a(\bar{r},0)\right\rangle$:

$$\left\langle G_a(\bar{r},0)\right\rangle = G_{ao}(\bar{r},0)e^{-\frac{1}{2}\left\langle |\psi_1(x,\bar{y}_\alpha)|^2\right\rangle} \qquad (4.19)$$

Here, the unperturbed term $G_{ao}(\bar{r},0)$ is damped by the factor $\exp[-\left\langle |\psi_1(x,\bar{y}_\alpha)|^2\right\rangle/2]$ in a turbulent medium because of complex-phase interference. From Eqs. (4.1), (4.19), and (A.20), the coherence length is

$$x_c = \left[\frac{54.8\ (1.833 - m_a)}{C_{no}^2\ k_a^2\ A^{5/3}\ x_o^{m_a}}\right]^{6/(11-6\ m_a)} \qquad (4.20)$$

At altitudes of the acoustic pulse $x \ll x_c$, the effect of turbulence is negligible. From Fig. 3, it can be concluded that the coherence length varies inversely with frequency and the strength of turbulence.

The incoherence length of propagation x_i is defined as

$$x_i = \left[\frac{54.8(1.833 - m_a)}{C_{no}^2\ k_a^2\ B^{5/3}\ x_o^{m_a}}\right]^{6/(11-6\ m_a)} \qquad (4.21)$$

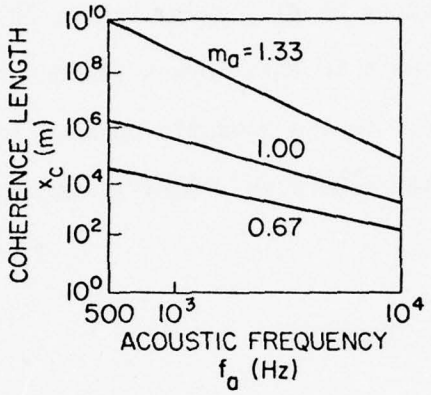

Fig. 3. COHERENCE LENGTH VS ACOUSTIC FREQUENCY.
$C_{no}^2 = 10^{-6} m^{-2/3}$, $x_o = 1$ m,
$c_o = 340$ m/sec, and $A = 2$.

The incoherence length of propagation is the altitude over which the transverse coherence length of the field is of the order of the inner scale of turbulence. For $x_i \ll x$, the acoustic wave is incoherent as a result of random fluctuations in the atmosphere. This incoherence length of propagation is typically three to five orders of magnitude larger than the coherence length.

B. Second Moment of Acoustic-Wave Propagation

The coherence function $M(\bar{r}',\bar{r}'')$ of an acoustic wave propagating in a turbulent atmosphere is defined by

$$\left\langle G_a(\bar{r}',0)G_a^*(\bar{r}'',0)\right\rangle = G_{ao}(\bar{r}',0)G_{ao}^*(\bar{r}'',0)M(\bar{r}',\bar{r}'') \qquad (4.22)$$

The quantity $\langle G_a(\bar{r}',0)G_a^*(\bar{r}'',0)\rangle$ is the second statistical moment of Green's function. This function has been widely used when a measure of coherence between two points in the same wavefront is required [Tatarskii, 1971; Prokhorov et al., 1975; Fante, 1975]; however, the definition and requirements in this investigation are more general because $\bar{r}'$ and $\bar{r}''$ lie in the acoustic pulse. To compute $M(\bar{r}',\bar{r}'')$, the Bethe-Salpeter equation [Frisch, 1968] is solved using Feynman's diagrammatic technique.

1. Bethe-Salpeter Equation

The coherence function is a measure of fluctuations between two points (not necessarily in the same plane). To compute $M(\bar{r}',\bar{r}'')$, the second statistical moment of the acoustic wave must be determined. This second moment, the ensemble average of the double Green's function $G_a(\bar{r}',0)G_a^*(\bar{r}'',0)$. This double Green's function is defined as

$$G_a(\bar{r}',0) \otimes G_a^*(\bar{r}'',0) = G_a(\bar{r}',0)G_a^*(\bar{r}'',0) \tag{4.23}$$

that is, the tensor product of Green's function and its complex conjugate. In terms of "double diagrams" and Eq. (4.15a),

$G_a(\bar{r}',0) \otimes G_a^*(\bar{r}'',0) =$ 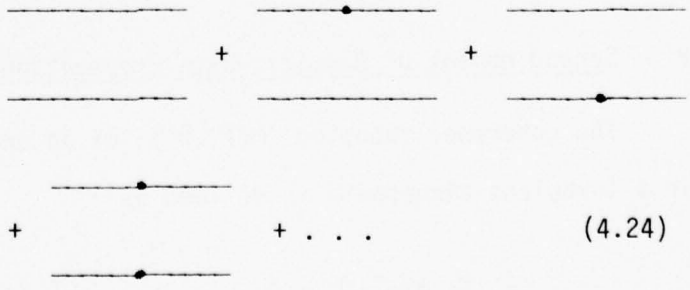 (4.24)

Each double diagram is the tensor product of the operator representing the upper line and the complex conjugate of the operator representing the lower line. For example,

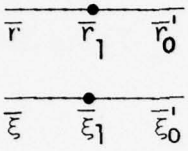

$$= (-2k_a^2)^2 \int_{V_s}\int_{V_s} G_{ao}(\bar{r},\bar{r}_1)n_1(\bar{r}_1)G_{ao}(\bar{r}_1,\bar{r}_0') \cdot G_{ao}^*(\bar{\xi},\bar{\xi}_1)n_1(\bar{\xi}_1)G_{ao}^*(\bar{\xi}_1,\bar{\xi}_0')\, d^3\bar{r}_1\, d^3\bar{\xi}_1 \tag{4.25}$$

The mean double Green's function $\langle G_a(\bar{r}',0) \otimes G_a^*(\bar{r}'',0)\rangle$ is expressed in the following diagrammatic series:

$\langle G_a(\bar{r}',0)G_a^*(\bar{r}'',0)\rangle =$

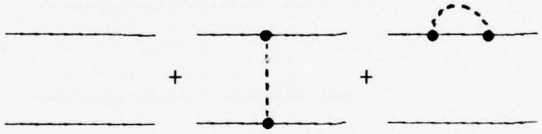

$+ \ldots$ (4.26)

where

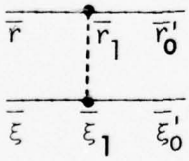

$$= (-2k_a^2)^2 \int_{V_s}\int_{V_s} G_{ao}(\bar{r},\bar{r}_1)G_{ao}(\bar{r}_1,\bar{r}_0')\langle n_1(\bar{r}_1)n_1(\bar{\xi}_1)\rangle \cdot G_{ao}^*(\bar{\xi},\bar{\xi}_1)G_{ao}^*(\bar{\xi}_1,\bar{\xi}_0')\, d^3\bar{r}_1 d^3\bar{\xi}_1 \tag{4.27}$$

In operator notation, $\langle G_a \otimes G_a^*\rangle$ can be computed from the following Bethe-Salpeter equation [Frisch, 1968]:

$$\langle G_a \otimes G_a^*\rangle = \langle G_a\rangle\langle G_a^*\rangle + \langle G_a\rangle\langle G_a^*\rangle \mathfrak{A} \langle G_a \otimes G_a^*\rangle \tag{4.28}$$

where $\mathcal{I}$ is the "intensity operator" because it is used in calculating the mean intensity of the propagating wave. Under a weak forward-scattering condition, the diagrammatic representation of this equation is

$\langle G_a \otimes G_a^* \rangle =$ 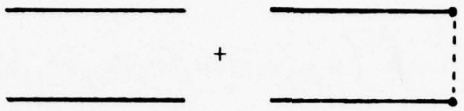 $\langle G_a \otimes G_a^* \rangle$ (4.29)

The top line denotes $\langle G_a \rangle$ and the bottom one designates $\langle G_a^* \rangle$. This diagrammatic equation can be solved by iteration as follows:

$\langle G_a \otimes G_a^* \rangle =$ 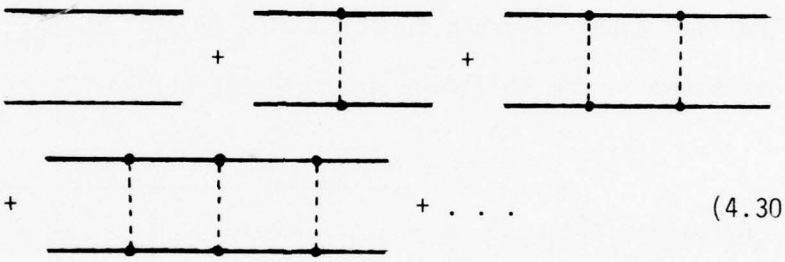 (4.30)

which is the "ladder" approximation of the solution to the Bethe-Salpeter equation [Tatarskii, 1971]. The Eq.(4.29) can be rewritten as

$$\langle G_a(\bar{r}',0)G_a^*(\bar{r}'',0)\rangle$$

$$= \langle G_a(\bar{r}',0)\rangle \langle G_a^*(\bar{r}'',0)\rangle$$

$$+ (-2k_a^2)^2 \int_{V_s}\int_{V_s} \langle G_a(\bar{r}',\bar{r}_1)\rangle \langle G_a^*(\bar{r}'',\bar{r}_2)\rangle \langle n_1(\bar{r}_1)n_1(\bar{r}_2)\rangle$$

$$\cdot \langle G_a(\bar{r}_1,0)G_a^*(\bar{r}_2,0)\rangle \, d^3\bar{r}_1 d^3\bar{r}_2 \qquad (4.31)$$

Normalizing this equation by $G_{ao}(\bar{r}',0)G_{ao}^*(\bar{r}'',0)$ and using Eq. (4.22),

$$M(\bar{r}',\bar{r}'')$$

$$= \frac{\left\langle G_a(\bar{r}',0)\right\rangle \left\langle G_a^*(\bar{r}'',0)\right\rangle}{G_{ao}(\bar{r}',0)G_{ao}^*(\bar{r}'',0)}$$

$$+ (-2k_a^2)^2 \int_{V_s}\int_{V_s} \frac{\left\langle G_a(\bar{r}',\bar{r}_1)\right\rangle \left\langle G_a^*(\bar{r}'',\bar{r}_2)\right\rangle}{G_{ao}(\bar{r}',0)G_a^*(\bar{r}'',0)} \left\langle n_1(\bar{r}_1)n_1(\bar{r}_2)\right\rangle$$

$$\cdot\, G_{ao}(\bar{r}_1,0)G_{ao}^*(\bar{r}_2,0)M(\bar{r}_1,\bar{r}_2)d^3\bar{r}_1 d^3\bar{r}_2 \qquad (4.32)$$

which, used to solve for $M(\bar{r}',\bar{r}'')$ through Eqs. (4.19), (A.16), (A.17), and (A.20) becomes

$$M(\bar{r}',\bar{r}'') = \exp\left\{-\frac{1}{2}\left[\left\langle|\psi_1(\bar{r}')|^2\right\rangle + \left\langle|\psi_1(\bar{r}'')|^2\right\rangle - 2\left\langle\psi_1(\bar{r}')\psi_1^*(\bar{r}'')\right\rangle\right]\right\} \qquad (4.33a)$$

Here, $\bar{r}' = (x',\bar{y}'_\alpha)$, $\bar{r}'' = (x'',\bar{y}''_\alpha)$, and

$$\frac{1}{2}\left[\left\langle|\psi_1(\bar{r}')|^2\right\rangle + \left\langle|\psi_1(\bar{r}'')|^2\right\rangle - 2\left\langle\psi_1(\bar{r}')\psi_1^*(\bar{r}'')\right\rangle\right] =$$

$$4\pi^2 k_a^2 \int_0^x\int_0^\infty \left[1 - J_0\left(\kappa_\alpha y_{\alpha m}\frac{\eta}{x}\right)\right] \kappa_\alpha\, \Phi_n(\eta,\kappa_\alpha)d\kappa_\alpha\, d\eta \qquad (4.33b)$$

where

$x = (x' + x'')/2$ and $y_{\alpha m} = |\bar{y}'_\alpha - \bar{y}''_\alpha|$.

2. Coherence Function

The coherence function is a measure of the sphericity of the acoustic wavefronts propagating vertically into the turbulent atmosphere;

it also determines the coherency in and between the wavefronts of an acoustic pulse. This function is examined in the following cases.

Case 1: $x << x_c$

At these altitudes, the acoustic wavefronts are almost coherent,

$$M(\bar{r}', \bar{r}'') \simeq 1 \tag{4.34}$$

and the effect of turbulence is negligible.

Case 2: $x_c << x << x_i$

In this case, Eq. (4.33a) is evaluated using the following relation [Abramowitz and Stegun, 1968; Formula 11.4.18]:

$$\int_0^\infty [1 - J_0(t)]\, t^{-8/3}\, dt = 1.118 \tag{4.35}$$

Based on Eqs. (2.23) and (4.33), the coherence function is

$$M(\bar{r}', \bar{r}'') = \exp\left[-3.73 \frac{(11/6 - m_a)}{(8/3 - m_a)} \left(\frac{y_{\alpha m}}{\ell_0(x)}\right)^{5/3} \left(\frac{x}{x_c}\right)^{(11/6 - m_a)}\right] \tag{4.36}$$

which holds for $\ell_0(x) << y_{\alpha m} << \ell_0(x)$. As can be seen in Fig. 4, the coherence function decreases as x/x_c and $y_{\alpha m}/\ell_0(x)$ increase, and it increases as m_a increases.

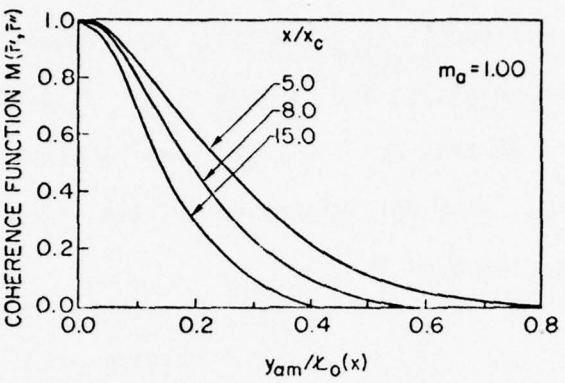

a. Parametric variation in normalized altitude

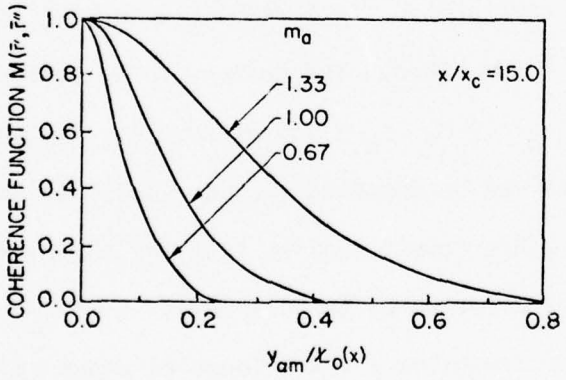

b. Parametric variation in m_a

Fig. 4. COHERENCE FUNCTION VS $y_{\alpha m}/\ell_o(x)$.

Case 3: $x_i \ll x$

At these altitudes, $y_{\alpha m} < \ell_o(x)$; as a result κ_α is integrated from 0 to $\ell_o^{-1}(\eta)$, and $J_o(\kappa_\alpha y_{\alpha m}\eta/x)$ is expanded in a small-argument approximation as $1 - (\kappa_\alpha y_{\alpha m}\eta/x)^2/4$ in the right-hand side of Eq. (4.33b). Using this expansion and Eqs. (2.23), (4.21), and (4.33) the coherence function is

$$M(\bar{r}',\bar{r}'') = \exp\left[-2.5\left(\frac{11 - 6m_a}{17 - 6m_a}\right)\left(\frac{y_{\alpha m}}{\ell_o(x)}\right)^2\left(\frac{x}{x_i}\right)^{(11/6-m_a)}\right] \qquad (4.37)$$

C. Summary

Feynman's diagrammatic technique has been used to describe mathematically the coherency of spherical acoustic waves traveling vertically into the turbulent atmosphere. If a RASS is operating at an acoustic frequency of $f_a = 1$ kHz, [Brown and Keeler, 1975; Taylor, 1968] $C_{no}^2 = 10^{-6}\ m^{-2/3}$, $x_o = 1$ m, $c_o = 340$ m/sec, $A = 2$, and $m_a = 1.33$, the coherence length can be computed via Eq. (4.20) to obtain $x_c = 6.4 \times 10^8$ m. This result implies that the coherency of an acoustic wave is not affected by turbulence at $x \ll x_c$ when the acoustic frequencies are below a few kilocycles under typical atmospheric conditions.

Chapter V

SCATTERING OF ELECTROMAGNETIC WAVES FROM AN ACOUSTIC PULSE

This chapter describes the scattering of electromagnetic waves from an acoustic pulse traveling vertically into the lower atmosphere. Marshall [1972] studied this phenomenon in a static atmosphere (without turbulence or winds). The effects of turbulence, mean wind, and temperature parameters are included to obtain a more realistic expression for the electromagnetic power reflected from an acoustic pulse. The fundamentals of the physical phenomenon are discussed in Section A, and an expression for the backscattered electromagnetic energy for a monostatic RASS is derived. In Sections B and C, the effects of turbulence and mean atmospheric parameters on the backscattered energy are considered, and Section D summarizes the results.

A. Interaction between Electromagnetic and Acoustic Waves

A physical basis for the scattering of electromagnetic energy from an acoustic pulse is established in this section.

1. Maxwell's Equations

The electromagnetic refractive index $n_e(\bar{r})$ of the medium is defined by

$$n_e(\bar{r}) = 1 + n_{e1}(\bar{r}) \tag{5.1}$$

where $n_{e1}(\bar{r})$ is its varying part; typically, $|n_{e1}(\bar{r})| \ll 1$. The variations in $n_e(\bar{r})$ can be caused by naturally occurring phenomena in the atmosphere or they may be man-made.

Assuming that the lower atmosphere is nonionized and that its permeability μ_o is a constant, the electromagnetic refractive index is

$$n_e(\bar{r}) = \sqrt{\frac{\varepsilon(\bar{r})}{\varepsilon_o}} \tag{5.2}$$

where

$$\varepsilon(\bar{r}) = \varepsilon_o + \Delta\varepsilon(\bar{r}) \tag{5.3}$$

Here, the free-space permittivity ε_o is a constant, and $\Delta\varepsilon(\bar{r})$ is the deviation of permittivity $\varepsilon(\bar{r})$ of the medium from ε_o. Given a sinusoidal time-varying electric field $\bar{E}(\bar{r})e^{-i\omega_e t}$ and a magnetic field $\bar{H}(\bar{r})e^{-i\omega_e t}$, Maxwell's equations can be expressed (using vector notation) as

$$\nabla \times \bar{E}(\bar{r}) = i\mu_o\omega_e\bar{H}(\bar{r}) \tag{5.4a}$$

$$\nabla \times \bar{H}(\bar{r}) = -i\varepsilon(\bar{r})\omega_e\bar{E}(\bar{r}) \tag{5.4b}$$

$$\nabla \cdot \bar{H}(\bar{r}) = 0 \tag{5.4c}$$

$$\nabla \cdot [\varepsilon(\bar{r})\bar{E}(\bar{r})] = 0 \tag{5.4d}$$

where

$$\omega_e = 2\pi f_e \tag{5.5}$$

is the angular electromagnetic frequency and f_e is the electromagnetic frequency. The above equations can be combined as

$$\nabla^2\bar{E}(\bar{r}) + \omega_e^2\mu_o\varepsilon(\bar{r})\bar{E}(\bar{r}) + \nabla[\bar{E}(\bar{r}) \cdot \nabla(\ln\varepsilon(\bar{r}))] = 0 \tag{5.6a}$$

The gradient term can be neglected if $\Delta\varepsilon(\bar{r})/\varepsilon_o$ is small over one wavelength λ_e [Bremmer, 1964]. This is a valid simplification because

this term, which contributes to the depolarization of the electromagnetic wave, is negligible under the atmospheric conditions [Strohbehn, 1971] pertinent to this study. Neglecting the gradient and applying Eq. (5.3),

$$\nabla^2\bar{E}(\bar{r}) + \omega_e^2\mu_o\varepsilon_o\bar{E}(\bar{r}) = -\omega_e^2\mu_o\Delta\varepsilon(\bar{r})\bar{E}(\bar{r}) \qquad (5.6b)$$

Using $k_e^2 = \omega_e^2\mu_o\varepsilon_o$, where $k_e = 2\pi/\lambda_e$ is the electromagnetic wavenumber, the above equation simplifies to

$$\nabla^2\bar{E}(\bar{r}) + k_e^2\bar{E}(\bar{r}) = -k_e^2\left(\frac{\Delta\varepsilon(\bar{r})}{\varepsilon_o}\right)\bar{E}(\bar{r}) \qquad (5.7)$$

which can be solved in a perturbation series because $|\Delta\varepsilon(\bar{r})/\varepsilon_o| \ll 1$.

2. Perturbation of Permittivity of Air by a Propagating Sound Wave

Neglecting the effect of water vapor [Bean and Dutton, 1968], the electromagnetic refractive index above 30 MHz can be approximated by

$$(n_e - 1) = \frac{K_{re}P}{T} \qquad (5.8)$$

where pressure P is in Nw/m^2, temperature T is in °K, and K_{re} is a constant equal to 77.7×10^{-8} °K/Nw/m^2. Equations (5.2) and (5.3) yield

$$(n_e - 1) = \frac{(\varepsilon - \varepsilon_o)}{2\varepsilon_o} \qquad (5.9)$$

therefore,

$$\frac{d\varepsilon}{\varepsilon - \varepsilon_o} = \frac{dP}{P} - \frac{dT}{T} \tag{5.10}$$

Because the propagation of a sound wave is an adiabatic process in the lower troposphere,

$$\frac{dP}{P} = -\gamma \frac{dV_d}{V_d} \tag{5.11}$$

where γ is the ratio of specific heats of air and V_d is its volume density. Using the above equation and the perfect gas equation PV_d/T = constant,

$$\frac{dT}{T} = \left(\frac{\gamma - 1}{\gamma}\right) \frac{dP}{P} \tag{5.12}$$

then

$$\frac{d\varepsilon}{\varepsilon_o} = \frac{2K_{re}}{\gamma} \frac{dP}{T} \tag{5.13}$$

which, in incremental notation, is

$$\frac{\Delta\varepsilon}{\varepsilon_o} = \frac{2K_{re}}{\gamma} \frac{\Delta P}{T} \tag{5.14}$$

Defining

$$P = p_o + p_a \tag{5.15a}$$

where p_o is the static atmospheric pressure and p_a is the external acoustic pressure, then

$$\Delta P = p_a \tag{5.15b}$$

The external source is assumed to have a sinusoidal amplitude variation with a maximum value of p_{amax}. If P_a is the radiated acoustic power (in watts), $g_a(\theta)$ is the gain function of the acoustic source, and G_{as} is the maximum value of $g_a(\theta)$, then

$$g_a(\theta) = G_{as}\, f_a^2(\theta) \tag{5.16a}$$

and

$$f_a(0) = 1 \tag{5.16b}$$

According to Landau and Lifshitz [1959], the intensity $I(r)$ at distance r is

$$I(r) = \frac{p_{amax}^2}{2\rho_o c_o} = \frac{P_a g_a(\theta)}{4\pi r^2} \tag{5.17}$$

Consequently combining Eqs. (5.15) and (5.17) yield

$$\left(\frac{\Delta\varepsilon}{\varepsilon_o}\right)^2_{max} = \left(\frac{2K_{re}^2 \rho_o c_o}{\pi\gamma^2 T^2}\right)\left(\frac{P_a g_a}{r^2}\right) \tag{5.18}$$

For the following typical values in the lower troposphere, $K_{re} = 77.7 \times 10^{-8}$ °K/Nw/m^2, $\rho_o = 1.23$ Kg/m^3, $c_o = 330$ m/sec, $T = 273$ °K, and $\gamma = 1.4$,

$$\left(\frac{2K_{re}^2 \rho_o c_o}{\pi\gamma^2 T^2}\right) \simeq 10^{-15} \tag{5.19}$$

and

$$\left(\frac{\Delta\varepsilon}{\varepsilon_o}\right)_{max} = \frac{K_1}{r} \tag{5.20}$$

where, assuming $g_a(\theta) \simeq G_{as}$ over the effective scattering volume V_{as},

$$K_1^2 = 10^{-15} P_a G_{as} \tag{5.21}$$

3. Born Approximation

Equation (5.7) can be written as

$$\nabla^2 E(\bar{r}) + k_e^2 E(\bar{r}) = -k_e^2 \delta_e \left(\frac{\Delta\varepsilon(\bar{r})}{\varepsilon_o}\right) E(\bar{r}) \tag{5.22}$$

for each cartesian component of $E(\bar{r})$, where δ_e is a dimensionless dummy parameter denoting a measure of deviation of relative permittivity from unity. The electric-field component $E(\bar{r})$ can be expanded in a power series of δ_e as

$$E(\bar{r}) = \sum_{j=0}^{\infty} \delta_e^j E_j(\bar{r}) \tag{5.23}$$

which, when substituting into Eq. (5.22) and equating terms of the same order in δ_e, results in

$$\nabla^2 E_o + k_e^2 E_o = 0 \tag{5.24}$$

$$\nabla^2 E_1 + k_e^2 E_1 + k_e^2 \left(\frac{\Delta\varepsilon(\bar{r})}{\varepsilon_o}\right) E_o = 0 \tag{5.25}$$

$$\vdots$$

$$\nabla^2 E_m + k_e^2 E_m + k_e^2 \left(\frac{\Delta\varepsilon(\bar{r})}{\varepsilon_o}\right) E_{m-1} = 0 \tag{5.26}$$

In the above set of equations, E_1 produces only single-scattering and higher order terms yield multiple-scattering effects; m^{th} order scattering is a result of E_j, $m \geq j \geq 0$. A sufficient condition for the validity of the above series is

$$\frac{1}{2} \left|\frac{\Delta\varepsilon}{\varepsilon_o}\right|_{max} k_e^2 \, d_{scv}^2 < 1$$

where d_{scv} is the diameter of the scattering volume. If

$$\frac{1}{2} \left|\frac{\Delta\varepsilon}{\varepsilon_o}\right|_{max} k_e^2 \, d_{scv}^2 << 1$$

then,

$$E(\bar{r}) \simeq E_o(\bar{r}) + E_1(\bar{r}) \tag{5.27}$$

This is known as the Born approximation [Bremmer, 1964]. If P_t is the transmitted electromagnetic power (in watts), G_t is the maximum gain of the electromagnetic transmitter, and η_o is the free-space impedance, then

$$E_o(\bar{r}) = E_{oo}(\bar{r}) \, e^{i(k_e r - \omega_e t)} \tag{5.28}$$

where

$$\frac{E_{oo}^2(\bar{r})}{2\eta_o} = \frac{P_t G_t}{4\pi r^2} \tag{5.29}$$

Using Green's function theory and imposing the radiation condition [Yeh and Liu, 1972] the scattered field at the receiver for monostatic geometry of the RASS is

$$E_1(0) = \frac{k_e^2}{4\pi} \int_{V_{as}} \frac{e^{ik_e r'}}{r'} \frac{\Delta\varepsilon(\bar{r}')}{\varepsilon_o} E_o(\bar{r}')\, d^3\bar{r}' \qquad (5.30)$$

where V_{as} is the scattering volume.

4. Scattering Geometry

The electromagnetic signal scattered from the acoustic pulse traveling in a turbulent atmosphere is computed for the RASS monostatic geometry illustrated in Fig. 5. The half-power beamwidths of the acoustic source and the electromagnetic antenna are $\hat{\theta}_a$ and $\hat{\theta}_e$,

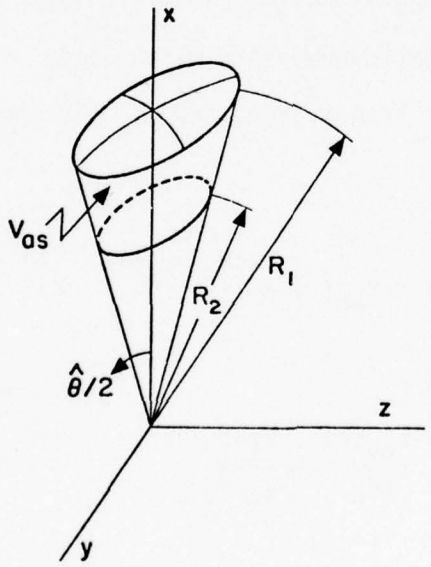

Fig. 5. RASS MONOSTATIC GEOMETRY.

respectively, and $\hat{\theta}$ is the minimum of each. The effective scattering volume V_{as} is limited by two spheres of radii R_1 and R_2 centered at the origin and by a cone of vertical angle $\hat{\theta}$. If n_{ac} is the number of cycles in the acoustic pulse, then

$$R_1 - R_2 = n_{ac} \lambda_a \tag{5.31}$$

The maximum gains of the electromagnetic transmitting and receiving antennas are G_r and G_t, respectively. These antenna patterns are

$$g_r(\theta) = G_r f_r^2(\theta) \tag{5.32a}$$

$$f_r(0) = 1 \tag{5.32b}$$

$$g_t(\theta) = G_t f_t^2(\theta) \tag{5.32c}$$

$$f_t(0) = 1 \tag{5.32d}$$

Here $g_r(\theta)$, $g_t(\theta)$, and the acoustic source pattern $g_a(\theta)$ defined in Eqs. (5.16) are considered to be substantially constant over V_{as}, as is $E_{oo}(\bar{r})$ from Eq. (5.29). These simplifying assumptions do not significantly affect the calculations because the variation in these patterns and amplitude over V_{as} is small. If the effective area of the receiving antenna is A_r and the received power is P_r,

$$A_r = \frac{\lambda_e^2}{4\pi} G_r \tag{5.33a}$$

and

$$\frac{P_r}{A_r} = \frac{\langle |E_1|^2 \rangle}{2\eta_o} \tag{5.33b}$$

The diameter of the scattering volume is

$$d_{scv} = \max \left\{ R\hat{\theta}, n_{ac}\lambda_a \right\} \tag{5.34}$$

where $R \simeq x$ is the height of the acoustic pulse. As a result, it can be noted from the previous subsection that the condition for the validity of the Born approximation is

$$K_1 k_e^2 x\hat{\theta}^2/2 << 1 \qquad \text{if} \quad d_{scv} = x\hat{\theta}$$

$$K_1 k_e^2 n_{ac}^2 \lambda_a^2/(2x) << 1 \qquad \text{if} \quad d_{scv} = n_{ac}\lambda_a$$

These conditions are typically valid in the lower troposphere.

B. Received Power in the Presence of Turbulence

In computing the scattered electromagnetic energy from an acoustic pulse in a turbulent atmosphere, the mean atmospheric parameters are assumed to be absent. The effect of these mean parameters, however, is considered in the next section. From the results obtained in Eqs. (3.32) and (5.20)

$$\frac{\Delta\varepsilon(\bar{r})}{\varepsilon_o} = \frac{K_1}{r} \operatorname{Re} \left\{ e^{[ik_a r + \psi(\bar{r}) - \psi_o(\bar{r})]} \right\} \tag{5.35}$$

Based on this equation plus (4.22), (4.33a), (5.28), and (5.30) and imposing the Bragg condition $2k_e = k_a$,

$$\left\langle |E_1|^2 \right\rangle = \left(\frac{K_1^2}{4}\right)\left(\frac{k_e^2}{4\pi}\right)^2 \int_{V_{as}} \int_{V_{as}} \frac{M(\bar{r}',\bar{r}'')}{(r'r'')^2} E_{oo}(\bar{r}')E_{oo}^*(\bar{r}'')d^3\bar{r}'d^3\bar{r}'' \qquad (5.36)$$

where $\bar{r}' = (x',\bar{y}_\alpha')$ and $\bar{r}'' = (x'',\bar{y}_\alpha'')$. Making the transformation of variables $x = (x'+x'')/2$, $\bar{y}_{\alpha m} = (\bar{y}_\alpha'-\bar{y}_\alpha'')$, and $\bar{y}_{\alpha p} = (\bar{y}_\alpha'+\bar{y}_\alpha'')/2$, and neglecting amplitude variations, which are less significant compared to phase variations,

$$\left\langle |E_1|^2 \right\rangle = \left(\frac{K_1^2}{4}\right)\left(\frac{k_e^2}{4\pi}\right)^2 (n_{ac}\lambda_a)^2 \frac{E_{oo}^2}{x^4} I(x, \hat{\theta}/2, y_{\alpha m}) \qquad (5.37)$$

where

$$I(x, \hat{\theta}/2, y_{\alpha m}) = \int_{D'} \int_{D''} M(x, y_{\alpha m})\, d^2\bar{y}_\alpha' d^2\bar{y}_\alpha'' \qquad (5.38)$$

In the above equation D' and D'' are circles of radii $d_a' = x' \hat{\theta}/2$ and $d_a'' = x'' \hat{\theta}/2$, respectively; and $I(x,\hat{\theta}/2,y_{\alpha m})$ is evaluated in Appendix C. Using Eqs. (5.21), (5.29), (5.33), and (5.37), the received power P_r is

$$P_r = \frac{n_{ac}^2 P_a P_t G_r G_t G_{as}}{256\, x^6} I(x, \hat{\theta}/2, y_{\alpha m})\, 10^{-15} \qquad (5.39)$$

Defining $d_a = x \hat{\theta}/2$, the received power P_r is evaluated for the following three cases.

Case 1: $x \ll x_c$

At this altitude, the acoustic wavefronts are almost fully coherent; therefore, from Eqs. (4.34), (5.39), and (C.9)

$$I(x, \hat{\theta}/2, y_{\alpha m}) = \left(\pi d_a^2\right)^2$$

$$= \left[\pi\left(\frac{x\hat{\theta}}{2}\right)^2\right]^2 \tag{5.40}$$

and

$$P_r = \frac{\pi^2 n_{ac}^2 P_a P_t G_r G_t G_{as} [(\hat{\theta}/2)^2/2]^2}{x^2} \left(\frac{10^{-15}}{64}\right)$$

$$= \frac{n_{ac}^2 P_a P_t G_r G_t G_{as}}{x^2} \left[\frac{(\hat{\theta}/2)^2}{2}\right]^2 (1.54 \times 10^{-16}) \tag{5.41}$$

This equation is identical to the one derived by Marshall [1972] who assumed a static environment. At these altitudes, his derivations are valid even in the presence of atmospheric turbulence.

Case 2: $x_c \ll x \ll x_i$

In this range, $A_a(x, \hat{\theta}/2, y_{\alpha m})$ can be approximated by πd_a^2 in the integrand of Eq. (C.9); then,

$$I(x, \hat{\theta}/2, y_{\alpha m}) = (2\pi)(\pi d_a^2) \int_0^{2d_a} y_{\alpha m} M(x, y_{\alpha m}) dy_{\alpha m} \tag{5.42}$$

Because, generally, $2d_a \gg \ell_o(x)$, the upper limit of this integral can be extended to infinity. Based on Eq. (4.36),

$$I(x, \hat{\theta}/2, y_{\alpha m}) = (2\pi)(\pi d_a^2)(0.113)\left(\frac{8/3 - m_a}{11/6 - m_a}\right)^{6/5} \rho_o^2(x)$$

$$\cdot\left(\frac{x_c}{x}\right)^{(11/6-m_a)(6/5)} \tag{5.43}$$

and

$$I(x, \hat{\theta}/2, y_{\alpha m})_{max} = (\pi d_a^2)^2 \tag{5.44}$$

As a result,

$$\frac{I(x, \hat{\theta}/2, y_{\alpha m})}{I(x, \hat{\theta}/2, y_{\alpha m})_{max}} = 0.226\left(\frac{8/3 - m_a}{11/6 - m_a}\right)^{6/5}\left(\frac{\rho_o(x)}{d_a}\right)^2$$

$$\cdot\left(\frac{x_c}{x}\right)^{(11-6m_a)/5} \tag{5.45}$$

If P_{rmax} given by Eq. (5.41) is the maximum received power in the absence of turbulence, then from Eqs. (5.39) and (5.45), it follows that

$$\frac{P_r}{P_{rmax}} = \frac{I(x, \hat{\theta}/2, y_{\alpha m})}{I(x, \hat{\theta}/2, y_{\alpha m})_{max}}$$

$$= 0.226\left(\frac{8/3 - m_a}{11/6 - m_a}\right)^{6/5}\left(\frac{\rho_o(x)}{d_a}\right)^2$$

$$\cdot\left(\frac{x_c}{x}\right)^{(11-6m_a)/5} \tag{5.46}$$

from which it can be observed (Fig. 6) that the received power decreases as altitude increases.

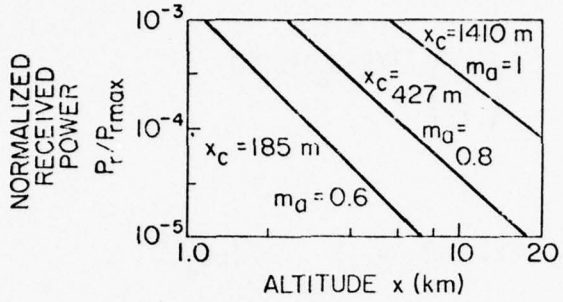

Fig. 6. NORMALIZED RECEIVED POWER VS ALTITUDE OF ACOUSTIC PULSE. $C_{no}^2 = 10^{-6}\ m^{-2/3}$, $x_o = 1$ m, $c_o = 340$ m/sec, $f_a = 10^4$ Hz, $A = 2$, $\hat{\theta} = 0.1$ rad, $x_c << x << x_i$.

Case 3: $x_i << x$

At these altitudes, it can be shown by using Eqs. (4.37), (5.39), (C.8) and (C.9) that

$$\frac{P_r}{P_{rmax}} = 0.4\left(\frac{17 - 6m_a}{11 - 6m_a}\right)\left(\frac{\ell_o(x)}{d_a}\right)^2\left(\frac{x_i}{x}\right)^{(11/6-m_a)} \qquad (5.47)$$

It can be concluded from the results obtained for the three cases considered above that, in the lower troposphere ($x \lesssim 10$ km), the effect of turbulence on the received RF power in a RASS is negligible at acoustic frequencies less than a few kilohertz. At frequencies greater than $\gtrsim 10$ kHz, however, turbulence must be considered when evaluating the RASS performance when the altitude of the acoustic pulse is greater than about 1 km.

C. Interaction between Electromagnetic and Acoustic Waves in the Presence of Mean Atmospheric Parameters

In addition to the fluctuating parameters, the atmosphere is characterized by such mean parameters as temperature and winds. In the lower atmosphere, a linear temperature profile can be observed at heights up to the first 10 km; its temperature gradient, typically -6.5 °K/km [Yeh and Liu, 1972], tends to disperse the acoustic wave train. The atmosphere is also characterized by vertical winds that alter the effective velocity of sound and by horizontal winds that shift the focus of electromagnetic energy from its origin. In the analysis to follow, these winds are assumed to be constant, and each parameter is studied separately.

1. Received Power in an Atmosphere with a Linear Temperature Profile

The linear temperature profile in the lower atmosphere can be described as

$$T(\bar{r}) = T' + a_g r \tag{5.48}$$

where a_g is the temperature gradient, T' is the temperature at ground, and $T(\bar{r})$ is the temperature at $\bar{r}$. The beamwidth of the acoustic source is assumed to be sufficiently narrow so that the temperature variations across the acoustic wavefront can be neglected. This is a valid assumption for acoustic-wave propagation in the troposphere [Yeh and Liu, 1972] and for beamwidths less than 1 radian. The endpoint of the vector $\bar{r}$ falls within the half-power beamwidth of the acoustic source. Because $|a_g r| \ll T'$ at altitudes below a few

kilometers, T' will be replaced by the average temperature T_o in the ensuing calculations.

From Tatarskii [1971] and Eqs. (3.24), (3.25) and (5.48), the phase $S_T(\bar{r})$ of the acoustic wave is given by

$$S_T(\bar{r}) = k_a r - \eta r^2 \tag{5.49a}$$

where

$$\eta = \frac{a_g k_a}{4T_o} \tag{5.49b}$$

In the geometry in Fig. 5 (page 58), the strength of the RASS received signal is proportional to the magnitude of F, where

$$F = \int_{R_2}^{R_1} \cos S_T(r)\, e^{-i(2k_e r - \alpha)}\, dr \tag{5.50}$$

and α is a constant introduced to simplify the calculations of $|F|^2$. In the absence of temperature gradients,

$$|F|^2 = \left(\frac{\eta_{ac}\lambda_a}{2}\right)^2 \tag{5.51}$$

For a linear temperature profile in the lower atmosphere, F calculated in Appendix D is

$$F = \sqrt{\frac{\pi}{8\eta}} \Big\{ \cos(\eta R_m^2 + \alpha)[C_f(A_m) - C_f(B_m)] + \sin(\eta R_m^2 + \alpha)[S_f(A_m) - S_f(B_m)]$$

$$
\begin{aligned}
&+ \cos(\eta R_p^2 - \alpha)[C_f(A_p) - C_f(B_p)] \\
&+ \sin(\eta R_p^2 - \alpha)[S_f(A_p) - S_f(B_p)] \\
&+ i\Big[\cos(\eta R_m^2 + \alpha)[-S_f(A_m) + S_f(B_m)] \\
&+ \sin(\eta R_m^2 + \alpha)[C_f(A_m) - C_f(B_m)] \\
&+ \cos(\eta R_p^2 - \alpha)[S_f(A_p) - S_f(B_p)] \\
&- \sin(\eta R_p^2 - \alpha)[C_f(A_p) - C_f(B_p)]\Big]\Big\} \qquad (5.52)
\end{aligned}
$$

where $C_f(\cdot)$, $S_f(\cdot)$ are Fresnel cosine and sine integrals, the normalized temperature gradient β is defined as

$$\beta = \frac{a_g \lambda_a}{T_o} \qquad (5.53)$$

and

$$R_1' = \frac{R_1}{\lambda_a} \qquad (5.54a)$$

$$R_2' = \frac{R_2}{\lambda_a} \qquad (5.54b)$$

$$A_m = \sqrt{\beta}\, R_1' - \frac{2}{\sqrt{\beta}}\left(1 - \frac{2\lambda_a}{\lambda_e}\right) \qquad (5.55a)$$

$$B_m = \sqrt{\beta}\, R_2' - \frac{2}{\sqrt{\beta}}\left(1 - \frac{2\lambda_a}{\lambda_e}\right) \qquad (5.55b)$$

$$A_p = \sqrt{\beta}\, R_1' - \frac{2}{\sqrt{\beta}}\left(1 + \frac{2\lambda_a}{\lambda_e}\right) \qquad (5.55c)$$

$$B_p = \sqrt{\beta}\, R_2' - \frac{2}{\sqrt{\beta}}\left(1 + \frac{2\lambda_a}{\lambda_e}\right) \qquad (5.55d)$$

$$R_m = \frac{2\lambda_a}{\beta}\left(1 - \frac{2\lambda_a}{\lambda_e}\right) \tag{5.56a}$$

$$R_p = \frac{2\lambda_a}{\beta}\left(1 + \frac{2\lambda_a}{\lambda_e}\right) \tag{5.56b}$$

$$\eta R_m^2 = \frac{2\pi}{\beta}\left(1 - \frac{2\lambda_a}{\lambda_e}\right)^2 \tag{5.56c}$$

$$\eta R_p^2 = \frac{2\pi}{\beta}\left(1 + \frac{2\lambda_a}{\lambda_e}\right)^2 \tag{5.56d}$$

Defining the power-reflection coefficient to be $|F|^2/(n_{ac}\lambda_a/2)^2$, it can be observed that a match between the electromagnetic and acoustic wavelengths depends on the temperature difference over the length of the acoustic wave train. For an acoustic pulse at an altitude x, the reflection of electromagnetic energy is maximized when

$$\frac{\lambda_e}{\lambda_a} \simeq 2\left(1 + \frac{a_g x}{2T_o}\right) \tag{5.57}$$

This represents a modified Bragg-scatter condition when a RASS is operating in the presence of a linear temperature profile. For $|\beta| \ll 1$, under modified Bragg-scatter condition and small wave-train lengths, the power-reflection coefficient is almost unity. It can be seen in Fig. 7 that the wavelength ratios that produce a peak in the power-reflection coefficient for positive and negative temperature gradients are different; this can also be observed in Eq. (5.57). The conclusion drawn from these results is that, for short wave-train lengths and wavelengths below a few meters, typical temperature gradients in the lower atmosphere have a negligible effect on the received power of a RASS.

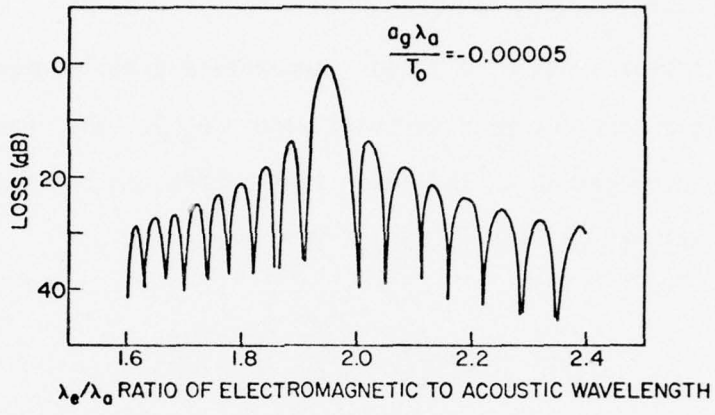

a. Negative temperature gradient

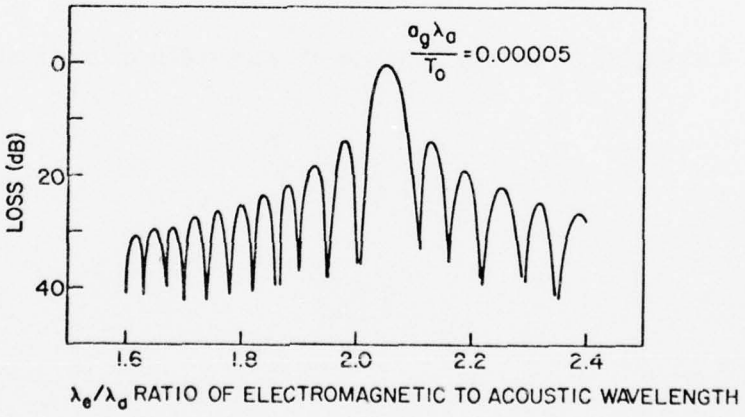

b. Positive temperature gradient

Fig. 7. EFFECT OF LINEAR TEMPERATURE PROFILE ON POWER-REFLECTION COEFFICIENT VS WAVELENGTH RATIO; altitude = 1000 λ_a, pulse length = 40 λ_a.

2. Received Power in an Atmosphere with a Linear Temperature Profile and Mean Vertical Wind

In the presence of a linear temperature profile described by Eq. (5.48) and a constant mean vertical wind $\langle w_x \rangle$, the phase of an acoustic wave propagating in the lower troposphere can be determined from Eqs. (3.24), (3.25) and (5.49b). This phase is

$$S_v(\bar{r}) = k_a r \left(1 - \frac{\langle w_x \rangle}{c_o}\right) - \eta r^2 \tag{5.58}$$

In the geometry in Fig. 5 (page 58), the strength of the RASS received signal is proportional to the magnitude of F_v, where

$$F_v = \int_{R_2}^{R_1} \cos S_v(r)\, e^{-i(2k_e r - \alpha)}\, dr \tag{5.59}$$

and α is a constant. In the absence of temperature gradients and winds,

$$|F_v|^2 = \left(\frac{n_{ac}\lambda_a}{2}\right)^2 \tag{5.60}$$

Defining

$$\alpha_v = \frac{\langle w_x \rangle}{c_o} \tag{5.61}$$

then, F_v can be calculated as in Appendix D,

$$F_v = \sqrt{\frac{\pi}{8\eta}} \Big\{ \cos(\eta R_{mv}^2 + \alpha)[C_f(A_{mv}) - C_f(B_{mv})] + \sin(\eta R_{mv}^2 + \alpha)[S_f(A_{mv}) - S_f(B_{mv})]$$

$$+ \cos(\eta R_{pv}^2 - \alpha)[C_f(A_{pv}) - C_f(B_{pv})]$$

$$+ \sin(\eta R_{pv}^2 - \alpha)[S_f(A_{pv}) - S_f(B_{pv})]$$

$$+ i\Big[\cos(\eta R_{mv}^2 + \alpha)[-S_f(A_{mv}) + S_f(B_{mv})]$$

$$+ \sin(\eta R_{mv}^2 + \alpha)[C_f(A_{mv}) - C_f(B_{mv})]$$

$$+ \cos(\eta R_{pv}^2 - \alpha)[S_f(A_{pv}) - S_f(B_{pv})]$$

$$- \sin(\eta R_{pv}^2 - \alpha)[C_f(A_{pv}) - C_f(B_{pv})]\Big]\Big\} \qquad (5.62)$$

where

$$A_{mv} = \sqrt{\beta}\, R_1' - \frac{2}{\sqrt{\beta}}\left(1 - \alpha_v - \frac{2\lambda_a}{\lambda_e}\right) \qquad (5.63a)$$

$$B_{mv} = \sqrt{\beta}\, R_2' - \frac{2}{\sqrt{\beta}}\left(1 - \alpha_v - \frac{2\lambda_a}{\lambda_e}\right) \qquad (5.63b)$$

$$A_{pv} = \sqrt{\beta}\, R_1' - \frac{2}{\sqrt{\beta}}\left(1 - \alpha_v + \frac{2\lambda_a}{\lambda_e}\right) \qquad (5.63c)$$

$$B_{pv} = \sqrt{\beta}\, R_2' - \frac{2}{\sqrt{\beta}}\left(1 - \alpha_v + \frac{2\lambda_a}{\lambda_e}\right) \qquad (5.63d)$$

$$R_{mv} = \frac{2\lambda_a}{\beta}\left(1 - \alpha_v - \frac{2\lambda_a}{\lambda_e}\right) \qquad (5.64a)$$

$$R_{pv} = \frac{2\lambda_a}{\beta}\left(1 - \alpha_v + \frac{2\lambda_a}{\lambda_e}\right) \qquad (5.64b)$$

$$\eta R_{mv}^2 = \frac{2\pi}{\beta}\left(1 - \alpha_v - \frac{2\lambda_a}{\lambda_e}\right)^2 \qquad (5.64c)$$

$$\eta R_{pv}^2 = \frac{2\pi}{\beta}\left(1 - \alpha_v + \frac{2\lambda_a}{\lambda_e}\right)^2 \qquad (5.64d)$$

Figure 8 illustrates the power-reflection coefficient defined by $|F_v|^2/(n_{ac}\lambda_a/2)^2$ as a function of λ_e/λ_a whose shape is determined by the temperature gradient. The optimal ratio of λ_e/λ_a, however, is obtained by the temperature gradient, altitude of the acoustic pulse, mean temperature T_o, and normalized mean vertical wind α_v. The modified Bragg-scatter condition is

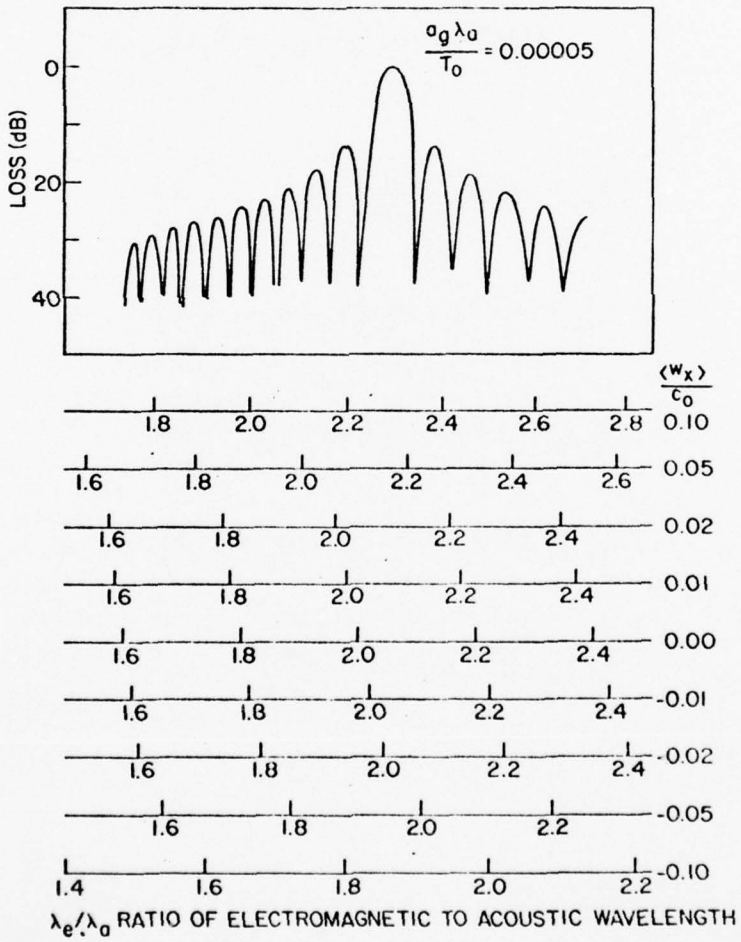

Fig. 8. EFFECT OF LINEAR TEMPERATURE PROFILE AND VERTICAL WIND ON POWER-REFLECTION COEFFICIENT VS WAVELENGTH RATIO: Altitude = 1000 λ_a, pulse length = 40 λ_a.

$$\frac{\lambda_e}{\lambda_a} \simeq 2\left(1 + \frac{\langle w_x \rangle}{c_o} + \frac{a_g x}{2T_o}\right) \tag{5.65}$$

When $\langle w_x \rangle / c_o = -a_g x/(2T_o)$, then $\lambda_e = 2\lambda_a$ which is a condition for the maximum return of electromagnetic energy in a static atmosphere. It can be concluded, as in the previous subsection, that the loss in received electromagnetic power is negligible in the presence of temperature gradients and mean vertical winds.

3. Received Power in the Presence of Horizontal Winds

Horizontal winds displace the acoustic wavefront laterally. This results in a shifting of the focus of reflected electromagnetic energy from its origin, thereby resulting in a decrease in the received signal level when a monostatic RASS is used. The effect of constant mean horizontal winds w_h is investigated as follows.

Consider an electromagnetic wavefront interacting with an acoustic wavefront. The phase-matching error between the two wavefronts is illustrated in Fig. 9. The error between paths P and P' with angular separation θ is $2(R-R')$, where $\bar{R}$ and $\bar{R}'$ are the vectors corresponding to the two paths. The factor 2 is the result of the forward and reverse travel of electromagnetic energy. Because the phase-match error is small for small θ, the electromagnetic energies from P and P' add nearly in phase at the receiver located at the origin of the coordinate system. If P is fixed and θ is increased, the phase-match error will become larger, and this will increase the phase difference in the electromagnetic energies reflected from the two paths. When this error is half of an electrical wavelength, the energies will

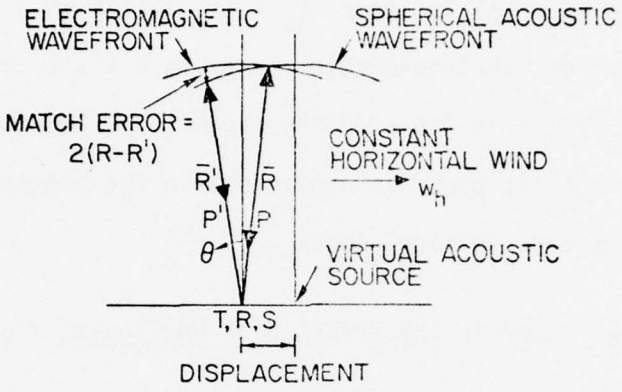

Fig. 9. SHIFT OF ACOUSTIC WAVEFRONTS IN THE PRESENCE OF HORIZONTAL WINDS. T - Radar Transmitter, R - Radar Receiver, S - Acoustic Source.

cancel. If θ is further increased this error may become a full electrical wavelength and the energies will add constructively. From this discussion, it can be concluded that a smaller beamwidth $\hat{\theta}$ reduces the susceptibility of reflected electromagnetic energy to horizontal winds.

Each acoustic wavefront in an acoustic pulse contributes a phase-match error. This error is substantially constant over an acoustic pulse containing a few tens of cycles for typical values of beamwidths and horizontal wind velocities; however, the alignment between electromagnetic and acoustic wavefronts is important.

From Tatarskii [1971], and Eqs. (3.24) and (3.25), the phase $S_w(\bar{r})$ of the acoustic wave is

$$S_w(\bar{r}) = k_a r \left(1 - \frac{\langle \bar{w} \rangle}{c_o} \cdot \hat{r}\right) \tag{5.66}$$

where $\hat{r} = \bar{r}/r$ and $\langle \bar{w} \rangle$ is the mean wind vector. For the geometry in Fig. 5 (page 58), the magnitude of the RASS received signal is proportional to F_w, where

$$F_w = \int_{V_{as}} \cos S_w(\bar{r}') \, e^{-i(2k_e r' - \alpha)} \, d^3\bar{r}' \tag{5.67}$$

and α is a constant. In the absence of horizontal winds $\bar{w}_h$, the maximum value of F_w is

$$F_{wmax} = \pi x^2 n_{ac} \lambda_a \left(\frac{\hat{\theta}}{2}\right)^2 \frac{1}{2} \tag{5.68}$$

where x is the height of the acoustic pulse. Note that, for $x >> \lambda_a$ and $w_h/c_o << 1$, the acoustic wavefronts shift laterally through $k_a x w_h/c_o$ radians in the presence of horizontal winds. The effects of horizontal winds on the received power are negligible when $k_a x w_h/c_o << 1$; in this case, $F_w \simeq F_{wmax}$. When $k_a x \hat{\theta} w_h/c_o >> 1$ and $\lambda_e = 2\lambda_a$, then from Eq.(E.15) in Appendix E, for small pulse length,

$$\frac{P_{rw}}{P_{rmax}} = \frac{20.37 \cos^2[k_a x \hat{\theta} w_h/(2c_o) - 3\pi/4]}{(k_a x \hat{\theta} w_h/c_o)^3} \tag{5.69}$$

Here P_{rw} and P_{rmax} are the power received in the presence of horizontal winds and in a static atmosphere, respectively. The functional behavior of Eq. (5.69) is illustrated in Fig. 10.

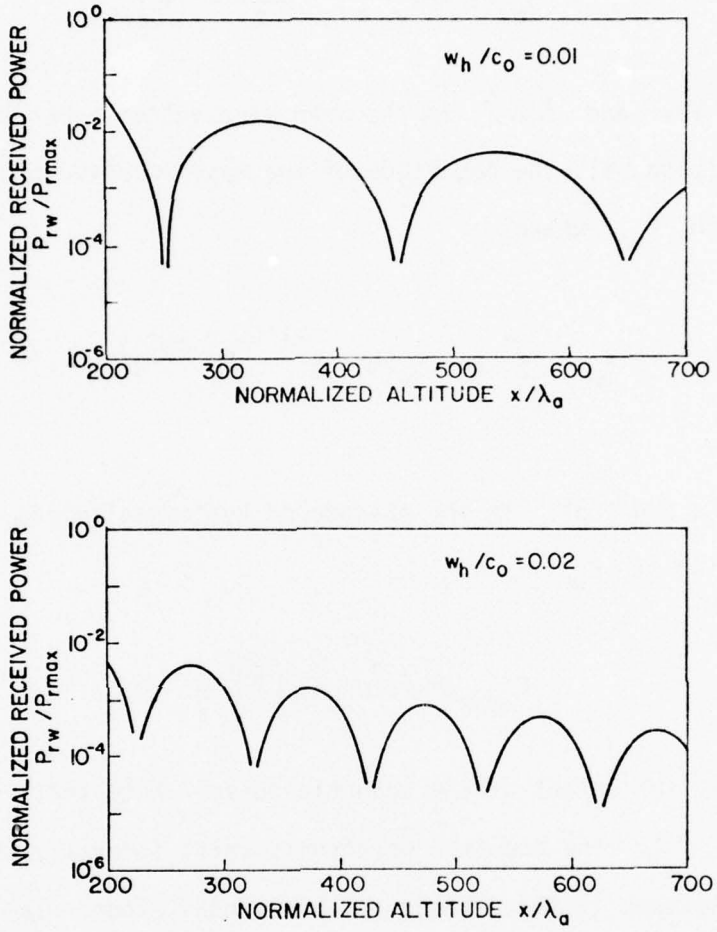

Fig. 10. ASYMPTOTIC NORMALIZED RECEIVED POWER VS NORMALIZED ALTITUDE FOR ACOUSTIC PULSE ALTITUDES LESS THAN COHERENCE LENGTH IN THE PRESENCE OF CONSTANT HORIZONTAL WINDS. $\hat{\theta} = 0.5$ rad.

If $x = 200\ \lambda_a$, $w_h/c_o = 0.01$, and $\hat{\theta} = 0.5$ rad, then $P_{rw}/P_{rmax} \simeq 4 \times 10^{-2}$. When $\lambda_a = 4$ m and $c_o = 340$ m/s, then $f_a = 85$ Hz which is the operating frequency of the Stanford RASS [Frankel and Peterson, 1976]; the loss in received power as a result of horizontal winds at an altitude of 800 m is $P_{rw}/P_{rmax} \simeq 4 \times 10^{-2}$. If the operating acoustic frequency is the only parameter changed to $f_a = 1$ kHz

and if the beamwidth remains constant at $\hat{\theta} = 0.5$ rad, then at $x = 200\ \lambda_a = 68$ m, $P_{rw}/P_{rmax} \simeq 4 \times 10^{-2}$.

The above decrease in the received signal level results because horizontal winds shift the focal point of the reflected electromagnetic energy from the origin, and this shift is a measure of the horizontal wind. Applying the principle of specular reflection (Fig. 11), a bistatic radar configuration with space-diversified receiving antennas can be used to collect this reflected energy [Frankel et al., 1977] and measure horizontal winds.

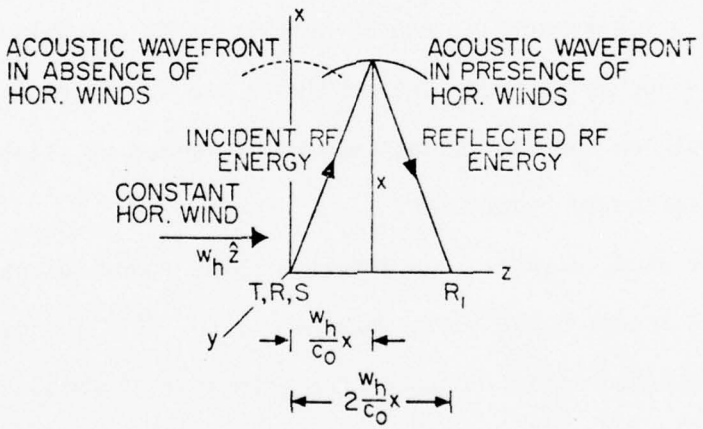

Fig. 11. SPECULAR REFLECTION OF ELECTROMAGNETIC ENERGY FROM ACOUSTIC WAVEFRONT. T - radar transmitter, R - radar receiver at the origin, R_1 - displaced receiver, S - acoustic source, x - altitude of the acoustic wavefront.

D. Summary

Scattering of electromagnetic waves from an acoustic pulse traveling in a realistic atmosphere has been considered. The effects of such atmospheric parameters as turbulence and mean winds were considered independently. These phenomena can be combined to analyze their effect on the scattering of electromagnetic waves; however, the basic physical ideas remain unchanged. The asymptotic results of the different cases can be combined to obtain a composite view, but only at the expense of clarity.

It has been concluded that turbulence has little influence on the scattered electromagnetic energy of acoustic pulses with carrier frequencies below a few kilocycles and at heights up to a few kilometers. Mean vertical winds and temperature gradients are functions of altitude, and their effects on the RASS signal can be minimized by establishing a modified Bragg-scatter condition.

Horizontal winds displace the acoustic pulse downwind resulting in received signal levels below those computed in Eq. (5.41). By using a bistatic RASS configuration, however, the principle of specular reflection of RF energy from the acoustic wavefronts can be applied to measure horizontal winds. In this RASS geometry, the radar antennas and acoustic sources are aligned in the wind direction -- the transmit antenna upwind from the acoustic source and the receive antenna downwind. If the separation between the antennas is much less than the altitude of the acoustic pulse, the received signal level can be obtained from Eq. (5.41).

Chapter VI

DOPPLER SHIFT IN THE REFLECTED ELECTROMAGNETIC SIGNAL

The electromagnetic energy reflected from a traveling acoustic wave train shifts from the frequency of the incident electromagnetic wave. This is called the doppler shift, and it depends on atmospheric parameters and on the position of the acoustic wave train with respect to the RASS geometry.

The influence of mean winds on the received doppler signal will be discussed in Section A. In Section B, the doppler shift for a bistatic RASS is described. Because deviation from unity in the acoustic refractive index caused by turbulence is smaller than that resulting from typical mean wind fields in the troposphere (by at least one order of magnitude), the effect of turbulence is ignored in this chapter.

A. RASS Doppler Measurements in the Presence of Mean Wind Field

In monostatic geometry, the doppler shift in the received electromagnetic signal $\Delta f(x)$ from an acoustic signal at an altitude x in the absence of winds is

$$\Delta f(x) = -\frac{2}{\lambda_e} c(x) \tag{6.1}$$

$$c(x) = K_d[T(x)]^{1/2} \tag{6.2}$$

where $K_d = 20.053$ [North, 1974] and the speed of sound $c(x)$ at x is measured in meters per second. From Eqs. (6.1) and (6.2), the temperature $T(x)$ at x can be measured by determining $\Delta f(x)$.

Because horizontal winds contribute negligible error in the computation of $T(x)$ for a monostatic RASS geometry, only vertical winds w_x need be considered. The doppler frequency in the presence of these winds is

$$\Delta f(x) = - \frac{2}{\lambda_e} [c(x) + w_x] \tag{6.3}$$

Knowledge of w_x and $\Delta f(x)$ produces a correct indication of temperature. If vertical winds are ignored, the error in the calculation of $T(x)$ is [North, 1974] approximately

$$\Delta T(x) \simeq 1.7\ w_x \tag{6.4}$$

and this error becomes significant when the vertical wind is greater than 1/2 m/sec.

The functional error in the computation of the height of the acoustic pulse will be on the order of w_x/c_o. This error should also be corrected because it becomes increasingly significant as the magnitude of the vertical wind and the altitudes grow larger. It can be eliminated, however, by a suitable averaging process, one of which is described by North [1974].

In the bistatic geometry of Fig. 12, the doppler shift $\Delta f(x)$ in the received electromagnetic signal caused by the traveling acoustic signal is

$$\Delta f(x) = - \frac{2}{\lambda_e} c(x) \cos [\alpha(x)] \tag{6.5}$$

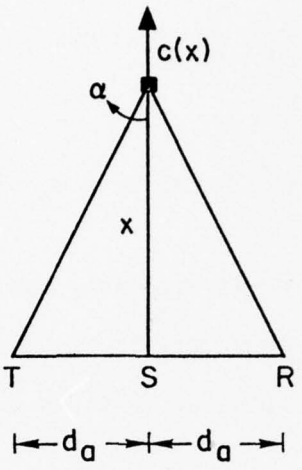

Fig. 12. DOPPLER-TRACKING BISTATIC RASS GEOMETRY. T - transmitter, S - acoustic source, R - receiver, x - altitude of the acoustic wavefront, d_a = TS = SR.

which differs from Eq. (6.1) because of the additional multiplicative factor $\cos [\alpha(x)]$, where

$$\cos [\alpha(x)] = \left(1 + \frac{d_a^2}{x^2}\right)^{-1/2} \tag{6.6}$$

and d_a is the separation between the acoustic source and the electromagnetic transmitter or receiver. At an altitude x, the temperature $T(x)$ can be computed via Eqs. (6.2), (6.5) and (6.6). At $x \gg d_a$, $\cos [\alpha(x)] \simeq 1$ and temperature can be determined from Eqs. (6.1) and (6.2).

In the presence of horizontal winds, w_h, the doppler shift for the bistatic RASS for small values of α is given by

AD-A047 953 STANFORD UNIV CALIF STANFORD ELECTRONICS LABS F/G 20/5
INTERACTION OF ELECTROMAGNETIC AND ACOUSTIC WAVES IN A STOCHAST--ETC(U)
JUL 77 N BHATNAGAR N00014-75-C-0601
UNCLASSIFIED SU-SEL-77-031 NL

2 OF 2
ADA047953

END
DATE FILMED
1-78
DDC

$$\Delta f(x) = -\frac{2}{\lambda_e} c'(x) \cos [\alpha(x)] \qquad (6.7a)$$

where

$$c'(x) = c(x) \cos \alpha_h + w_h \sin \alpha_h \qquad (6.7b)$$

In Eq. (6.7b) $\alpha_h = w_h/c_o$ is typically much smaller than unity. Hence $c'(x) \simeq c(x)$, and therefore it can be concluded that the effect of horizontal winds on the doppler shift in a bistatic RASS is insignificant.

B. Averaged Doppler Shift of the RASS in a Bistatic Configuration

A static atmosphere is assumed in this analysis. The bistatic geometry of Fig. 12 is considered. As the acoustic pulse spreads over a distance of $n_{ac}\lambda_a$ in the vertical direction, the effective altitude x_p of the acoustic pulse should correspond to the maximum intensity in the doppler-frequency spectrum [Gill, 1965]. Note that $x_2 \leq x_p \leq x_1$, where x_1 and x_2 are the heights of the upper and lower edges of the acoustic-pulse train. Beam power patterns of the electromagnetic transmitter and receiver antennas determine x_p. For example, if this pattern has a gaussian variation, x_p will be close to the top of its edge x_1 at low altitudes of the acoustic pulse. At higher altitudes, however, variation in the beam power pattern over the spread of the acoustic wave train in the vertical direction is negligible; therefore, $x_p = (x_1 + x_2)/2$.

If the doppler shift is obtained by an averaging measurement of $\Delta f(x)$ when the acoustic pulse occupies two different positions in the vertical direction, then

$$\Delta f_{av}(x) = - \frac{2c(x)}{\lambda_e (x_{p1} - x_{p2})} \int_{x_{p2}}^{x_{p1}} \cos [\alpha(x')] \, dx' \qquad (6.8)$$

where heights x_{p1} and x_{p2} indicate the maximum power return of electromagnetic energy from the acoustic pulse at the two positions. Note that x is any point between x_{p2} and x_{p1} and that the speed of sound $c(x)$ is assumed to be constant over x_{p2} to x_{p1}. At high altitudes, $\cos [\alpha(x)] \simeq 1$ and the averaged doppler shift can once again be computed by Eq. (6.1). At low altitudes and for a finite spread of the acoustic-wave train, however, Eq. (6.8) should be used. Based on Eqs. (6.6) and (6.8), $\Delta f_{av}(x)$ can be simplified to

$$\Delta f_{av}(x) = - \frac{2c(x)}{\lambda_e (x_{p1} - x_{p2})} \left[\left(d_a^2 + x_{p1}^2 \right)^{1/2} - \left(d_a^2 + x_{p2}^2 \right)^{1/2} \right] \qquad (6.9)$$

Consequently, the temperature at x can be computed from Eqs. (6.2) and (6.9).

Chapter VII

CONCLUSION

In this study, the interaction of electromagnetic and acoustic waves in a stochastic atmosphere has been discussed for a monostatic RASS geometry. Spectral expansions for the physical parameters describing acoustic-wave propagation in a dissipative atmosphere were developed from basic conservation equations. Using Rytov's transformation and Feynman's diagrammatic method, it has been theoretically demonstrated that, for acoustic pulses with carrier frequencies below a few kilohertz and propagating under typical atmospheric conditions, turbulence has little effect on the strength of the backscattered RASS radio signal at heights up to a few kilometers. This result implies that focusing of radio-frequency energy by the acoustic wavefronts is primarily a function of sound intensity which decreases as x^{-2}, where x is the altitude.

The effect of mean vertical winds and temperature profiles on the strength of the received signal was also shown to be insignificant. Horizontal winds shift the focus of the reflected electromagnetic energy from its origin, thereby resulting in a decrease in the received signal level when a monostatic RASS is used. The principle of specular reflections, however, can be utilized in a bistatic radar configuration with space-diversified receiving antennas to measure remotely the horizontal wind component in the lower troposphere.

The doppler performance of the RASS has also been described. It has been observed that the doppler shift is sensitive to the presence of winds, but this sensitivity can be eliminated by an averaging process.

A modified expression for the doppler shift was also obtained for a bistatic RASS geometry, which takes into account the finite spread of the acoustic pulse in the vertical direction.

This research has been theoretical in nature. The conclusions drawn, however, need to be verified experimentally.

Appendix A

SIMPLIFICATION OF $\langle \psi_1(\bar{r}')\psi_1^*(\bar{r}'') \rangle$

The coherency of a spherical acoustic wave propagating vertically into the lower atmosphere can be described by its first and second statistical moments. These moments, in turn, depend on the perturbation $[\psi(\bar{r}) - \psi_o(\bar{r})]$ of its complex phase. Consequently, it can be observed from Eq. (3.28) that, to compute these moments, it is necessary to compute $\langle \psi_1(\bar{r}')\psi_1^*(\bar{r}'') \rangle$. Therefore, $\langle \psi_1(\bar{r}')\psi_1^*(\bar{r}'') \rangle$ is calculated in this appendix for spherical wave propagation. From Eqs. (3.30) and (3.31)

$$\psi_1(\bar{r}) = \frac{k_a^2}{2\pi} \int_{V_s} n_1(\bar{r}_1) e^{ik_a(r_1 - r)} \frac{r}{r_1} \frac{e^{ik_a|\bar{r}-\bar{r}_1|}}{|\bar{r}-\bar{r}_1|} d^3\bar{r}_1 \tag{A.1}$$

$B_n(\bar{r}', \bar{r}'')$, the covariance function of the acoustic refractive index, is

$$B_n(\bar{r}', \bar{r}'') = \langle n_1(\bar{r}')n_1(\bar{r}'') \rangle \tag{A.2}$$

Then

$$\langle \psi_1(\bar{r}')\psi_1^*(\bar{r}'') \rangle = \left(\frac{k_a^2}{2\pi}\right)^2 (r'r'')\, e^{-ik_a(r'-r'')} \iint_{V_s} \iint_{V_s} \frac{B_n(\bar{r}_1, \bar{r}_2)}{r_1 r_2}$$

$$\cdot \frac{\exp[ik_a\{(r_1 - r_2) + |\bar{r}' - \bar{r}_1| - |\bar{r}'' - \bar{r}_2|\}]}{|\bar{r}' - \bar{r}_1||\bar{r}'' - \bar{r}_2|}$$

$$\cdot\, d^3\bar{r}_1 d^3\bar{r}_2 \tag{A.3}$$

where $\bar{r}_1 = (x_1, \bar{y}_{\alpha 1})$; $\bar{r}_2 = (x_2, \bar{y}_{\alpha 2})$. Under paraxial approximation [Strohbehn, 1968], and forward scatter;

$$r = \sqrt{x^2 + y_\alpha^2} \simeq x + \frac{y_\alpha^2}{2x}$$

$$\left\langle \psi_1(\bar{r}')\psi_1^*(\bar{r}'') \right\rangle = \left(\frac{k_a^2}{2\pi}\right)^2 x'x'' e^{-ik_a\left[\frac{y_\alpha'^2}{2x'} - \frac{y_\alpha''^2}{2x''}\right]}$$

$$\cdot \iint_{V_s} \iint_{V_s} \frac{B_n(\bar{r}_1, \bar{r}_2)}{x_1 x_2 (x'-x_1)(x''-x_2)} \exp\left[ik_a\left\{\frac{y_{\alpha 1}^2}{2x_1} - \frac{y_{\alpha 2}^2}{2x_2}\right.\right.$$

$$\left.\left. + \frac{|\bar{y}_\alpha' - \bar{y}_{\alpha 1}|^2}{2(x'-x_1)} - \frac{|\bar{y}_\alpha'' - \bar{y}_{\alpha 2}|^2}{2(x''-x_2)}\right\}\right] d^3\bar{r}_1 d^3\bar{r}_2 \qquad (A.4)$$

The representation of r as a quadratic function of y_α is valid only for small y_α. But for larger values of y_α the integrand oscillates rapidly. Hence the integration over $\bar{y}_\alpha$ coordinates has been extended to infinity. The two dimensional spectral representation of $B_n(\bar{r}_1, \bar{r}_2)$ in a locally homogeneous, isotropic atmosphere, with smooth variations in vertical direction as in Eqs. (2.10e), (2.13) and (2.16) is

$$B_n(\bar{r}_1, \bar{r}_2) = \iint_{-\infty}^{\infty} F_n\left(\frac{x_1+x_2}{2}, x_1-x_2, \bar{\kappa}_\alpha\right) e^{-i\bar{\kappa}_\alpha \cdot (\bar{y}_{\alpha 1} - \bar{y}_{\alpha 2})} d^2\bar{\kappa}_\alpha \qquad (A.5)$$

Substituting the above expansion in the expression for $\left\langle \psi_1(\bar{r}')\psi_1^*(\bar{r}'') \right\rangle$,

$$\left\langle \psi_1(\bar{r}')\psi_1^*(\bar{r}'') \right\rangle = \left(\frac{k_a^2}{2\pi}\right)^2 x'x'' e^{-ik_a\left[\frac{y_\alpha'^2}{2x'} - \frac{y_\alpha''^2}{2x''}\right]} \int_{-\infty}^{\infty}\int_0^{x'}\int_0^{x''}$$

$$\cdot \frac{F_n\left(\frac{x_1+x_2}{2}\ ,\ x_1-x_2,\ \bar{\kappa}_\alpha\right)}{x_1x_2(x'-x_1)(x''-x_2)} I_1(x_1,\ \bar{y}_\alpha')I_2(x_2,\bar{y}_\alpha'')$$

$$\cdot\ dx_2\ dx_1\ d^2\bar{\kappa}_\alpha \qquad \text{(A.6)}$$

where

$$I_1(x_1,\bar{y}_\alpha') = \int_{-\infty}^{\infty}\int \exp\left[ik_a\left\{\frac{y_{\alpha 1}^2}{2x_1} + \frac{|\bar{y}_\alpha'-\bar{y}_{\alpha 1}|^2}{2(x'-x_1)}\right\} - i\bar{\kappa}_\alpha\cdot\bar{y}_{\alpha 1}\right] d^2\bar{y}_{\alpha 1} \qquad \text{(A.7)}$$

$$I_2(x_2,\bar{y}_\alpha'') = \int_{-\infty}^{\infty}\int \exp\left[-ik_a\left\{\frac{y_{\alpha 2}^2}{2x_2} + \frac{|\bar{y}_\alpha''-\bar{y}_{\alpha 2}|^2}{2(x''-x_2)}\right\} + i\bar{\kappa}_\alpha\cdot\bar{y}_{\alpha 2}\right] d^2\bar{y}_{\alpha 2} \qquad \text{(A.8)}$$

After some algebra,

$$I_1(x_1,\bar{y}_\alpha') = \left[\frac{2\pi i x_1(x'-x_1)}{x'k_a}\right] \exp\left[\frac{ik_a y_\alpha'^2}{2x'} - \frac{i\kappa_\alpha^2 x_1}{2k_a x'}(x'-x_1) - i\bar{\kappa}_\alpha\cdot\bar{y}_\alpha'\frac{x_1}{x'}\right] \qquad \text{(A.9)}$$

$$I_2(x_2,\bar{y}_\alpha'') = \left[\frac{-2\pi i x_2(x''-x_2)}{x''k_a}\right] \exp\left[-\frac{ik_a y_\alpha''^2}{2x''} + i\frac{\kappa_\alpha^2 x_2}{2k_a x''}(x''-x_2) + i\bar{\kappa}_\alpha\cdot\bar{y}_\alpha''\frac{x_2}{x''}\right] \qquad \text{(A.10)}$$

Then,

$$\left\langle \psi_1(\bar{r}')\psi_1^*(\bar{r}'') \right\rangle = k_a^2 \int_0^{x'}\int_0^{x''}\int_{-\infty}^{\infty}\int F_n\left(\frac{x_1+x_2}{2}\ ,\ x_1-x_2,\ \bar{\kappa}_\alpha\right)$$

$$\cdot\ \exp\left[\frac{-i\kappa_\alpha^2}{2k_a}\left\{\frac{x_1}{x'}(x'-x_1) - \frac{x_2}{x''}(x''-x_2)\right\}\right.$$

$$-i\bar{\kappa}_\alpha \cdot \left\{ \bar{y}'_\alpha \frac{x_1}{x'} - \bar{y}''_\alpha \frac{x_2}{x''} \right\} \Bigg] d^2\bar{\kappa}_\alpha dx_2 dx_1 \qquad \text{(A.11)}$$

Let $\frac{x'+x''}{2} = x$; $x'-x'' = \delta x$; $\frac{x_1+x_2}{2} = \eta$; $x_1-x_2 = \xi$

$\bar{y}_{\alpha p} = \frac{\bar{y}'_\alpha+\bar{y}''_\alpha}{2}$; $\bar{y}_{\alpha m} = \bar{y}'_\alpha-\bar{y}''_\alpha$; $F_n(\eta, |\xi|, \bar{\kappa}_\alpha) \simeq 0$ for $|\xi| \gtrsim L_0$, the outer scale of turbulence. δx is of the order of few λ_a; its maximum value being the number of cycles in the acoustic pulse times λ_a. Contributions to the expression in the above equation come from lower values of ξ, also $|\delta x/x| \ll 1$. Hence terms that include ξ and $\delta x/x$ in the exponent will be neglected. Extending the limits of integration on ξ to ∞

$$\left\langle \psi_1(\bar{r}')\psi_1^*(\bar{r}'') \right\rangle = 2k_a^2 \int_0^x \int_0^\infty \iint_{-\infty}^{\infty} F_n(\eta,\xi, \bar{\kappa}_\alpha)$$

$$\cdot \exp\left[-i\frac{\kappa_\alpha^2}{2k_a} \delta x \left(\frac{\eta}{x}\right)^2 - i\bar{\kappa}_\alpha \cdot \bar{y}_{\alpha m} \frac{\eta}{x} \right] d^2\bar{\kappa}_\alpha d\xi d\eta \qquad \text{(A.12)}$$

since $\int_0^\infty F_n(\eta,\xi, \bar{\kappa}_\alpha)d\xi = \pi\Phi_n(\eta, \bar{\kappa}_\alpha)$ (A.13)

$$\left\langle \psi_1(\bar{r}')\psi_1^*(\bar{r}'') \right\rangle = 2\pi k_a^2 \int_0^x \iint_{-\infty}^{\infty} \Phi_n(\eta, \bar{\kappa}_\alpha)$$

$$\cdot \exp\left[-i\frac{\kappa_\alpha^2}{2k_a} \delta x \left(\frac{\eta}{x}\right)^2 - i\bar{\kappa}_\alpha \cdot \bar{y}_{\alpha m} \frac{\eta}{x} \right] d^2\bar{\kappa}_\alpha d\eta \qquad \text{(A.14)}$$

Since the turbulence is isotropic, and

$$\int_0^{2\pi} \exp\left[-i\kappa_\alpha y_{\alpha m} \frac{\eta}{x} \cos\theta\right] d\theta = 2\pi J_0\left(\kappa_\alpha y_{\alpha m} \frac{\eta}{x}\right) \tag{A.15}$$

where $J_0(\cdot)$ is a Bessel function of first kind and zeroth order, then

$$\left\langle \psi_1(\bar{r}')\psi_1^*(\bar{r}'')\right\rangle = 4\pi^2 k_a^2 \int_0^x \int_0^\infty \kappa_\alpha \Phi_n(\eta, \kappa_\alpha) \exp\left[-i\frac{\kappa_\alpha^2}{2k_a} \delta x \left(\frac{\eta}{x}\right)^2\right]$$

$$\cdot J_0\left(\kappa_\alpha y_{\alpha m} \frac{\eta}{x}\right) d\kappa_\alpha d\eta \tag{A.16}$$

For a Kolmogorov spectrum, the exponent part of the integrand is almost unity over the useful range of integrating variables for typical values of acoustic pulse length. As a result

$$\left\langle \psi_1(\bar{r}')\psi_1^*(\bar{r}'')\right\rangle = 4\pi^2 k_a^2 \int_0^x \int_0^\infty \kappa_\alpha \Phi_n(\eta, \kappa_\alpha) J_0\left(\kappa_\alpha y_{\alpha m} \frac{\eta}{x}\right) d\kappa_\alpha d\eta \tag{A.17}$$

This equation is used in computing the coherence length and coherence function of vertical acoustic wave propagation. Evaluation of $\left\langle |\psi_1(x, \bar{y}_\alpha)|^2\right\rangle$ is as follows. From Eq. (A.17),

$$\left\langle |\psi_1(x, \bar{y}_\alpha)|^2\right\rangle = (2\pi k_a)^2 \int_0^x \int_0^\infty \kappa_\alpha \Phi_n(\eta, \kappa_\alpha) d\kappa_\alpha d\eta \tag{A.18}$$

Using Eqs. (2.20) and (2.23),

$$\left\langle |\psi_1(x, \bar{y}_\alpha)|^2 \right\rangle = (2\pi k_a)^2 \int_0^x \int_{t_o^{-1}(\eta)}^{\infty} \kappa_\alpha \, 0.033 \, C_{no}^2 \left(\frac{\eta}{x_o}\right)^{-m_a} \kappa_\alpha^{-11/3} d\kappa_\alpha d\eta \qquad (A.19)$$

$$\left\langle |\psi_1(x, \bar{y}_\alpha)|^2 \right\rangle = (0.0365) C_{no}^2 k_a^2 A^{5/3} \left(\frac{x}{x_o}\right)^{-m_a} \frac{x^{11/6}}{\left(\frac{11}{6} - m_a\right)} \qquad (A.20)$$

Appendix B

CONTRIBUTION OF DOUBLE-SCATTERING TERM TO THE MEAN GREEN'S FUNCTION OF A SPHERICAL ACOUSTIC WAVE PROPAGATING IN A TURBULENT ATMOSPHERE

To compute the first statistical moment of the acoustic wave, it is necessary to determine the contribution of the double-scattering term in Eq. (4.17) to the mean of a spherical acoustic wave propagating in a turbulent atmosphere. The second term in the diagrammatic series in Eq. (4.17) is defined as $G_{ao}(\bar{r},0)\, I(x,\bar{y}_\alpha)$, and $I(x,\bar{y}_\alpha)$ is computed in this appendix. The mathematics is the same as in Appendix A, and like algebra follows in Eq. (4.18).

$$I(x,\bar{y}_\alpha) = \left(\frac{-2k_a^2}{4\pi}\right)^2 \iint\limits_{x_2 \geq x_1} \left\langle n_1(\bar{r}_1) n_1(\bar{r}_2) \right\rangle \cdot \frac{e^{ik_a\{|\bar{r}-\bar{r}_2| + |\bar{r}_2-\bar{r}_1| + r_1 - r\}}}{|\bar{r}-\bar{r}_2|\,|\bar{r}_2-\bar{r}_1|} \frac{r}{r_1} d^3\bar{r}_1 d^3\bar{r}_2 \qquad (B.1)$$

Using the paraxial approximation

$$I(x,\bar{y}_\alpha) = x\left(\frac{k_a^2}{2\pi}\right)^2 \iint\limits_{x_2 \geq x_1} \frac{B_n(\bar{r}_1,\bar{r}_2)}{(x-x_2)(x_2-x_1)x_1} \cdot \exp\left[ik_a\left\{\frac{|\bar{y}_\alpha-\bar{y}_{\alpha 2}|^2}{2(x-x_2)} + \frac{|\bar{y}_{\alpha 2}-\bar{y}_{\alpha 1}|^2}{2(x_2-x_1)} + \frac{y_{\alpha 1}^2}{2x_1} - \frac{y_\alpha^2}{2x}\right\}\right] \cdot d^3\bar{r}_1 d^3\bar{r}_2 \qquad (B.2)$$

From Eqs. (2.10e), (2.13) and (2.16)

$$B_n(\bar{r}_1,\bar{r}_2) = \iint_{-\infty}^{\infty} F_n\left(\frac{x_1+x_2}{2},\ |x_1-x_2|,\ \bar{\kappa}_\alpha\right) e^{-\bar{\kappa}_\alpha \cdot (\bar{y}_{\alpha 1}-\bar{y}_{\alpha 2})}\, d^2\bar{\kappa}_\alpha \qquad (B.3)$$

Note that F_n depends on $|x_1-x_2|$. From Eqs. (B.2) and (B.3)

$$I(x,\bar{y}_\alpha) = x\left(\frac{k_a^2}{2\pi}\right)^2 \int_0^x \int_0^{x_2} \iint_{-\infty}^{\infty} \frac{F_n\left(\frac{x_1+x_2}{2},\ |x_1-x_2|,\ \bar{\kappa}_\alpha\right)}{(x-x_2)(x_2-x_1)x_1}$$

$$\cdot\ I_a(x,\bar{y}_\alpha)\, d^2\bar{\kappa}_\alpha\, dx_1\, dx_2 \qquad (B.4)$$

where

$$I_a(x,\bar{y}_\alpha) = \iint_{-\infty}^{\infty}\iint_{-\infty}^{\infty} \exp\left[ik_a\left\{\frac{|\bar{y}_\alpha-\bar{y}_{\alpha 2}|^2}{2(x-x_2)} + \frac{|\bar{y}_{\alpha 2}-\bar{y}_{\alpha 1}|^2}{2(x_2-x_1)} + \frac{y_{\alpha 1}^2}{2x_1} - \frac{y_\alpha^2}{2x}\right\}\right.$$

$$\left. - i\bar{\kappa}_\alpha \cdot (\bar{y}_{\alpha 1}-\bar{y}_{\alpha 2})\right] d^2\bar{y}_{\alpha 1}\, d^2\bar{y}_{\alpha 2} \qquad (B.5)$$

Because

$$\int_{-\infty}^{\infty}\exp\left[ik_a\left\{\frac{|\bar{y}_{\alpha 2}-\bar{y}_{\alpha 1}|^2}{2(x_2-x_1)} + \frac{y_{\alpha 1}^2}{2x_1}\right\} - i\bar{\kappa}_\alpha\cdot\bar{y}_{\alpha 1}\right] d^2\bar{y}_{\alpha 1} =$$

$$\left[\frac{2\pi i x_1(x_2-x_1)}{x_2 k_a}\right]\exp\left[\frac{ik_a y_{\alpha 2}^2}{2x_2} - \frac{i\kappa_\alpha^2 x_1(x_2-x_1)}{2k_a x_2} - i\bar{\kappa}_\alpha\cdot\bar{y}_{\alpha 2}\frac{x_1}{x_2}\right] \qquad (B.6)$$

then,

$$I_a(x,\bar{y}_\alpha) = \left[\frac{2\pi i x_1(x_2-x_1)}{x_2 k_a}\right]\exp\left[-ik_a\frac{y_\alpha^2}{2x} - \frac{i\kappa_\alpha^2 x_1(x_2-x_1)}{2k_a x_2}\right]$$

$$\cdot \int_{-\infty}^{\infty}\exp\left[ik_a\left\{\frac{|\bar{y}_\alpha-\bar{y}_{\alpha 2}|^2}{2(x-x_2)} + \frac{y_{\alpha 2}^2}{2x_2}\right\} - i\bar{\kappa}_\alpha\cdot\bar{y}_{\alpha 2}\left(-1+\frac{x_1}{x_2}\right)\right] d^2\bar{y}_{\alpha 2} = \qquad (B.7)$$

$$\left[\frac{2\pi i x_1(x_2-x_1)}{x_2 k_a}\right] \exp\left[-ik_a \frac{y_\alpha^2}{2x} - \frac{i\kappa_\alpha^2 x_1(x_2-x_1)}{2k_a x_2}\right]\left[\frac{2\pi i x_2(x-x_2)}{x k_a}\right]$$

$$\cdot \exp\left[\frac{ik_a y_\alpha^2}{2x} - \frac{i\kappa_\alpha^2}{2k_a}\left(\frac{x_1}{x_2}-1\right)^2 \frac{x_2}{x}(x-x_2) - i\bar{\kappa}_\alpha \cdot \bar{y}_\alpha\left(\frac{x_1}{x_2}-1\right)\frac{x_2}{x}\right] \qquad \text{(B.7 contd.)}$$

$$I_a(x,\bar{y}_\alpha) = -\left(\frac{2\pi}{k_a}\right)^2 \frac{x_1(x-x_2)(x_2-x_1)}{x}$$

$$\cdot \exp\left[i\bar{\kappa}_\alpha \cdot \bar{y}_\alpha \frac{(x_2-x_1)}{x} - \frac{i\kappa_\alpha^2}{2k_a}(x_2-x_1)\left\{1 - \frac{(x_2-x_1)}{x}\right\}\right] \qquad \text{(B.8)}$$

From Eqs. (B.4) and (B.8)

$$I(x,\bar{y}_\alpha) = -k_a^2 \int_0^x \int_0^{x_2} \iint_{-\infty}^{\infty} F_n\left(\frac{x_1+x_2}{2}, x_2-x_1, \bar{\kappa}_\alpha\right)$$

$$\cdot \exp\left[i\bar{\kappa}_\alpha \cdot \bar{y}_\alpha \frac{(x_2-x_1)}{x} - \frac{i\kappa_\alpha^2}{2k_a}(x_2-x_1)\left\{1 - \frac{(x_2-x_1)}{x}\right\}\right] d^2\bar{\kappa}_\alpha \, dx_1 \, dx_2 \qquad \text{(B.9)}$$

Let $x_2 - x_1 = \xi$; $\frac{x_1+x_2}{2} = \eta$ and as in Appendix A,

$$I(x,\bar{y}_\alpha) = -k_a^2 \int_0^x \int_{-\infty}^{\infty} \iint_{-\infty}^{\infty} F_n(\eta,\xi,\bar{\kappa}_\alpha)\, d^2\bar{\kappa}_\alpha \, d\xi \, d\eta \qquad \text{(B.10)}$$

It then follows from Eq. (A.12) that

$$I(x,\bar{y}_\alpha) = -\frac{1}{2}\left\langle |\psi_1(x,\bar{y}_\alpha)|^2 \right\rangle \qquad \text{(B.11)}$$

APPENDIX C

SIMPLIFICATION OF $I(x, \hat{\theta}/2, y_{\alpha m})$

To determine the intensity of the RASS received signal, it is necessary to compute $\langle |E_1|^2 \rangle$ which is the ensemble average of $|E_1|^2$. This quantity is derived by the simplification of $I(x, \hat{\theta}/2, y_{\alpha m})$ in Eq. (5.38).

$$I(x, \hat{\theta}/2, y_{\alpha m}) = \int_{D'} \int_{D''} M(x, y_{\alpha m})\, d^2\bar{y}'_\alpha d^2\bar{y}''_\alpha \qquad (C.1)$$

D' and D" are circles of radii $x'\hat{\theta}/2$ and $x''\hat{\theta}/2$, respectively. Repeating for convenience, the definitions given in Chapter V,

$$x = (x' + x'')/2;\ \bar{y}_{\alpha m} = (\bar{y}'_\alpha - \bar{y}''_\alpha);\ \bar{y}_{\alpha p} = (\bar{y}'_\alpha + \bar{y}''_\alpha)/2 \qquad (C.2)$$

$$d'_a = x'\,\hat{\theta}/2;\ d''_a = x''\,\hat{\theta}/2;\ \text{and}\ d_a = x\,\hat{\theta}/2 \qquad (C.3)$$

$$W(y_\alpha) = \begin{cases} 1 & y_\alpha \le d_a \qquad (C.4a) \\ 0 & y_\alpha > d_a \qquad (C.4b) \end{cases}$$

the above integral can be written as

$$I(x, \hat{\theta}/2, y_{\alpha m}) = \iint W(y'_\alpha)\, W(y''_\alpha)\, M(x, y_{\alpha m})\, d^2\bar{y}'_\alpha\, d^2\bar{y}''_\alpha \qquad (C.5)$$

Making the change of variables to $\bar{y}_{\alpha m}$ and $\bar{y}_{\alpha p}$ results in

$$I(x,\hat{\theta}/2,\ y_{\alpha m}) = \int M(x,y_{\alpha m})\ \ A_a(x,\hat{\theta}/2,y_{\alpha m})d^2\bar{y}_{\alpha m} \qquad (C.6)$$

where

$$A_a(x,\hat{\theta}/2,y_{\alpha m}) = \int W\left(|\bar{y}_{\alpha p} + \frac{\bar{y}_{\alpha m}}{2}|\right)\ W\left(\left|\bar{y}_{\alpha p} - \frac{\bar{y}_{\alpha m}}{2}\right|\right)\ d^2\bar{y}_{\alpha p} \qquad (C.7)$$

This double integral, is the overlap area of two circles of radii d_a' and d_a''. Since $x' \simeq x''$; $A_a(x,\hat{\theta}/2,\ y_{\alpha m})$ is evaluated as in Fried [1967]

$$A_a(x,\hat{\theta}/2,y_{\alpha m}) = \begin{cases} 1/2\left[4d_a^2\ \cos^{-1}\left\{y_{\alpha m}/(2d_a)\right\} - y_{\alpha m}(4d_a^2 - y_{\alpha m}^2)^{1/2}\right] & \\ & y_{\alpha m} \le 2d_a \\ 0 & y_{\alpha m} > 2d_a \end{cases} \qquad (C.8)$$

The maximum value of the above expression is πd_a^2. $A_a(x,\hat{\theta}/2,y_{\alpha m})/(\pi d_a^2)$ is plotted in Fig. 13. From Eq. (C.6), $I(x,\hat{\theta}/2,y_{\alpha m})$ does

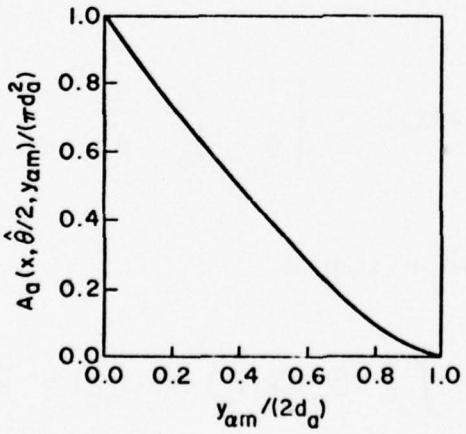

FIG. 13. THE OVERLAP INTEGRAL VS $y_{\alpha m}/(2d_a)$

not depend on the orientation of $\bar{y}_{\alpha m}$; therefore,

$$I(x,\hat{\theta}/2,y_{\alpha m}) = 2\pi \int_0^{2d_a} y_{\alpha m}\, M(x,y_{\alpha m})\, A_a(x,\hat{\theta}/2,y_{\alpha m})\, dy_{\alpha m} \qquad (C.9)$$

APPENDIX D.

COMPUTATION OF POWER-REFLECTION COEFFICIENT IN THE PRESENCE OF A LINEAR TEMPERATURE PROFILE

The mathematics involving the computation of received power in an atmosphere with a linear temperature profile is considered in this Appendix. It can be observed from Eq. (5.49) that the phase of the acoustic wave has a quadratic dependence, and, therefore, use is made of Fresnel sine and cosine integrals. The quantity F [defined in Eqs. (5.49) and (5.50)] is evaluated

$$F = \int_{R_2}^{R_1} \cos[k_a r - \eta r^2]\, e^{-i(2k_e r - \alpha)}\, dr \qquad (D.1)$$

$$\eta = a_g k_a/(4T_o) \; . \qquad (D.2)$$

and α is a constant. Initially, the Fresnel sine and cosine integrals are defined as follows [Abramowitz and Stegun, 1968],

$$C_f(x) = \int_0^x \cos\left(\frac{\pi}{2} t^2\right) dt \qquad (D.3a)$$

$$S_f(x) = \int_0^x \sin\left(\frac{\pi}{2} t^2\right) dt \qquad (D.3b)$$

Some useful properties of these integrals are

$$C_f(x) \to 1/2 \; ; \; S_f(x) \to 1/2 \quad \text{as} \quad x \to \infty \qquad (D.4)$$

$$C_f(x) \simeq x \; ; \; S_f(x) \simeq \frac{\pi}{6} x^3 \quad \text{as} \quad x \to 0 \qquad (D.5)$$

$$C_f(-x) = -C_f(x) \; ; \; S_f(-x) = -S_f(x) \qquad (D.6)$$

Using these properties, F is evaluated to be

$$
\begin{aligned}
F = \sqrt{\frac{\pi}{8\eta}} \Bigg\{ & \cos(\eta R_m^2 + \alpha)[C_f(A_m) - C_f(B_m)] \\
& + \sin(\eta R_m^2 + \alpha)[S_f(A_m) - S_f(B_m)] \\
& + \cos(\eta R_p^2 - \alpha)[C_f(A_p) - C_f(B_p)] \\
& + \sin(\eta R_p^2 - \alpha)[S_f(A_p) - S_f(B_p)] \\
+ i \Bigg[& \cos(\eta R_m^2 + \alpha)[-S_f(A_m) + S_f(B_m)] \\
& + \sin(\eta R_m^2 + \alpha)[C_f(A_m) - C_f(B_m)] \\
& + \cos(\eta R_p^2 - \alpha)[S_f(A_p) - S_f(B_p)] \\
& - \sin(\eta R_p^2 - \alpha)[C_f(A_p) - C_f(B_p)] \Bigg] \Bigg\}
\end{aligned}
\tag{D.7}
$$

where

$$\beta = a_g \lambda_a / T_o \tag{D.8}$$

$$R_m = \frac{2\lambda_a}{\beta}\left(1 - \frac{2\lambda_a}{\lambda_e}\right); \quad R_p = \frac{2\lambda_a}{\beta}\left(1 + \frac{2\lambda_a}{\lambda_e}\right) \tag{D.9}$$

$$A_m = \sqrt{\frac{2}{\pi}\eta}\,(R_1 - R_m); \quad B_m = \sqrt{\frac{2}{\pi}\eta}\,(R_2 - R_m) \tag{D.10}$$

$$A_p = \sqrt{\frac{2}{\pi}\eta}\,(R_1 - R_p); \quad B_p = \sqrt{\frac{2}{\pi}\eta}\,(R_2 - R_p) \tag{D.11}$$

After scaling the variables by λ_a

$$R_1' = R_1/\lambda_a \quad ; \quad R_2' = R_2/\lambda_a \tag{D.12}$$

$$R_m' = R_m/\lambda_a = \frac{2}{\beta}\left(1 - \frac{2\lambda_a}{\lambda_e}\right) \tag{D.13}$$

$$R_p' = R_p/\lambda_a = \frac{2}{\beta}\left(1 + \frac{2\lambda_a}{\lambda_e}\right) \tag{D.14}$$

$$\sqrt{\frac{2\eta}{\pi}} = \frac{\sqrt{\beta}}{\lambda_a} \quad ; \sqrt{\frac{\pi}{8\eta}} = \frac{\lambda_a}{2\sqrt{\beta}} \tag{D.15}$$

$$A_m = \sqrt{\beta}\ R_1' - \frac{2}{\sqrt{\beta}}\left(1 - \frac{2\lambda_a}{\lambda_e}\right) \tag{D.16}$$

$$B_m = \sqrt{\beta}\ R_2' - \frac{2}{\sqrt{\beta}}\left(1 - \frac{2\lambda_a}{\lambda_e}\right) \tag{D.17}$$

$$A_p = \sqrt{\beta}\ R_1' - \frac{2}{\sqrt{\beta}}\left(1 + \frac{2\lambda_a}{\lambda_e}\right) \tag{D.18}$$

$$B_p = \sqrt{\beta}\ R_2' - \frac{2}{\sqrt{\beta}}\left(1 + \frac{2\lambda_a}{\lambda_e}\right) \tag{D.19}$$

$$\eta R_m^2 = \frac{2\pi}{\beta}\left(1 - \frac{2\lambda_a}{\lambda_e}\right)^2 \tag{D.20}$$

$$\eta R_p^2 = \frac{2\pi}{\beta}\left(1 + \frac{2\lambda_a}{\lambda_e}\right)^2 \tag{D.21}$$

For $a_g \simeq 10$ °K/km and $T_o \simeq 300$°K; $|R_p| > |(2\lambda_a)/\beta| = |(2T_o)/a_g| \simeq$ 60 km. Hence $|R_p|$ is much larger than R_1 and R_2 for ranges under consider ($\leq$ 10 kilometers). Then,

$$|S_f(A_p) - S_f(B_p)| \to 0 \; ; \qquad |C_f(A_p) - C_f(B_p)| \to 0$$

Therefore,

$$F \simeq \frac{1}{2} e^{i(\eta R_m^2 + \alpha)} \int_{R_2 - R_m}^{R_1 - R_m} e^{-i\eta x^2} dx \tag{D.22}$$

If $\alpha = -\eta R_m^2$, x is the altitude of the acoustic pulse, the length of the acoustic-wave train is short, and $R_1 - R_2 = n_{ac}\lambda_a$, then $|F| \simeq n_{ac}\lambda_a/2$ which is the maximum value of $|F|$. This maximum value of $|F|$ occurs when $2\lambda_a/\lambda_e = [1 - \beta x/(2\lambda_a)]$. The modified Bragg-scatter condition for the coherent reflection of electromagnetic energy from an acoustic pulse at x for $|\beta x/(2\lambda_a)| << 1$, therefore, is

$$\frac{\lambda_e}{\lambda_a} \simeq 2\left[1 + \frac{a_g x}{2\bar{T}_o}\right] \tag{D.23}$$

which can be explained by the fact that peak power is reflected back when the interaction between electromagnetic and acoustic waves is maximum.

APPENDIX E

COMPUTATION OF NORMALIZED RECEIVED POWER IN THE PRESENCE OF HORIZONTAL WINDS

The mathematical details involving the computation of received power in the presence of constant horizontal winds are presented in this appendix. An asymptotic expression for the received power is derived, using an asymptotic expression for a Bessel function of the first kind and zeroth order $J_o(x)$. Equations (5.66) and (5.67) define F_w as a quantity proportional to the strength of the received signal

$$F_w = \int_{V_{as}} \cos S_w(\bar{r}') \, e^{-i(2k_e r' - \alpha)} \, d^3\bar{r}' \tag{E.1}$$

$$S_w(\bar{r}) = k_a r \left[1 - \frac{\langle \bar{w} \rangle}{c_o} \cdot \hat{r} \right] \tag{E.2}$$

where

$$\hat{r} = (\cos\theta, \cos\zeta \sin\theta, \sin\zeta \sin\theta) \tag{E.3a}$$

$$\langle \bar{w} \rangle = \left(\langle w_x \rangle, \langle w_y \rangle, \langle w_z \rangle \right) \tag{E.3b}$$

$$\langle w_x \rangle = 0; \quad \langle w_y \rangle = \text{constant}; \quad \langle w_z \rangle = \text{constant}$$

$$\langle w_y \rangle = w_h \cos\phi_w \; ; \quad \langle w_z \rangle = w_h \sin\phi_w \tag{E.3c}$$

$$\text{and} \quad w_h^2 = \langle w_y \rangle^2 + \langle w_z \rangle^2 \tag{E.3d}$$

then from Eq. (E.2)

$$S_w(\bar{r}) = k_a r \left[1 - \frac{w_h}{c_o} \cos(\zeta - \phi_w) \sin\theta \right] \tag{E.4}$$

Some useful definitions and properties of the Bessel function of first kind and zeroth order are listed below [Watson, 1966]:

$$J_o(x) = \frac{1}{2\pi} \int_{\alpha}^{2\pi+\alpha} e^{-ix \sin\theta} \, d\theta \quad \text{where } \alpha \text{ is any angle} \tag{E.5}$$

$$J_o(-x) = J_o(x) \tag{E.6}$$

$$J_o(x) \simeq 1 - \frac{x^2}{4} \quad \text{for } x \to 0 \tag{E.7}$$

$$J_o(x) \simeq \sqrt{\frac{2}{\pi x}} \cos\left(x - \frac{\pi}{4}\right) \quad \text{for } x \gg 1 \tag{E.8}$$

Using these properties,

$$F_w = \pi x^2 \int_{R_2}^{R_1} \int_{0}^{\hat{\theta}/2} \left[e^{i\{(k_a-2k_e)r'+\alpha\}} + e^{i\{(-k_a-2k_e)r'+\alpha\}}\right] \cdot J_o\left(k_a r' \frac{w_h}{c_o} \sin\theta\right) \sin\theta \, d\theta \, dr' \tag{E.9}$$

Let x be the height of the acoustic pulse. Because $|\sin\theta| \leq 1$, $k_a x \, w_h/c_o \ll 1$ implies that the effect of horizontal winds can be neglected and $F_w \simeq F_{wmax}$ as in Eq.(5.68). For $k_a x \hat{\theta} w_h/c_o \gg 1$ and $\hat{\theta} < 1$, a large-argument approximation for $J_o(\cdot)$ in Eq. (E.9) can be used. This approximation, however, is not good over the entire range of θ because the argument of the Bessel function becomes 0 for $\theta = 0$. This approximation gives rise to a minor error in the final result because the integrand has $\sin\theta$ as a factor. In addition, $\sin\theta \simeq \theta$ for $\sin(\hat{\theta}/2)$ is small; therefore

$$F_w = \pi x^2 \int_{R_2}^{R_1} \left[e^{i\{(k_a-2k_e)r'+\alpha\}} + e^{i\{(-k_a-2k_e)r'+\alpha\}}\right] \cdot I_\theta(r') dr' \tag{E.10}$$

where

$$I_\theta(r') = \left(\frac{2}{\pi k_a r' \, w_h/c_o}\right)^{1/2} \int_0^{\hat{\theta}/2} \theta^{1/2} \cos\left(k_a r' \frac{w_h}{c_o}\theta - \frac{\pi}{4}\right) d\theta \quad \text{(E.11)}$$

Using Erdélyi's theorem [Popoulis, 1968], $I_\theta(r')$ is evaluated asymptotically to be

$$I_\theta(r') = \left(\frac{\hat{\theta}}{\pi}\right)^{1/2}\left(k_a r' \frac{w_h}{c_o}\right)^{-3/2} \sin\left(k_a r' \frac{w_h}{c_o}\frac{\hat{\theta}}{2} - \frac{\pi}{4}\right) \quad \text{(E.12)}$$

Note that the sinusoidal term in this equation varies little over the acoustic pulse when $n_{ac}(w_h/c_o)(\hat{\theta}\,\pi)$ is much less than unity. Under the Bragg-scatter condition $\lambda_e = 2\lambda_a$ and using Eqs. (5.68), (E.10), and (E.12), therefore

$$\frac{|F_w|^2}{F_{wmax}^2} = \frac{20.37 \cos^2[k_a x\,\hat{\theta}\, w_h/(2c_o) - 3\pi/4]}{(k_a x\,\hat{\theta}\, w_h/c_o)^3} \quad \text{(E.13)}$$

Because

$$P_{rw}/P_{rmax} = |F_w|^2/F_{wmax}^2 \quad \text{(E.14)}$$

where P_{rw} is the power received in presence of horizontal winds and P_{rmax}, given by Eq. (5.41), is the power received in a static atmosphere. Therefore

$$\frac{P_{rw}}{P_{rmax}} = \frac{20.37 \cos^2[k_a x\,\hat{\theta}\, w_h/(2c_o) - 3\pi/4]}{(k_a x\,\hat{\theta}\, w_h/c_o)^3} \quad \text{(E.15)}$$

where $k_a x\,\hat{\theta}\, w_h/c_o \gg 1$.

BIBLIOGRAPHY

Abramowitz, M. and I. A. Stegun (1968), Handbook of Mathematical Functions, Dover Publications, Inc., New York.

Barabanenkov, Yu. N., Yu. A. Kravtsov, S. M. Rytov, and V. I. Tatarskii (1971), "Status of the Theory of Propagation of Waves in a Randomly Inhomogeneous Medium," Soviet Physics, Uspekhi, Vol. 13, No. 5, pp. 551-575.

Bogoliubov, N. N. and Y. A. Mitropolsky (1961), Asymptotic Methods in the Theory of Non-linear Oscillations, Translated from Russian, Hindustan Publishing Corp., Delhi.

Bean, B. R. and E. J. Dutton (1968), Radio Meteorology, Dover Publications, Inc., New York.

Bremmer, H. (1964), "Random Volume Scattering," Radio Science, Vol. 68D, No. 9, pp. 967-981.

Brown, E. H., and R. J. Keeler (1975), "Application of Propagation Parameters to Atmospheric Echosondes," Radar Meteorology Conference, Vol. 16, Houston, Amer. Meteor. Soc., Boston, Mass., pp. 272-277.

Clifford, S. F. and E. H. Brown (1970), "Propagation of Sound in a Turbulent Atmosphere," J. Acoustical Society of America, Vol. 48, No. 5 (Part 2), pp. 1123-1127.

Fante, R. L. (1975), "Electromagnetic Beam Propagation in Turbulent Media," Proc. of the IEEE, Vol. 63, No. 12, pp. 1669-1692.

Feynman, R. P. (1948), "Space time Approach to Nonrelativistic Quantun Mechanics," Rev. Modern Phys., 20, pp. 367-387.

Frankel, M. S, N. J. F. Chang and M. J. Sanders (1977), "A High Frequency Radio Acoustic-Sounder for Remote Measurement of Atmospheric Winds and Temperature," submitted to Bull. Amer. Meteorol. Soc.

Frankel, M. S and A. M. Peterson (1976), "Remote temperature profiling in the lower troposphere," Radio Science, Vol. 11, No. 3, pp. 157-166.

Fried, D. L. (1967), "Optical Heterodyne Detection of an Atmospherically Distorted Signal Wave-Front," Proc. of the IEEE, Vol. 55, No. 1, pp. 57-67.

Frisch, U. (1968), "Wave Propagation in Random Medium," Probabilistic Methods in Applied Mathematics, Vol. I, Ed. A. T. Bharucha-Reid, Academic Press, New York, pp. 75-198.

Gray, D. A. and A. T. Waterman (1970), "Measurement of fine-scale atmospheric structure using an optical propagation technique," J. Geophys. Res., Vol. 75, No. 6, pp. 1077-1083.

Gill, T. P. (1965), The Doppler Effect, Logos Press Ltd. and Elek Books Ltd., London.

Kolmogorov, A. N. (1941), "The local structure of turbulence in incompressible viscous fluid for very large Reynold's numbers," Doklady Akad. Nauk SSR, 30(4):229; English translation in Turbulence, Classic Papers on Statistical Theory, S. K. Friedlander and L. Topper, Eds., Interscience, N. Y., pp. 151-155, 1961.

Landau, L. D. and E. M. Lifshitz (1959), Fluid Mechanics, Pergammon Press, London Addison-Wesley Publishing Company, Inc., Reading, Mass.

Lawrence, R. S. and J. W. Strohbehn (1970), "A Survey of Clear-Air Propagation Effects Relevant to Optical Communication," Proc. of the IEEE, Vol. 58, No. 10, pp. 1523-1545.

Little, C. G. (1969), "Acoustic Methods for the Remote Sensing of the Lower Atmosphere," Proc. of the IEEE, Vol. 57, No. 4, pp. 571-578.

Lutomirski, R. and H. Yura (1971), "Wave Structure Function and Mutual Coherence Function of an Optical Wave in a Turbulent Atmosphere," J. Optical Society of America, Vol. 61, No. 4, pp. 482-487.

Marshall, J. M. (1972), A Radio Acoustic Sounding System for the Remote Measurement of Atmospheric Parameters, Sci. Rep. No. 39, SU-SEL-72-003, Stanford Electronics Laboratories, Stanford, California.

Nayfeh, A. H. (1973), Perturbation Methods, John Wiley & Sons, Inc., New York.

North, E. M. (1974), A Radio Acoustic Sounding System for Remote Measurement of Atmospheric Temperature, Tech. Rep. No. 1, SU-SEL-73-021, Stanford Electronics Laboratories, Stanford, California.

Papoulis, A. (1968), Systems and Transforms with Applications in Optics, McGraw Hill, New York.

Prokhorov, A. M., F. V. Bunkin, K. S. Gochelashvily, and V. I. Shishov (1975), "Laser Irradiance Propagation in Turbulent Media," Proc. of the IEEE, Vol. 63, No. 5, pp. 790-811.

Schmeltzer, R. A. (1967), "Means, Variances, and Covariances for Laser Beam Propagation Through a Random Medium," Quart. Appl. Math., Vol. 24, pp. 339-354.

Strohbehn, J. W. (1968), "Line of Sight Wave Propagation through the Turbulent Atmosphere," Proc. of the IEEE, Vol. 56, No. 8, pp. 1301-1318.

Strohbehn, J. W. (1971), "Optical Propagation through the Turbulent Atmosphere," Progress in Optics, Vol. IX, Ed. E. Wolf, North Holland Publishing Co., Amsterdam, London.

Tatarskii, V. I. (1961), Wave Propagation in a Turbulent Medium, English Translation by R. A. Silverman, McGraw Hill, New York.

Tatarskii, V. I. (1971), The Effects of the Turbulent Atmosphere on Wave Propagation, NTIS, U.S. Dept. of Commerce, Springfield, Virginia.

Taylor, L. S. (1968), "Validity of Ray-Optics Calculations in a Turbulent Atmosphere," J. Optical Society of America, Vol. 58, No. 1, pp. 57-59.

Watson, G. N. (1966), A Treatise on the Theory of Bessel Functions, Cambridge University Press, London.

Yaglom, A. M. (1962), An Introduction to the Theory of Stationary Random Functions, Dover Publications Inc., New York.

Yeh, K. C. and C. H. Liu (1972), Theory of Ionospheric Waves, Academic Press, New York.

Yura, H. (1972), "Mutual Coherence Function of a Finite Cross-Section Optical Beam Propagating in a Turbulent Medium," Appl. Opt., Vol. 11, pp. 1399-1406.

SECURITY CLASSIFICATION OF THIS PAGE (When Data Entered)

REPORT DOCUMENTATION PAGE		READ INSTRUCTIONS BEFORE COMPLETING FORM
1. REPORT NUMBER SEL-77-031	2. GOVT ACCESSION NO.	3. RECIPIENT'S CATALOG NUMBER
4. TITLE (and Subtitle) Interaction of Electromagnetic and Acoustic Waves in a Stochastic Atmosphere		5. TYPE OF REPORT & PERIOD COVERED Final Report
		6. PERFORMING ORG. REPORT NUMBER SEL-77-031
7. AUTHOR(s) Nirdosh Bhatnagar		8. CONTRACT OR GRANT NUMBER(s) N00014-75-C-0601
9. PERFORMING ORGANIZATION NAME AND ADDRESS Center for Radar Astronomy Stanford Electronics Laboratories Stanford University, Stanford CA 94305		10. PROGRAM ELEMENT, PROJECT, TASK AREA & WORK UNIT NUMBERS
11. CONTROLLING OFFICE NAME AND ADDRESS U. S. Navy Office of Naval Research		12. REPORT DATE July 1977 13. NO. OF PAGES 111
14. MONITORING AGENCY NAME & ADDRESS (if diff. from Controlling Office)		15. SECURITY CLASS. (of this report) Unclassified 15a. DECLASSIFICATION/DOWNGRADING SCHEDULE

16. DISTRIBUTION STATEMENT (of this report)
This document has been approved for public release and sale; its distribution is unlimited. Reproduction in whole or in part is permitted for any purpose of the United States Government.

17. DISTRIBUTION STATEMENT (of the abstract entered in Block 20, if different from report)

18. SUPPLEMENTARY NOTES

19. KEY WORDS (Continue on reverse side if necessary and identify by block number)
Electromagnetic waves, acoustic waves, stochastic atmosphere, atmospheric temperature, horizontal winds.

20. ABSTRACT (Continue on reverse side if necessary and identify by block number)
In the Stanford Radio Acoustic Sounding System (RASS), an electromagnetic signal is made to scatter from a moving acoustic pulse train. Under a Bragg-scatter condition, maximum electromagnetic scattering occurs. The scattered radio signal contains temperature and wind information as a function of the acoustic pulse position.

In the theoretical work on RASS to date, the effects of such atmospheric parameters as turbulence, humidity, mean temperature, and mean wind fields on the propagating acoustic pulse train have been ignored. By neglecting these parameters, the quantitative analyses have assumed that the acoustic wavefronts act as large perfect

DD FORM 1 JAN 73 1473
EDITION OF 1 NOV 65 IS OBSOLETE

Unclassified
SECURITY CLASSIFICATION OF THIS PAGE (When Data Entered)

19. KEY WORDS (Continued)

20 ABSTRACT (Continued)

spherical reflectors. In this investigation, RASS performance is assessed in a real atmosphere where "coherency" of the acoustic pulse is degraded as it propagates vertically into the lower atmosphere. The only assumption made is that the electromagnetic wave is not affected by stochastic perburbations in the atmosphere.

It is concluded that, for acoustic pulses with carrier frequencies below a few kilohertz propagating under typical atmospheric conditions, turbulence has little effect on the strength of the received radio signal at heights up to a few kilometers. This result implies that focusing of RF energy by the acoustic wavefronts is primarily a function of sound intensity which decreases as x^{-2}, where x denotes altitude.

The effect of mean vertical wind and mean temperature on the strength of the received signal is also demonstrated to be insignificant. Mean horizontal winds, however, shift the focus of the reflected electromagnetic energy from its origin, resulting in a decrease in received signal level when a monostatic RF system is used. For a bistatic radar configuration with space-diversified receiving antennas, the shifting of the acoustic pulse makes possible the remote measurement of the horizontal wind component.

JSEP REPORTS DISTRIBUTION LIST

Department of Defense

Director
National Security Agency
Attn: Dr. T. J. Beahn
Fort George G. Meade, MD 20755

Defense Documentation Center (12)
Attn: DDC-TCA (Mrs. V. Caponio)
Cameron Station
Alexandria, VA 22314

Assistant Director
Electronics and Computer Sciences
Office of Director of Defense
Research and Engineering
The Pentagon
Washington, D.C. 20315

Defense Advanced Research
Projects Agency
Attn: (Dr. R. Reynolds)
1400 Wilson Boulevard
Arlington, VA 22209

Department of the Army

Commandant
US Army Air Defense School
Attn: ATSAD-T-CSM
Fort Bliss, TX 79916

Commander
US Army Armament R&D Command
Attn: DRSAR-RD
Dover, NJ 07801

Commander
US Army Ballistics Research Lab.
Attn: DRXRD-BAD
Aberdeen Proving Ground
Aberdeen, MD 21005

Commandant
US Army Command and
General Staff College
Attn: Acquisitions, Library Div.
Fort Leavenworth, KS 66027

Commander
US Army Communication Command
Attn: CC-OPS-PD
Fort Huachuca, AZ 85613

Commander
US Army Materials and
Mechanics Research Center
Attn: Chief, Materials Sci. Div.
Watertown, MA 02172

Commander
US Army Materiel Development
and Readiness Command
Attn: Technical Lib., Rm. 7S 35
5001 Eisenhower Avenue
Alexandria, VA 22333

Commander
US Army Missile R&D Command
Attn: Chief, Document Section
Redstone Arsenal, AL 35809

Commander
US Army Satellite Communications
Agency
Fort Monmouth, NJ 07703

Commander
US Army Security Agency
Attn: IARD-T
Arlington Hall Station
Arlington, VA 22212

Project Manager
ARTADS
EAI Building
West Long Branch, NJ 07764

NOTE: One (1) copy to each addressee unless otherwise indicated.

Commander/Director
Atmospheric Sciences Lab. (ECOM)
Attn: DRSEL-BL-DD
White Sands Missile Range, NM 88002

Commander
US Army Electronics Command
Attn: DRSEL-NL-O
(Dr. H. S. Bennett)
Fort Monmouth, NJ 07703

Director
TRI-TAC
Attn: TT-AD (Mrs. Briller)
Fort Monmouth, NJ 07703

Commander
US Army Electronics Command
Attn: DRSEL-CT-L (Dr. R. Buser)
Fort Monmouth, NJ 07703

Director
Electronic Warfare Lab. (ECOM)
Attn: DRSEL-WL-MY
White Sands Missile Range, NM 88002

Executive Secretary, TAC/JSEP
US Army Research Office
P. O. Box 12211
Research Triangle Park, NC 27709

Commander
Frankford Arsenal
Deputy Director
Pitman-Dunn Laboratory
Philadelphia, PA 19137

Project Manager
Ballistic Missile Defense
Program Office
Attn: DACS-DMP (Mr. A. Gold)
1300 Wilson Boulevard
Arlington, VA 22209

Commander
Harry Diamond Laboratories
Attn: Mr. John E. Rosenberg
2800 Powder Mill Road
Adelphi, MD 20783

HQDA (DAMA-ARZ-A)
Washington, D.C. 20310

Commander
US Army Electronics Command
Attn: DRSEL-TL-E (Dr. J. A. Kohn)
Fort Monmouth, NJ 07703

Commander
US Army Electronics Command
Attn: DRSEL-TL-EN
(Dr. S. Kroenenberg)
Fort Monmouth, NJ 07703

Commander
US Army Electronics Command
Attn: DRSEL-NL-T (Mr. R. Kulinyi)
Fort Monmouth, NJ 07703

Commander
US Army Electronics Command
Attn: DRSEL-NL-B (Dr. E. Lieblein)
Fort Monmouth, NJ 07703

Commander
US Army Electronics Command
Attn: DRSEL-TL-MM (Mr. N. Lipetz)
Fort Monmouth, NJ 07703

Commander
US Army Electronics Command
Attn: DRSEL-RD-O (Dr. W. S. McAfee)
Fort Monmouth, NJ 07703

Director
Night Vision Laboratory
Attn: DRSEL-NV-D
Fort Belvoir, VA 22060

Col. Robert Noce
Senior Standardization Representative
US Army Standardization Group, Canada
Canadian Force Headquarters
Ottawa, Ontario, Canada KIA)K2

Commander
US Army Electronics Command
Attn: DRSEL-NL-B (Dr. D. C. Pearce)
Fort Monmouth, NJ 07703

Commander
Picatinny Arsenal
Attn: SMUPA-TS-T-S
Dover, NJ 07801

Dr. Sidney Ross
Technical Director
SARFA-TD
Frankford Arsenal
Philadelphia, PA 19137

Commander
US Army Electronics Command
Attn: DRSEL-NL-RH-1
(Dr. F. Schwering)
Fort Monmouth, NJ 07703

Commander
US Army Electronics Command
Attn: DRSEL-TL-I
(Dr. C. G. Thornton)
Fort Monmouth, NJ 07703

US Army Research Office (3)
Attn: Library
P. O. Box 12211
Research Triangle Park, NC 27709

Director
Division of Neuropsychiatry
Walter Reed Army Institute
of Research
Washington, D.C. 20012

Commander
White Sands Missile Range
Attn: STEWS-ID-R
White Sands Missile Range, NM 88002

Department of the Air Force

Mr. Robert Barrett
RADC/ETS
Hanscom AFB, MA 01731

Dr. Carl E. Baum
AFWL (ES)
Kirtland AFB, NM 87117

Dr. E. Champagne
AFAL/DH
Wright-Patterson AFB, OH 45433

Dr. R. P. Dolan
RADC/ETSD
Hanscom AFB, MA 01731

Mr. W. Edwards
AFAL/TE
Wright-Patterson AFB, OH 45433

Professor R. E. Fontana
Head, Dept. of Electrical Engineering
AFIT/ENE
Wright-Patterson AFB, OH 45433

Dr. Alan Garscadden
AFAPL/POD
Wright-Patterson AFB, OH 45433

USAF European Office of
Aerospace Research
Attn: Major J. Gorrell
Box 14, FPO, New York 09510

LTC Richard J. Gowen
Department of Electrical Engineering
USAF Academy, CO 80840

Mr. Murray Kesselman (ISCA)
Rome Air Development Center
Griffiss AFB, NY 13441

Dr. G. Knausenberger
Air Force Member, TAC
Air Force Office of Scientific
Research, (AFSC) AFSOR/NE
Bolling Air Force Base, DC 20332

Dr. L. Kravitz
Air Force Member, TAC
Air Force Office of Scientific
Research, (AFSC) AFSOR/NE
Bolling Air Force Base, DC 20332

Mr. R. D. Larson
AFAL/DHR
Wright-Patterson AFB, OH 45433

Dr. Richard B. Mack
RADC/ETER
Hanscom AFB, MA 01731

Mr. John Mottsmith (MCIT)
HQ ESD (AFSC)
Hanscom AFB, MA 01731

Dr. Richard Picard
RADC/ETSL
Hanscom AFB, MA 01731

Dr. J. Ryles
Chief Scientist
AFAL/CA
Wright-Patterson AFB, OH 45433

Dr. Allan Schell
RADC/ETE
Hanscom AFB, MA 01731

Mr. H. E. Webb, Jr. (ISCP)
Rome Air Development Center
Griffiss AFB, NY 13441

LTC G. Wepfer
Air Force Office of Scientific
Research, (AFSC) AFOSR/NP
Bolling Air Force Base, DC 20332

LTC G. McKemie
Air Force Office of Scientific
Research, (AFSC) AFOSR/NM
Bolling Air Force Base, DC 20332

Department of the Navy

Dr. R. S. Allgaier
Naval Surface Weapons Center
Code WR-303
White Oak
Silver Spring, MD 20910

Naval Weapons Center
Attn: Code 5515, H. F. Blazek
China Lake, CA 93555

Dr. H. L. Blood
Technical Director
Naval Undersea Center
San Diego, CA 95152

Naval Research Laboratory
Attn: Code 5200, A. Brodzinsky
4555 Overlook Avenue, SW
Washington, D.C. 20375

Naval Research Laboratory
Attn: Code 7701, J. D. Brown
4555 Overlook Avenue, SW
Washington, D.C. 20375

Naval Research Laboratory
Attn: Code 5210, J. E. Davey
4555 Overlook Avenue, SW
Washington, D.C. 20375

Naval Research Laboratory
Attn: Code 5460/5410, J. R. Davis
4555 Overlook Avenue, SW
Washington, D.C. 20375

Naval Ocean Systems Center
Attn: Code 75, W. J. Dejka
271 Catalina Boulevard
San Diego, CA 92152

Naval Weapons Center
Attn: Code 601, F. C. Essig
China Lake, CA 93555

Naval Research Laboratory
Attn: Code 5510, W. L. Faust
4555 Overlook Avenue, SW
Washington, D.C. 20375

Naval Research Laboratory
Attn: Code 2627, Mrs. D. Folen
4555 Overlook Avenue, SW
Washington, D.C. 20375

Dr. Robert R. Fossum
Dean of Research
Naval Postgraduate School
Monterey, CA 93940

Dr. G. G. Gould
Technical Director
Naval Coastal System Laboratory
Panama City, FL 32401

Naval Ocean Systems Center
Attn: Code 7203, V. E. Hildebrand
271 Catalina Boulevard
San Diego, CA 92152

Naval Ocean Systems Center
Attn: Code 753, P. H. Johnson
271 Catalina Boulevard
San Diego, CA 92152

Donald E. Kirk
Professor and Chairman
Electronic Engineer, SP-304
Naval Postgraduate School
Monterey, CA 93940

Naval Air Development Center
Attn: Code 01, Dr. R. K. Lobb
Johnsville
Warminster, PA 18974

Naval Research Laboratory
Attn: Code 5270, B. D. McCombe
4555 Overlook Avenue, SW
Washington, D.C. 20375

Capt. R. B. Meeks
Naval Sea Systems Command
NC #3
2531 Jefferson Davis Highway
Arlington, VA 20362

Dr. H. J. Mueller
Naval Air Systems Command
Code 310
JP #1
1411 Jefferson Davis Highway
Arlington, VA 20360

Dr. J. H. Mills, Jr.
Naval Surface Weapons Center
Electronics Systems Department
Code DF
Dahlgren, VA 22448

Naval Ocean Systems Center
Attn: Code 702, H. T. Mortimer
271 Catalina Boulevard
San Diego, CA 92152

Naval Air Development Center
Attn: Technical Library
Johnsville
Warminster, PA 18974

Naval Ocean Systems Center
Attn: Technical Library
271 Catalina Boulevard
San Diego, CA 92152

Naval Research Laboratory
Underwater Sound Reference Division
Technical Library
P. O. Box 8337
Orlando, FL 32806

Naval Surface Weapons Center
Attn: Technical Library
Code DX-21
Dahlgren, VA 22448

Naval Surface Weapons Center
Attn: Technical Library
Building 1-330, Code WX-40
White Oak
Silver Spring, MD 20910

Naval Training Equipment Center
Attn: Technical Library
Orlando, FL 32813

Naval Undersea Center
Attn: Technical Library
San Diego, CA 92152

Naval Underwater Systems Center
Attn: Technical Library
Newport, RI 02840

Office of Naval Research
Electronic and Solid State
Sciences Program (Code 427)
800 North Quincy Street
Arlington, VA 22217

Office of Naval Research
Mathematics Program (Code 432)
800 North Quincy Street
Arlington, VA 22217

Office of Naval Research
Naval Systems Division
Code 220/221
800 North Quincy Street
Arlington, VA 22217

Director
Office of Naval Research
New York Area Office
715 Broadway, 5th Floor
New York, NY 10003

Office of Naval Research
San Francisco Area Office
One Hallidie Plaza, Suite 601
San Francisco, CA 94102

Director
Office of Naval Research
Branch Office
495 Summer Street
Boston, MA 02210

Director
Office of Naval Research
Branch Office
536 South Clark Street
Chicago, IL 60605

Director
Office of Naval Research
Branch Office
1030 East Green Street
Pasadena, CA 91101

Mr. H. R. Riedl
Naval Surface Weapons Center
Code WR-34
White Oak Laboratory
Silver Spring, MD 20910

Naval Air Development Center
Attn: Code 202, T. J. Shopple
Johnsville
Warminster, PA 18974

Naval Research Laboratory
Attn: Code 5403, J. E. Shore
4555 Overlook Avenue, SW
Washington, D.C. 20375

A. L. Slafkovsky
Scientific Advisor
Headquarters Marine Corps
MC-RD-1
Arlington Annex
Washington, D.C. 20380

Harris B. Stone
Office of Research, Development,
Test and Evaluation
NOP-987
The Pentagon, Room 5D760
Washington, D.C. 20350

Mr. L. Sumney
Naval Electronics Systems Command
Code 3042, NC #1
2511 Jefferson Davis Highway
Arlington, VA 20360

David W. Taylor
Naval Ship Research and
Development Center
Code 522.1
Bethesda, MD 20084

Naval Research Laboratory
Attn: Code 4105, Dr. S. Teitler
4555 Overlook Avenue, SW
Washington, D.C. 20375

Lt. Cdr. John Turner
NAVMAT 0343
CP #5, Room 1044
2211 Jefferson Davis Highway
Arlington, VA 20360

Naval Ocean Systems Center
Attn: Code 746, H. H. Wieder
271 Catalina Boulevard
San Diego, CA 92152

Dr. W. A. Von Winkle
Associate Technical Director
for Technology
Naval Underwater Systems Center
New London, CT 06320

Dr. Gernot M. R. Winkler
Director, Time Service
US Naval Observatory
Massachusetts Avenue at
34th Street, NW
Washington, D.C. 20390

Other Government Agencies

Dr. Howard W. Etzel
Deputy Director
Division of Materials Research
National Science Foundation
1800 G Street
Washington, D.C. 20550

Mr. J. C. French
National Bureau of Standards
Electronics Technology Division
Washington, D.C. 20234

Dr. Jay Harris
Program Director
Devices and Waves Program
National Science Foundation
1800 G Street
Washington, D.C. 20550

Los Alamos Scientific Laboratory
Attn: Reports Library
P. O. Box 1663
Los Alamos, NM 87544

Dr. Dean Mitchell
Program Director
Solid-State Physics
Division of Materials Research
National Science Foundation
1800 G Street
Washington, D.C. 20550

Mr. F. C. Schwenk, RD-T
National Aeronautics and
Space Administration
Washington, D.C. 20546

M. Zane Thornton
Deputy Director, Institute for
Computer Sciences and Technology
National Bureau of Standards
Washington, D.C. 20234

Nongovernment Agencies

Director
Columbia Radiation Laboratory
Columbia University
538 West 120th Street
New York, NY 10027

Director
Coordinated Science Laboratory
University of Illinois
Urbana, IL 61801

Director of Laboratories
Division of Engineering and
Applied Physics
Harvard University
Pierce Hall
Cambridge, MA 02138

Director
Electronics Research Center
The University of Texas
Engineering-Science Bldg. 112
Austin, TX 78712

Director
Electronics Research Laboratory
University of California
Berkeley, CA 94720

Director
Electronics Sciences Laboratory
University of Southern California
Los Angeles, CA 90007

Director
Microwave Research Institute
Polytechnic Institute of New York
333 Jay Street
Brooklyn, NY 11201

Director
Research Laboratory of Electronics
Massachusetts Institute of Technology
Cambridge, MA 02139

Director
Stanford Electronics Laboratory
Stanford University
Stanford, CA 94305

Stanford Ginzton Laboratory
Stanford University
Stanford, CA 94305

Officer in Charge
Carderock Laboratory
Code 18 - G. H. Gleissner
David Taylor Naval Ship Research
and Development Center
Bethesda, MD 20084

Dr. Roy F. Potter
3868 Talbot Street
San Diego, CA 92106